OPTIMIZATION-BASED PROCESS SYNTHESIS FOR SUSTAINABLE CHEMICAL SYSTEMS

By

Joonjae Ryu

A dissertation submitted in partial fulfillment of the

requirements for the degree of

Doctor of Philosophy

(Chemical & Biological Engineering)

at the

UNIVERSITY OF WISCONSIN – MADISON

2022

Date of final oral examination: June 30, 2022

The dissertation is approved by the following members of the Final Oral Committee:

Maravelias, Christos T., Professor, Chemical & Biological Engineering

Swaney, Ross E., Associate Professor, Chemical & Biological Engineering

Zavala, Victor M., Professor, Chemical & Biological Engineering

Van Lehn, Reid C., Assistant Professor, Chemical & Biological Engineering

Noguera, Daniel R., Professor, Civil & Environment Engineering

Abstract

We propose optimization-based approaches for distillation network synthesis and heat integration, which can contribute to finding more energy efficient and sustainable chemical systems. For distillation network synthesis, we first propose unit models for distillation: 1) versatile shortcut distillation column and 2) separation energy targeting models. The models are to address systems where the components that are present in the feed can vary due to zero flow rates of some components, which naturally appear in process synthesis problems. The distillation column model can calculate component distributions and the energy requirement for a desired distillation task. The separation energy targeting model can be used to estimate an energy requirement target for the separation of a mixture without finding detail network configurations.

We also propose a generalized superstructure-based distillation network synthesis model with improved modeling capabilities. The model can assign multiple mixtures to be separated to different columns of the network while considering interactions between separation steps for each mixture. In terms of outlets, products with general specifications, including pure components and multi-component mixtures, as well as streams without strict specifications (e.g., reactor recycle streams), can be readily handled. Stream bypass and thermal coupling are simultaneously considered to find more energy efficient configurations. In addition, we propose an approach to leverage graphical insights in the optimization-based distillation network synthesis, where graphically-inspired feasibility constraints are combined with a superstructure-based approach.

For heat integration, we propose utility targeting and heat exchanger network synthesis models that account for variable stream temperatures and flow rates, as well as unclassified streams. Even with the extended capabilities, the model remains linear using discrete temperature grids, leading to a more tractable optimization model. The proposed model is well suited to problems where process configurations and the associated heat exchanger network are simultaneously synthesized. Several extensions are proposed, including nonisothermal mixing and phase changes.

Acknowledgements

During my PhD journey, I have been privileged to meet wonderful people who are indispensable for what I have done. First and foremost, I would like to extend my sincere gratitude to my advisor, Professor Christos Maravelias. His passion and dedication to research have always motivated me to be a better version of myself. He is a role model from which I could learn how to become an independent and dedicated researcher as well as a great advisor. Also, I sincerely appreciate his understanding and generous consideration during the difficult time due to the pandemic.

Next, I would like to thank all my dissertation committee members, Professors Ross Swaney, Victor Zavala, Reid Van Lehn, and Daniel Noguera, for their constructive feedback and encouragement.

I am thankful to all former and current members of the Maravelias group for unforgettable moments both in Madison and Princeton, especially Hojae, Garry, Arthur, Amin, Boeun, Jaewon, Ishan, and Juan. The precious memories will always remain in my heart. I also want to thank my friends Hochan and Sungho for being dependable friends while we are going through our journeys together.

I want to deeply appreciate my parents for their immeasurable love and support. Your love is the greatest crutch that holds me up whenever I face difficulties.

Finally, I want to thank my lovely better half Eunji for her understanding and being perseverant along the long journey. I cannot finish this journey without your endless love and warm support. You always bring joy and meaning to my life.

List of Figures

List of Tables

Contents

Chapter 1

Introduction

In this chapter, we first introduce process synthesis and superstructure-based approaches to address process synthesis problems. Then, we review approaches for distillation column modeling and distillation network synthesis, as well as approaches for heat integration. Lastly, we present the outline of this thesis.

1.1 Process Synthesis[1]

Process synthesis is a procedure to synthesize a process to meet specific goals while satisfying given constraints. There are, in general, two types of approaches to address process synthesis problems. The first relies on the decomposition of the problem into various subproblems which are solved sequentially. In this way, process alternatives are generated and assessed for each subproblem separately, and synthesis decisions are made hierarchically. A common strategy is to decompose the problem into: (1) reaction (or reactor) network synthesis, (2) separation network synthesis, and (3) heat exchanger network synthesis. The design decisions made in one subproblem bound the search space of a subsequent one; henceforth, some solutions can be excluded even if they might be better. For example, optimizing the solvent-to-reactant ratio based only on product

[1]The contents of this section appear in Ryu et al., *Comp. & Chem. Engr.* **2020**

yield can lead to very difficult and expensive downstream separations. Also, a reaction temperature resulting in a slightly lower selectivity may lead to better solutions when heat exchanger network is considered.

The second approach does not rely on the decomposition of the problem. Instead, a network which, in principle, includes all useful unit operations and relevant interconnections, referred to as a *superstructure*, is used. A superstructure for the overall process includes all alternative reactors, separators, heat exchangers, and their potential connections, thereby embedding all alternatives. Solving the optimization model based on such superstructures can yield the optimal process configuration and unit operating conditions considering interactions between elements in the superstructure.

1.2 Superstructure-based Process Synthesis[2]

Superstructure-based approaches can consider various interactions between different subsystems (e.g., reaction and separation systems), which would be ignored if each subsystem is synthesized separately. Papoulias and Grossmann proposed an approach to optimize a superstructure embedding several alternative reactors, separators, heat exchange networks, and utility system [74]. Later, superstructure-based approaches were formalized based on the State-Task-Network (STN) and State-Equipment-Network (SEN) representations, leading to a systematic way to represent superstructures and formulate synthesis problems [109]. Li et al. proposed a superstructure representation based on blocks [66]. For a detailed review on superstructure-based process synthesis, readers are referred to some excellent review papers [7, 16, 71, 105].

[2]The contents of this section appear in Ryu et al., *Comp. & Chem. Engr.* **2020**

For the approach to be effective, the connectivity among units of the postulated superstructure must be rich, while unnecessary connections should be excluded so that the resulting model is computationally efficient. Accordingly, Friedler et al. proposed a graph representation to generate the simplest superstructure that contains all relevant alternatives [37]. Wu et al. introduced a framework to generate rich but simple superstructures based on the concept of "minimal" and "feasible" sets [106].

Unit operations, which are key building blocks in the superstructure approach, can be modeled in various ways depending on the scope of the synthesis problem. Rigorous models based on mass/energy balances and thermodynamics can be used, but the resulting models can be highly challenging to solve when there are multiple unit operations in the superstructure. Accordingly, shortcut models or surrogate-based models are more widely used because of computational efficiency and simplicity [21, 25, 45, 80].

Superstructure-based approaches usually result in mixed-integer nonlinear programming (MINLP) models, which are computationally challenging to solve. Henceforth, the development of solution methods for these models has also received considerable attention [9, 23, 24, 57, 93, 111]

1.3 Distillation Network Synthesis[3]

In chemical/petrochemical facilities, distillation has been widely used, accounting for 10 $\sim$ 15 % of the world's industrial energy consumption [4, 56, 91, 94]. Thus, many efforts have been made to develop systematic and effective frameworks to synthesize more

[3]The contents of this section appear in Ryu and Maravelias, *Comp. & Chem. Engr.* **2020** and Ryu and Maravelias, *Chem. Eng. Sci.* **2021**

energy/cost efficient distillation networks [16, 73]. In early works, distillation network synthesis was addressed by heuristic rules obtained from numerical studies [99, 100] or thermodynamic insights [39]; later, heuristic rules were combined with evolutionary algorithms, where several initial flow sheets are generated and changed based on heuristic rules until there is no improvement [88, 95].

Superstructure-based approaches have also been proposed [3, 13, 31, 86, 109], and extended to handle dividing wall columns [14], non-sharp separations [2], multiple feeds system [33], and heat-integrated columns [32, 36].

Instead of solving a single optimization problem based on the superstructure, enumeration based approaches, where every configuration is generated and optimized individually, were proposed [38, 51, 72]. This approach, which is based on an efficient method of enumerating all useful configurations using a matrix, referred to as the *matrix method* [89], generated valuable insights into the characteristics of optimal solutions.

Distillation network has been also studied in conjunction with reactor systems because these two subsystems are interconnected in most chemical systems. Linke and Kokossis [67] studied interactions between reactor and separation systems, and Kong and Shah [62] proposed a superstructure-based approach for reaction screening while considering separation cost.

Notably, distillation column unit models are critical to model and solve the network synthesis problem, so various shortcut methods have been proposed. For the separation of an ideal or nearly ideal mixture, the Underwood equations [103, 104] was proposed to calculate minimum vapor flow rates, which are important indicators for distillation cost. Shortcut methods that can be applied to non-ideal mixtures have also been developed;

Doherty and coworkers developed the Boundary Value Method (BVM) to design a distillation column and check the feasibility of a task [29, 28, 53]; Koehler et al. introduced a reversible distillation model to calculate the minimum reflux [58]; Bausa et al. developed the Rectification Body Method (RBM) for the calculation of the minimum vapor flow rate [8]; Lucia et al. introduced the shortest stripping line method to calculate minimum energy [69, 70]; Kraemer et al. proposed a shortcut method for heteroazeotropic distillation [63], which was reformulated later for better numerical performance [92]. Recently, data-driven approaches have been used to develop efficient column models [87]. Although more accurate methods (e.g., with rigorous thermodynamics calculation) can be employed [23, 110], it remains challenging to find global solutions for large-scale distillation networks with these methods.

1.4 Heat Integration[4]

Using surplus energy in one process/stream to satisfy energy demand of other processes/streams, namely *heat integration*, can significantly reduce energy use of a chemical system. The area of heat integration has received renewed attention over the last few years due to an emphasis on the design of energy efficient and sustainable chemical systems. There are two main approaches to heat integration: *sequential* and *simultaneous*. In the former, the problem is decomposed into three sub-problems. The first sub-problem seeks to find the minimum utility consumption and the location of a pinch point, known as utility targeting [15, 75]. In the second sub-problem, several sub-networks are generated based on the location of the pinch point [75], and the optimal structure with the

[4]The contents of this section appear in Ryu and Maravelias, *Ind. Eng. Chem. Res.* **2019**

minimum number of matches to satisfy the utility target is obtained [40, 41, 42, 76]. In the third sub-problem, investment cost, based on heat exchanger area, is minimized [35]. The sequential method may lead to a sub-optimal solution because it does not consider the trade-off between utility cost and investment cost. Accordingly, approaches to alleviate this limitation have been proposed, where some of these sub-problems are combined. Floudas [34] used the concept of hyper-structure to solve the second and the third sub-problems simultaneously. Colberg [19] and Jezowski [50] proposed different models that can consider the first and the third sub-problems simultaneously. Later, approaches considering all decisions (i.e., utility, matches, and area) simultaneously were proposed to generate the optimal heat exchanger network (HEN) with the minimum total annualized cost. Ciric and Floudas [18] extended the hyper-structure to solve all the sub-problems simultaneously; Yee and Grossmann [107] proposed a stage-wise HENS model which has been extended by various works [1, 10, 20, 26, 48, 78, 79, 112]; Barbaro [6] proposed a linear model based on transportation/transshipment model; Swaney [97] extended the transportation model [15] to consider heat pump and heat engine.

1.5 Thesis Outline

The remainder of this thesis consists of five chapters, as follows. In Chapter 2, we present distillation unit models that are tailored for superstructure-based process synthesis. In Chapter 3, we present a superstructure-based approach for distillation network synthesis, which can be used to address generalized problems with its extended features. In Chapter 4, we introduce another approach for distillation network synthesis, where graphically-inspired feasibility constraints are combined with a superstructure-based optimization

approach. In Chapter 5, we present optimization-based heat integration approaches, which can facilitate simultaneous process synthesis and heat integration. In Chapter 6, we conclude and suggest future research directions. We use uppercase non-italic bold letters for sets and subsets, uppercase italic for variables, and lowercase greek for parameters.

Chapter 2

Distillation Unit Models[5]

2.1 Motivation

Due to their simplicity, shortcut methods have been extensively adopted in distillation network synthesis models. In most shortcut methods, it is necessary to know which components are present in the feed. However, when we consider the synthesis of a system (e.g., separation network or combined reactor-separation network), components that are present in the feed can change depending on decisions in other subsystems (e.g., reaction selections in upstream processes) [81]. For example, in **Figure 2.1A**, the synthesis of a reactor-separation network is shown, where the reactor network consists of five alternative reactors carrying out different reactions and the separation network separates the outlet from the reactor network. Since different reactions produce effluents with different components, we cannot determine which components are contained in the feed (i.e., outlet from the reactor network) a priori [60]; henceforth, such feed is termed as *undetermined*.

The presence of an undetermined feed makes the use of shortcut methods challenging because they would have to be used for each disaggregated stream (See **Figure 2.1B**), so that components that are present in the feed are known a priori, resulting in a

[5]The contents of this chapter appear in Ryu and Maravelias, *Comp. & Chem. Engr.* **2020**

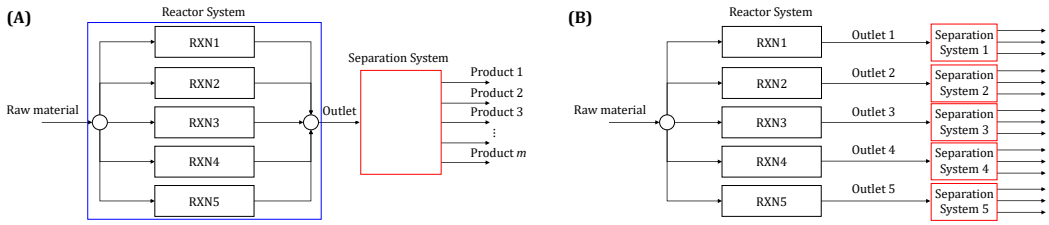

Figure 2.1: (A): A reactor network (blue box) is connected to a separation network (red box). Depending on the reactor/reaction selection, component molar flow rates in the outlet change, while some of them can be zero; (B): Each reactor is connected to a separate separation network.

computationally challenging optimization problem. Accordingly, when undetermined feeds are potentially present, relatively simple models with pre-calculation of separation energy/cost have been adopted [62, 102].

To handle problems with undetermined feed(s) in a more computationally efficient way, we propose generalized shortcut-based distillation unit models, which can be readily integrated with or utilized as submodules in other superstructure-based process synthesis models to calculate the energy requirement or cost for the separation.

2.2 Background

2.2.1 Underwood Equations

We define the ordered set $\mathbf{I} = \{\mathrm{A}, \mathrm{B}, \mathrm{C}, ...\}$ to denote the postulated components in the feed in decreasing order of volatility. We use the index i to denote the element (e.g., A or B) or the order of that element (e.g., 1 or 2). If we consider a feed mixture with n postulated components ($|\mathbf{I}| = n$), the relative volatility of component i (α_i) is defined as

the ratio of its vapor-liquid equilibrium constant (K_i) to that of the heaviest (i.e., the least volatile) component ($\alpha_i = K_i/K_{i'=n}$). Assuming that the relative volatilities are constant along the column, it is shown that the followings hold [103, 104],

$$\sum_{i\in\mathbf{I}} \frac{\alpha_i F_i}{\alpha_i - \phi_l} = (1-q)\sum_{i\in\mathbf{I}} F_i \qquad l \in \mathbf{L} \tag{2.1}$$

$$\sum_{i\in\mathbf{I}} \frac{\alpha_i D_i}{\alpha_i - \phi_l} = V1 \qquad l \in \mathbf{L}^{\mathrm{A}} \tag{2.2}$$

$$\sum_{i\in\mathbf{I}} \frac{-\alpha_i B_i}{\alpha_i - \phi_l} = V2 \qquad l \in \mathbf{L}^{\mathrm{A}} \tag{2.3}$$

where F_i denotes the molar flow rate of component i in the feed; D_i/B_i denotes the molar flow rate of component i in the distillate/bottom stream; $V1/V2$ denotes the minimum vapor molar flow rate in the top/bottom section of the distillation column; q denotes the liquid fraction of the feed (e.g., $q = 1/0$ for saturated liquid/vapor); and ϕ_l denotes an *Underwood root*. The set $\mathbf{L}$ is defined as $\{1, 2, ..., n-1\}$ to denote the index of the Underwood roots. Note that the Underwood equations were developed for systems where a feed mixture has an ideal or near-ideal behavior (i.e., constant relative volatilities). If the feed mixture is non-ideal, the Underwood equations can lead to significantly inaccurate solutions, so more rigorous methods (e.g., using tray-by-tray column models with rigorous energy/mass balance) are needed.

We refer to Eq. (2.1) as the *feed equation* while Eqs. (2.2) and (2.3) as the *vapor equations*. If all component flow rates in the feed (F_i) are given positive, we can solve the feed equation to calculate ϕ_l. Each root is bounded by the relative volatilities of each pair of adjacent components ($\alpha_i > \phi_l > \alpha_{i+1}, i = l$). For example, if we have a feed with four components, $\mathbf{I} = \{\mathrm{A}, \mathrm{B}, \mathrm{C}, \mathrm{D}\}$, then there are three roots satisfying:

$$\alpha_{\mathrm{A}} > \phi_1 > \alpha_{\mathrm{B}} > \phi_2 > \alpha_{\mathrm{C}} > \phi_3 > \alpha_{\mathrm{D}} = 1 \tag{2.4}$$

Also, we assume one light key (LK) and one heavy key (HK); the light key is the lightest component in the bottom stream while the heavy key is the heaviest component in the distillate stream. Also, we refer to the components between the light and heavy keys as *distributed components* and the components that are lighter than the light key (LLK) or heavier than the heavy key (HHK) as *non-distributed components*. Usually, the component molar flow rates of the key components in the distillate and bottom streams can be set from product specifications. Also, we assume that LLKs and HHKs are completely recovered in the distillate and bottom streams, respectively.

If root ϕ_l is between the relative volatilities of the light and heavy keys, it is termed as an *active root*, $l \in \mathbf{L}^{\mathrm{A}}$. If there are p distributed components, there are $1+p$ active roots. These active roots are used to calculate the minimum vapor flow rates in the vapor equations. For example, if we choose component A/C as the light/heavy key in the previous example, component B is distributed; thus, we need to use two active roots between α_{A} and α_{C} (i.e., ϕ_1 and ϕ_2) in the vapor equations. Also, $D_{\mathrm{D}} = 0$ and $B_{\mathrm{D}} = F_{\mathrm{D}}$ are enforced (HHK), and D_{A} (or B_{A}) and D_{C} (or B_{C}) are determined based on product specifications. Then, there are two unknowns in Eq. (2.2)/(2.3) (i.e., $V1/V2$ and $D_{\mathrm{B}}/B_{\mathrm{B}}$, respectively). With two active roots (i.e., ϕ_1 and ϕ_2), we can construct two equations from Eq. (2.2)/(2.3) to calculate the unknowns.

If root $\phi_{l'}$ is not between the relative volatilites of the keys (i.e., $\alpha_{\mathrm{LK}} < \phi_{l'}$ or $\alpha_{\mathrm{HK}} > \phi_{l'}$), it is referred to as an *inactive root*, $l' \in \mathbf{L}^{\mathrm{IA}}$. Underwood [103] and several researchers [44, 101] showed that if the distillation column is operated with the minimum

vapor flow rates, the following inequalities hold for all inactive roots,

$$V1 \geq \sum_{i \in \mathbf{I}} \frac{\alpha_i D_i}{\alpha_i - \phi_{l'}} \qquad i \in \mathbf{I}, l' \in \mathbf{L}^{\mathrm{IA}} \tag{2.5}$$

$$V2 \geq -\sum_{i \in \mathbf{I}} \frac{\alpha_i B_i}{\alpha_i - \phi_{l'}} \qquad i \in \mathbf{I}, l' \in \mathbf{L}^{\mathrm{IA}} \tag{2.6}$$

Thus, incorporating Eqs. (2.5) and (2.6) in a model can remove solutions with component distributions that cannot be obtained with the minimum vapor flow rates. Additional discussion can be found in appendix A.1 and other works [44, 101].

2.2.2 Undetermined Feed

Most approaches employing the Underwood equations assume that the components present in the feed are fixed, so the bounds on each root are known (e.g., Eq. (2.4)). However, when the feed is undetermined, the bounds may not be valid [61]. To illustrate,

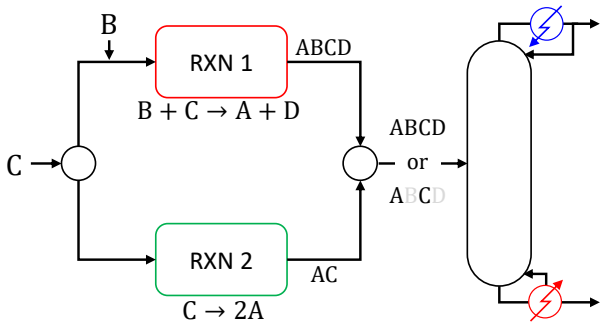

Figure 2.2: A reactor network is connected to a distillation column; depending on the reactor selection, the components present in the outlet stream change. If RXN1 is selected, components A, B, C, and D are included in the outlet. However, if RXN2 is selected, the flow rates of components B and D are zero, changing the number/location of the Underwood roots.

we consider the example in **Figure 2.2**, where there is a reactor network including two

alternative reactors (RXN1 and RXN2) performing different reactions (B + C $\rightarrow$ A + D and C $\rightarrow$ 2A) to produce final product A from reactant C. Depending on the reactor selection, the outlet stream from the reactor network consists of either $\{\mathrm{A}, \mathrm{B}, \mathrm{C}, \mathrm{D}\}$ or $\{\mathrm{A}, \mathrm{C}\}$. If we consider $\{\mathrm{A}, \mathrm{B}, \mathrm{C}, \mathrm{D}\}$ as the postulated components in the outlet stream, the flow rates of components B and D are zero if RXN2 is selected. Then, there is only one distinct root (not three) satisfying,

$$\alpha_{\mathrm{A}} > \phi_1 = \phi_2 = \phi_3 > \alpha_{\mathrm{C}} \tag{2.7}$$

where components B and D do not affect the location of the Underwood roots. Hence, if we find the Underwood roots based on the bounds from the postulated components (i.e., $\{\mathrm{A}, \mathrm{B}, \mathrm{C}, \mathrm{D}\}$), we cannot find any roots in $(\alpha_{\mathrm{C}}, \alpha_{\mathrm{D}})$; furthermore, we can find only one distinct root either in $(\alpha_{\mathrm{A}}, \alpha_{\mathrm{B}})$ or $(\alpha_{\mathrm{B}}, \alpha_{\mathrm{C}})$, which makes Eq. (2.4) infeasible. Therefore, the Underwood equations need to be reformulated with appropriate constraints on each root, rather than bounds, to address undetermined feeds.

2.2.3 Fully Thermally Coupled Distillation Network

Petluyk and coworkers [77] showed that the energy requirement in a distillation network can be reduced by removing intermediate heat exchangers between columns, referred to as *thermal coupling*. For instance, a condenser (or reboiler) of a column can be removed if the liquid reflux (or vapor load) is provided by a stream that is withdrawn from another column.

When the entire vapor load and liquid reflux are provided by a single reboiler and a single condenser, respectively, the configuration is termed as the *fully thermally coupled*

(FTC) configuration [77]. This configuration utilizes sloppy splits, where key components are not adjacent (e.g., A and C). In **Figure 2.3A**, a distillation network to separate a ternary mixture (ABC) is shown, where component A/C is selected as the light/heavy key in the first column, leading to a sloppy split. This configuration can be converted to a FTC configuration (See **Figure 2.3B**) by removing intermediate heat exchangers, resulting in only one condenser/reboiler in the network. Interestingly, it is proved that

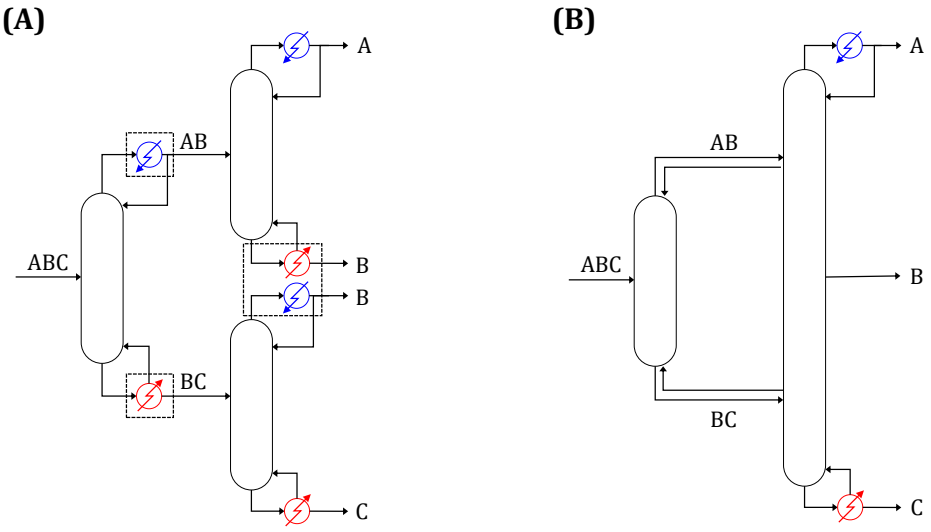

Figure 2.3: (A): Distillation network to separate a ternary mixture (ABC) into pure components. Sloppy split is performed in the first column (AB/BC). Intermediate heat exchangers are highlighted with black dashed boxes; (B): Fully thermally coupled (FTC) configuration. Intermediate heat exchangers are removed, so there is only one condenser/reboiler in the network.

the minimum energy to separate an ideal zeotropic mixture into pure components via distillation is always obtained by the FTC configuration [43, 44].

Using the FTC configuration, we can obtain a more reasonable energy target, compared to purely theoretical approaches (e.g., exergy analysis), for the separation of a mixture via distillation. For example, R. T. Gooty et al. [101] found that the optimal distillation network configuration almost always has an energy requirement which is less than 1.2 times that of the FTC configuration. Henceforth, we refer to the energy requirement for the FTC configuration as the *separation energy target*. This energy target can be highly useful for preliminary process synthesis such as an initial screening of reaction alternatives with the consideration of separation energy. Also, the minimum vapor flow rate that needs to be condensed/vaporized by the single condenser/reboiler ($V1^{FTC}/V2^{FTC}$) can be easily estimated by finding the maximum among the minimum vapor flow rates for splits between adjacent components [43, 44] as follows,

$$V1^{FTC} = \max_{i}(\overline{V1}_{i,i+1}) \tag{2.8}$$

$$V2^{FTC} = V1^{FTC} - (1-q)\sum_{i\in\mathbf{I}} F_i \tag{2.9}$$

where $\overline{V1}_{i,i+1}$ denotes the minimum vapor flow rate in the top section of the column to separate the feed between components i and $i+1$, calculated by the Underwood equations. This approach is called *Vmin* approach. For example, if we have a feed with $\mathbf{I} = \{\mathrm{A}, \mathrm{B}, \mathrm{C}, \mathrm{D}\}$, $V1^{FTC}$ can be obtained by calculating the minimum vapor flow rates for A/BCD, AB/CD, and ABC/D splits of the feed (i.e., $\overline{V1}_{\mathrm{A,B}}$, $\overline{V1}_{\mathrm{B,C}}$, and $\overline{V1}_{\mathrm{C,D}}$, respectively) and choosing the maximum among them. Then, $V2^{FTC}$ can be easily calculated with the feed information.

Therefore, if we can calculate minimum vapor flow rates for the splits between all pairs of adjacent components in the feed, we can also calculate the minimum vapor flow rates (and energy requirement) needed in the FTC configuration. However, for

systems with an undetermined feed, these calculations cannot be carried out using the Underwood equations or any other shortcut methods.

2.3 Generalized Shortcut-based Distillation Column Model

We propose a novel reformulation of the Underwood equations to address problems with undetermined feed(s) in a more computationally efficient way. The reformulation enables the calculation of all roots of Underwood equations. Then, we utilize this reformulation to develop a versatile shortcut distillation column model and a separation energy targeting model.

2.3.1 Detection of Lightest/Heaviest Component

We introduce binary variable Y_i to denote whether component i has a positive molar flow rate in the feed,

$$\underline{\delta}_i Y_i \leq F_i \leq \overline{\delta}_i Y_i \qquad i \in \mathbf{I} \tag{2.10}$$

where $\underline{\delta}_i/\overline{\delta}_i$ is a lower/upper bound on F_i. We introduce binary variable Y_i^L/Y_i^H to denote that component i is the lightest/heaviest component in the feed. The lightest/heaviest component should have positive molar flow rates,

$$Y_i^L \leq Y_i \qquad i \in \mathbf{I} \tag{2.11}$$

$$Y_i^H \leq Y_i \qquad i \in \mathbf{I} \tag{2.12}$$

and there should be one lightest component and one heaviest component in the feed.

$$\sum_{i \in \mathbf{I}} Y_i^L = 1 \tag{2.13}$$

$$\sum_{i \in \mathbf{I}} Y_i^H = 1 \tag{2.14}$$

Also, Y_i^L and Y_i^H are constrained as follows:

$$\sum_{i > i' \in \mathbf{I}} Y_{i'} \leq (i-1)(1 - Y_i^L) \qquad 1 < i \in \mathbf{I} \tag{2.15}$$

$$\sum_{i < i' \in \mathbf{I}} Y_{i'} \leq (n-i)(1 - Y_i^H) \qquad n > i \in \mathbf{I} \tag{2.16}$$

If $Y_i^L = 1$, the right hand side of Eq. (2.15) becomes zero, enforcing that there is no component that is lighter than i (i.e., $\sum_{i > i' \in \mathbf{I}} Y_{i'} = 0$). Similarly, if $Y_i^H = 1$, Eq. (2.16) enforces that there is no component that is heavier than i (i.e., $\sum_{i < i' \in \mathbf{I}} Y_{i'} = 0$). For example, in **Figure 2.4**, a system with five postulated components ($\mathbf{I} = \{\mathrm{A}, \mathrm{B}, \mathrm{C}, \mathrm{D}, \mathrm{E}\}$) is shown, where the molar flow rates of components A and E are zero ($Y_\mathrm{A} = 0$ and $Y_\mathrm{E} = 0$). Due to Eq. (2.11), component A cannot be selected as the lightest component

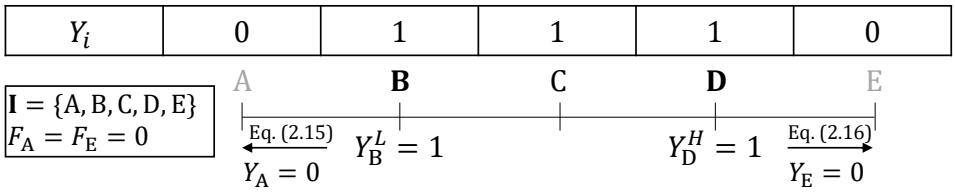

Figure 2.4: Detection of the lightest/heaviest component in the feed. Molar flow rates of components A and E are zero, so B/D is the lightest/heaviest component in the feed ($Y_\mathrm{B}^L = 1 / Y_\mathrm{D}^H = 1$).

($Y_\mathrm{A}^L = 0$). Thus, only Y_B^L can be activated because Eq. (2.15) is violated if another component is selected as the lightest component. Similarly, component E cannot be

selected as the heaviest component due to Eq. (2.12), and only Y_{D}^{H} can be activated because of Eq. (2.16).

2.3.2 Reformulation of Feed Equation

We define the set of intervals between adjacent postulated components as $\mathbf{I}^{\mathrm{R}} = \mathbf{I} \backslash \{i = n\}$. For example, if $\mathbf{I} = \{\mathrm{A}, \mathrm{B}, \mathrm{C}, \mathrm{D}\}$, then $\mathbf{I}^{\mathrm{R}} = \{\mathrm{A}, \mathrm{B}, \mathrm{C}\}$, where $i \in \mathbf{I}^{\mathrm{R}}$ denotes the interval between components i and $i+1$. Then, for each interval, we define the Underwood root ϕ_i, satisfying $\phi_i \geq \phi_{i+1}$. We define variable $U_{i,i'}^{F}$ as follows,

$$U_{i,i'}^{F} = \frac{\alpha_i F_i}{\alpha_i - \phi_{i'}}, \qquad i \in \mathbf{I},\ i' \in \mathbf{I}^{\mathrm{R}} \tag{2.17}$$

Note that $n-1$ Underwood roots are considered in Eq. (2.17). In the current form, Eq. (2.17) can lead to numerical instability because the denominator can become too small. To prevent this, it is reformulated as follows,

$$U_{i,i'}^{F}\big(1 - \frac{\phi_{i'}}{\alpha_i}\big) = F_i \qquad i \in \mathbf{I},\ i' \in \mathbf{I}^{\mathrm{R}} \tag{2.18}$$

$$-\frac{1}{\omega} F_i \leq U_{i,i'}^{F} \leq \frac{1}{\omega} F_i \qquad i \in \mathbf{I},\ i' \in \mathbf{I}^{\mathrm{R}} \tag{2.19}$$

where ω is a lower bound on $||1 - \phi_{i'}/\alpha_i||$ for which a sufficiently small number (e.g., $10^{-4} \sim 10^{-3}$) can be used. With this reformulation, the variable $U_{i,i'}^{F}$ is bounded by F_i, leading to better numerical stability. Then, the feed equation can be written as follows:

$$\sum_{i \in \mathbf{I}} U_{i,i'}^{F} = (1-q) \sum_{i \in \mathbf{I}} F_i \qquad i' \in \mathbf{I}^{\mathrm{R}} \tag{2.20}$$

2.3.3 Number of Distinct Underwood Roots

Consider a system with n postulated components. If there are r components with zero flow rates, the system actually has $n-r$ components; thus, there are only $n-r-1$

distinct Underwood roots. However, we consider $n-1$ roots in Eq. (2.17), so some roots must be identical.

For this, we define the set $\mathbf{I}^{\mathrm{RD}} = \mathbf{I}^{\mathrm{R}} \backslash \{i = n-1\}$ to denote the intervals between the Underwood roots. Then, the difference between adjacent Underwood roots, Δ_i, is constrained as follows,

$$\phi_i - \phi_{i+1} = \Delta_i \quad i \in \mathbf{I}^{\mathrm{RD}} \tag{2.21}$$

$$\epsilon(Y_{i+1} - Y_{i+1}^L - Y_{i+1}^H) \leq \Delta_i \leq (\overline{\alpha} - \underline{\alpha})(Y_{i+1} - Y_{i+1}^L - Y_{i+1}^H) \quad i \in \mathbf{I}^{\mathrm{RD}} \tag{2.22}$$

where ϵ can be set as a small number (e.g., $10^{-3} \sim 10^{-2}$); $\overline{\alpha}/\underline{\alpha}$ is an upper/lower bound on the roots, with $\overline{\alpha} = \alpha_{\mathrm{A}}$ and $\underline{\alpha} = 1$ being valid bounds. If component $i+1$ has zero flow rate ($Y_{i+1} = 0$), then $Y_{i+1}^L = 0$ and $Y_{i+1}^H = 0$ are enforced by Eqs. (2.11) and (2.12), leading to $\Delta_i = \phi_i - \phi_{i+1} = 0$. On the other hand, if component $i+1$ has positive molar flow rate while it is neither the lightest nor the heaviest component, $\Delta_i \geq \epsilon$ is enforced. Finally, if component $i+1$ is either the lightest or the heaviest component ($Y_{i+1}^L = 1$ or $Y_{i+1}^H = 1$), $Y_{i+1} - Y_{i+1}^L - Y_{i+1}^H = 0$ holds, enforcing $\Delta_i = 0$ again. For example, if a system

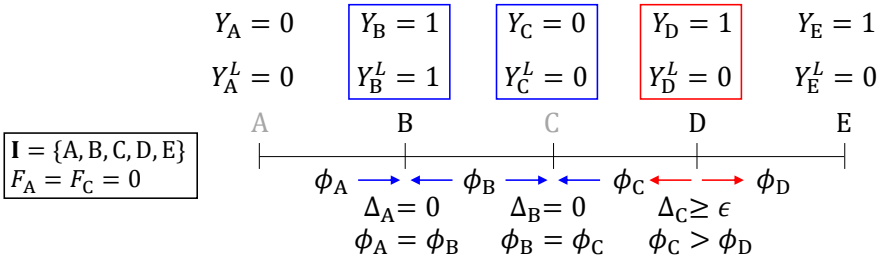

Figure 2.5: Distinct Underwood roots of a system with $\mathbf{I} = \{\mathrm{A}, \mathrm{B}, \mathrm{C}, \mathrm{D}, \mathrm{E}\}$ and $F_{\mathrm{A}} = F_{\mathrm{C}} = 0$.

has five postulated components ($\mathbf{I} = \{\mathrm{A}, \mathrm{B}, \mathrm{C}, \mathrm{D}, \mathrm{E}\}$), and components A and C have zero flow rates (See **Figure 2.5**), the system has three components and two distinct roots.

Component B has a positive molar flow rate ($Y_{\mathrm{B}} = 1$) and is the lightest component ($Y_{\mathrm{B}}^{L} = 1$), so $\Delta_{\mathrm{A}} = \phi_{\mathrm{A}} - \phi_{\mathrm{B}} = 0$ is enforced by Eq. (2.22). Component C has zero flow rate, so $\Delta_{\mathrm{B}} = \phi_{\mathrm{B}} - \phi_{\mathrm{C}} = 0$ is enforced. Component D is neither the lightest nor the heaviest component, so a positive difference between adjacent roots ($\Delta_{\mathrm{C}} = \phi_{\mathrm{C}} - \phi_{\mathrm{D}} \geq \epsilon$) is enforced. Thus, two distinct roots are enforced ($\phi_{\mathrm{A}} = \phi_{\mathrm{B}} = \phi_{\mathrm{C}} > \phi_{\mathrm{D}}$).

We refer to the model composed of Eqs. (2.10)∼(2.16), (2.18)∼(2.22) as **M1***. It can be used to calculate all the relevant Underwood roots for undetermined feeds.

2.3.4 Valid Constraints on Underwood Roots

In deterministic global optimization, introducing valid strong constraints can reduce the computation time to obtain the global optimal solution as well as to prove its global optimality [98]. Although all distinct roots can be found with **M1***, each root is not constrained as tight as possible. Accordingly, we propose valid constraints by utilizing the understanding of the Underwood equations, which can significantly enhance the computational performance of the model.

Consider a system with 5 components, $\mathbf{I} = \{\mathrm{A}, \mathrm{B}, \mathrm{C}, \mathrm{D}, \mathrm{E}\}$, where all components have positive molar flow rates. Then, in **M1***, the roots are constrained by Eqs. (2.21) and (2.22) and bounded by α_{A} and 1 as follows,

$$\alpha_{\mathrm{A}} > \phi_{\mathrm{A}} > \phi_{\mathrm{B}} > \phi_{\mathrm{C}} > \phi_{\mathrm{D}} > \alpha_{\mathrm{E}} = 1 \tag{2.23}$$

enforcing four distinct roots. From the knowledge about the Underwood equations, the roots should satisfy the followings,

$$\alpha_{\mathrm{A}} > \phi_{\mathrm{A}} > \alpha_{\mathrm{B}} > \phi_{\mathrm{B}} > \alpha_{\mathrm{C}} > \phi_{\mathrm{C}} > \alpha_{\mathrm{D}} > \phi_{\mathrm{D}} > \alpha_{\mathrm{E}} = 1 \tag{2.24}$$

Accordingly, we can introduce additional constraints as follows,

$$(Y_i = 1) \wedge (Y_i^L = 0) \rightarrow \alpha_i < \phi_{i-1} \qquad 1 < i \in \mathbf{I} \tag{2.25}$$

$$(Y_i = 1) \wedge (Y_i^H = 0) \rightarrow \alpha_i > \phi_i \qquad i \in \mathbf{I}^{\mathrm{R}} \tag{2.26}$$

where ϕ_{i-1}/ϕ_i is enforced to be greater/less than α_i if component i has a positive molar flow rate and is not the lightest/heaviest component in the feed. The logical propositions in Eqs. (2.25) and (2.26) can be expressed using binary variables as follows:

$$(\alpha_i + \sigma)(Y_i - Y_i^L) + \underline{\alpha}(1 - Y_i + Y_i^L) \leq \phi_{i-1} \qquad 1 < i \in \mathbf{I} \tag{2.27}$$

$$\phi_i \leq (\alpha_i - \sigma)(Y_i - Y_i^H) + \overline{\alpha}(1 - Y_i + Y_i^H) \qquad i \in \mathbf{I}^{\mathrm{R}} \tag{2.28}$$

Note that Eq. (2.27)/(2.28) becomes redundant when component i has zero flow rate or it is the lightest/heaviest component.

In the previous example where all components have positive flow rates, Eqs. (2.27) and (2.28) enforce $\alpha_i > \phi_i > \alpha_{i+1}, i \in \mathbf{I}^{\mathrm{R}}$. Even if some components have zero flow rates, Eqs. (2.27) and (2.28) constrain the roots to be between relevant relative volatilities. For example, if $F_{\mathrm{A}} = F_{\mathrm{C}} = 0$ ($Y_{\mathrm{A}} = Y_{\mathrm{C}} = 0$) in the previous system, then there are two distinct roots (not four) satisfying (See **Figure 2.6**),

$$\alpha_{\mathrm{B}} > \phi_{\mathrm{A}} = \phi_{\mathrm{B}} = \phi_{\mathrm{C}} > \alpha_{\mathrm{D}} > \phi_{\mathrm{D}} > \alpha_{\mathrm{E}} = 1 \tag{2.29}$$

whereas Eq. (2.22) enforces $\phi_{\mathrm{A}} = \phi_{\mathrm{B}} = \phi_{\mathrm{C}} > \phi_{\mathrm{D}}$. Then, $\phi_{\mathrm{C}} > \alpha_{\mathrm{D}}$ and $\phi_{\mathrm{D}} > \alpha_{\mathrm{E}}$ are enforced by Eq. (2.27) expressed for $i = \mathrm{D}$ and $i = \mathrm{E}$, respectively because $Y_{\mathrm{D}} = 1$ and $Y_{\mathrm{E}} = 1$. Note that Eq. (2.27) expressed for $i = \mathrm{B}$ is relaxed because $Y_{\mathrm{B}}^L = 1$. Also, $\alpha_{\mathrm{B}} > \phi_{\mathrm{B}}$ and $\alpha_{\mathrm{D}} > \phi_{\mathrm{D}}$ are enforced by Eq. (2.28) expressed for $i = \mathrm{B}$ and $i = \mathrm{D}$, respectively, because $Y_{\mathrm{B}} = 1$ and $Y_{\mathrm{D}} = 1$. Finally, Eqs. (2.27) and (2.28) expressed for the components with zero flow rates (i.e., components A and C) become redundant.

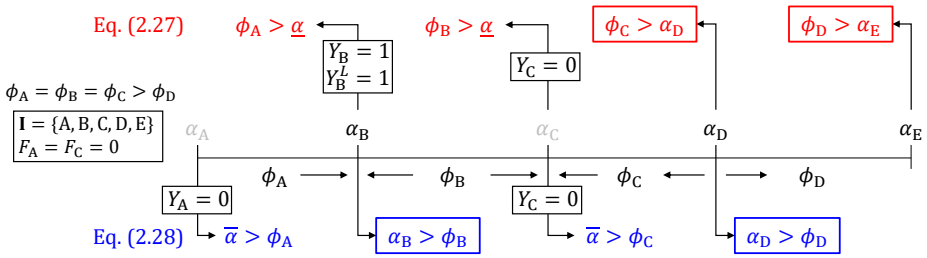

Figure 2.6: System with $\mathbf{I} = \{\mathrm{A}, \mathrm{B}, \mathrm{C}, \mathrm{D}, \mathrm{E}\}$ and $F_\mathrm{A} = F_\mathrm{C} = 0$. Constraints from Eq. (2.27)/(2.28) are colored in red/blue. Also, if a constraint is not redundant, it is highlighted with a colored box. Binary variables that relax Eqs (2.27) and (2.28) are represented in black boxes.

We refer to the model composed of **M1*** with Eqs. (2.27) and (2.28) as **M1**. In superstructure-based process synthesis approaches, **M1** can be used to calculate all relevant roots efficiently in the presence of undetermined feeds. Notably, when only active roots are needed, a simpler approach has been proposed [61], whose effective valid constraints and its extension for non-sharp splits are presented in appendix A.3 and appendix A.4, respectively.

2.3.5 Light/Heavy Key Selection

First, we introduce binary variable Y_i^{LK}/Y_i^{HK} to denote the selection of component i as the light/heavy key. There are one light and one heavy keys,

$$\sum_{i \in \mathbf{I}} Y_i^{LK} = 1 \tag{2.30}$$

$$\sum_{i \in \mathbf{I}} Y_i^{HK} = 1 \tag{2.31}$$

and they should have positive molar flow rates,

$$Y_i^{LK} \leq Y_i \qquad i \in \mathbf{I} \tag{2.32}$$

$$Y_i^{HK} \leq Y_i \qquad i \in \mathbf{I} \tag{2.33}$$

The binary variable Z_i is introduced to denote whether component i is a distributed component.

$$Z_i = \sum_{i' \leq i-1} Y_{i'}^{LK} - \sum_{i' \leq i} Y_{i'}^{HK} \qquad i \in \mathbf{I} \tag{2.34}$$

2.3.6 Reformulation of Vapor Equations

We define variables $U_{i,i'}^D, U_{i,i'}^B$,

$$U_{i,i'}^D = \frac{\alpha_i D_i}{\alpha_i - \phi_{i'}} \qquad i \in \mathbf{I},\ i' \in \mathbf{I}^{\mathrm{R}} \tag{2.35}$$

$$U_{i,i'}^B = -\frac{\alpha_i B_i}{\alpha_i - \phi_{i'}} \qquad i \in \mathbf{I},\ i' \in \mathbf{I}^{\mathrm{R}} \tag{2.36}$$

which can be reformulated as follows,

$$U_{i,i'}^D (1 - \frac{\phi_{i'}}{\alpha_i}) = D_i \qquad i \in \mathbf{I},\ i' \in \mathbf{I}^{\mathrm{R}} \tag{2.37}$$

$$U_{i,i'}^B (1 - \frac{\phi_{i'}}{\alpha_i}) = -B_i \qquad i \in \mathbf{I},\ i' \in \mathbf{I}^{\mathrm{R}} \tag{2.38}$$

$$-\frac{1}{\omega} D_i \leq U_{i,i'}^D \leq \frac{1}{\omega} D_i \qquad i \in \mathbf{I},\ i' \in \mathbf{I}^{\mathrm{R}} \tag{2.39}$$

$$-\frac{1}{\omega} B_i \leq U_{i,i'}^B \leq \frac{1}{\omega} B_i \qquad i \in \mathbf{I},\ i' \in \mathbf{I}^{\mathrm{R}} \tag{2.40}$$

Note that root ϕ_i is calculated by **M1**. Then, the vapor equations (i.e., Eqs. (2.2) and (2.3)) are reformulated as follows,

$$V1 - S_{i'} \leq \sum_{i \in \mathbf{I}} U_{i,i'}^D \leq V1 \qquad i' \in \mathbf{I}^{\mathrm{R}} \tag{2.41}$$

$$V2 - S_{i'} \leq \sum_{i \in \mathbf{I}} U_{i,i'}^B \leq V2 \qquad i' \in \mathbf{I}^{\mathrm{R}} \tag{2.42}$$

where the nonnegative slack variable $S_{i'}$ is constrained as follows,

$$S_{i'} \leq \beta(1 - Z_{i'}) \qquad i' \in \mathbf{I}^{\mathrm{R}} \tag{2.43}$$

$$S_{i'} \leq \beta(1 - Y_{i'}^{LK}) \qquad i' \in \mathbf{I}^{\mathrm{R}} \tag{2.44}$$

The parameter β is an upper bound on the vapor flow rate. If a corresponding root ($\phi_{i'}$) is active (i.e., $\alpha_{\mathrm{LK}} > \phi_{i'} > \alpha_{\mathrm{HK}}$), $S_{i'} = 0$ is enforced by Eqs. (2.43) and (2.44); then, $V1 = \sum_{i \in \mathbf{I}} U_{i,i'}^{D}$ and $V2 = \sum_{i \in \mathbf{I}} U_{i,i'}^{B}$ are enforced by Eqs. (2.41) and (2.42). Conversely, if the root is inactive, $S_{i'}$ can be positive, so only $V1 \geq \sum_{i \in \mathbf{I}} U_{i,i'}^{D}$ and $V2 \geq \sum_{i \in \mathbf{I}} U_{i,i'}^{B}$ are enforced.

For example, consider a system with $\mathbf{I} = \{\mathrm{A}, \mathrm{B}, \mathrm{C}, \mathrm{D}, \mathrm{E}\}$, where all components have positive flow rates (See **Figure 2.7**). If component B/D is selected as the light/heavy key ($Y_{\mathrm{B}}^{LK} = 1$ and $Y_{\mathrm{D}}^{HK} = 1$), component C is distributed ($Z_{\mathrm{C}} = 1$). Then, ϕ_{B} and ϕ_{C} are active (between α_{B} and α_{D}) while ϕ_{A} and ϕ_{D} are inactive. $S_{\mathrm{B}} = 0$ is enforced

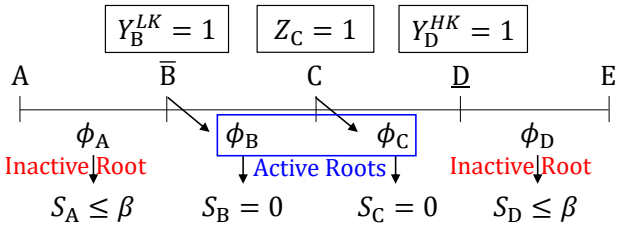

Figure 2.7: (De)activation of slack variable S_i depending on the light/heavy key selection. Component B/D is selected as the light/heavy key, so C is distributed. Thus, ϕ_{B} and ϕ_{C} are active (in blue box) while ϕ_{A} and ϕ_{D} are inactive. Accordingly, S_{B} and S_{C} are enforced to be 0 while S_{A} and S_{D} can be positive.

(i.e., ϕ_{B} is active) by Eq. (2.44) expressed for $i' = \mathrm{B}$ because $Y_{\mathrm{B}}^{LK} = 1$. Also, $S_{\mathrm{C}} = 0$ is enforced (i.e., ϕ_{C} is active) by Eq. (2.43) expressed for $i' = \mathrm{C}$ because $Z_{\mathrm{C}} = 1$. For

inactive roots, corresponding slack variables (i.e., S_{A} and S_{D}) can be positive.

We assume that LLKs/HHKs are completely recovered in the distillate/bottom stream. Thus, their component molar flow rates in the bottom/distillate stream are deactivated accordingly,

$$B_i \leq \overline{\delta}_i^B \sum_{i' \geq i} Y_{i'}^{HK} \qquad i \in \mathbf{I} \tag{2.45}$$

$$D_i \leq \overline{\delta}_i^D \sum_{i' \leq i} Y_{i'}^{LK} \qquad i \in \mathbf{I} \tag{2.46}$$

where $\overline{\delta}_i^B / \overline{\delta}_i^D$ is an upper bound on the molar flow rate of component i in the bottom/distillate stream. Product specifications such as recovery (ρ_i^R)

$$D_i \geq \rho_i^R F_i \qquad i \in \mathbf{I}^{\mathrm{P}} \tag{2.47}$$

$$B_i \geq \rho_i^R F_i \qquad i \in \mathbf{I}^{\mathrm{P}} \tag{2.48}$$

or purity (ρ_i^P)

$$D_i \geq \rho_i^P \sum_{i' \in \mathbf{I}} D_{i'} \qquad i \in \mathbf{I}^{\mathrm{P}} \tag{2.49}$$

$$B_i \geq \rho_i^P \sum_{i' \in \mathbf{I}} B_{i'} \qquad i \in \mathbf{I}^{\mathrm{P}} \tag{2.50}$$

can be specified, where $\mathbf{I}^{\mathrm{P}}$ is the set of components with product specifications. Finally, the distillation column model, referred to as **M2**, is formulated as follows:

Calculation of Underwood roots: **M1**

Distillation column modeling: Eqs. (2.30) $\sim$ (2.34), (2.37) $\sim$ (2.46) (**M2**)

Product specifications: Eqs. (2.47) $\sim$ (2.50)

2.4 Separation Energy Targeting Model

Using **M1**, a separation energy targeting model to separate an ideal zeotropic mixture can be formulated based on the FTC configuration. First, we introduce variable $\overline{D}_{i,i'}/\overline{B}_{i,i'}$ to denote the molar flow rate of component i in the distillate/bottom stream when the split between components i' and $i'+1$ is achieved. Assuming sharp splits, the following holds,

$$\overline{D}_{i,i'} = \begin{cases} F_i & \text{if } i \leq i', \\ 0 & \text{if } i > i' \end{cases} \qquad i \in \mathbf{I}, i' \in \mathbf{I}^R \tag{2.51}$$

$$\overline{B}_{i,i'} = F_i - \overline{D}_{i,i'}, \qquad i \in \mathbf{I}, i' \in \mathbf{I}^R \tag{2.52}$$

Then, we define $\overline{U}^D_{i,i'}$ and $\overline{U}^B_{i,i'}$ as follows:

$$\overline{U}^D_{i,i'} = \frac{\alpha_i \overline{D}_{i,i'}}{\alpha_i - \phi_{i'}} \qquad i \in \mathbf{I},\ i' \in \mathbf{I}^{\mathrm{R}} \tag{2.53}$$

$$\overline{U}^B_{i,i'} = -\frac{\alpha_i \overline{B}_{i,i'}}{\alpha_i - \phi_{i'}} \qquad i \in \mathbf{I},\ i' \in \mathbf{I}^{\mathrm{R}} \tag{2.54}$$

which are reformulated using the approaches followed for Eqs. (2.37)$\sim$(2.40) (See Eqs. (A.3)$\sim$(A.6)). Then, the minimum vapor flow rate for the split between components i' and $i'+1$ (i.e., $\overline{V1}_{i',i'+1}$) can be calculated as follows,

$$\overline{V1}_{i',i'+1} = \sum_{i \in \mathbf{I}} \overline{U}^D_{i,i'} \qquad i' \in \mathbf{I}^{\mathrm{R}} \tag{2.55}$$

Finally, the minimum vapor flow rate that should be condensed in the FTC configuration ($V1^{FTC}$) is the maximum among $\overline{V1}_{i',i'+1}$,

$$V1^{FTC} \geq \overline{V1}_{i',i'+1} - \overline{S}_{i'} \qquad i' \in \mathbf{I}^{\mathrm{R}} \tag{2.56}$$

$$\overline{S}_{i'} \leq \beta(2 - \sum_{i' \geq i \in \mathbf{I}} Y^L_i - \sum_{i' < i \in \mathbf{I}} Y^H_i) \qquad i' \in \mathbf{I}^{\mathrm{R}} \tag{2.57}$$

Note that the nonnegative slack variable $\overline{S}_{i'}$ can be positive when the feed keeps unchanged with the split between components i' and $i'+1$. For example, if a feed has four postulated components $\{\mathrm{A},\mathrm{B},\mathrm{C},\mathrm{D}\}$ while component D has zero flow rate (i.e., $Y_{\mathrm{D}}=0$), the feed remains the same after the split between C and D. However, its minimum vapor flow rate (i.e., $\overline{V1}_{\mathrm{C,D}}$) is calculated as positive because the feed is assumed to be recovered as the distillate stream by Eq. (2.51). In this case, $\overline{S}_{\mathrm{C}}$ can be positive

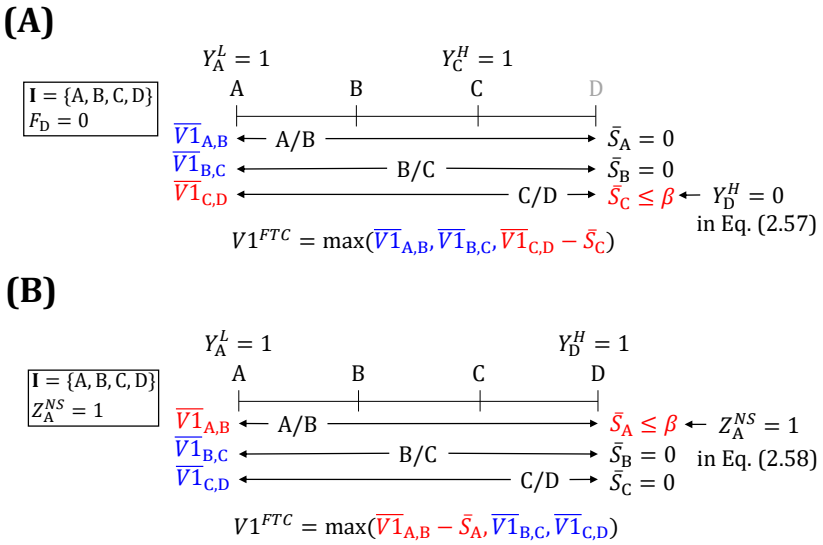

Figure 2.8: (De)activation of slack variable $\overline{S}_{i'}$; (A): The molar flow rate of component D is 0 ($Y_{\mathrm{D}}=0$). Thus, $\overline{S}_{\mathrm{C}}$ can be positive to relax the impact of $\overline{V1}_{\mathrm{C,D}}$ on $V1^{FTC}$; (B): Components A and B do not need to be separated, so $Z_{\mathrm{A}}^{NS}=1$ is set. Thus, $\overline{S}_{\mathrm{A}}$ can be positive to relax the impact of $\overline{V1}_{\mathrm{A,B}}$ on $V1^{FTC}$.

in Eq. (2.57) because $Y_{\mathrm{D}}^{H}=0$, relaxing the impact of $\overline{V1}_{\mathrm{C,D}}$ on $V1^{FTC}$ in Eq. (2.56) (See **Figure 2.8A**). Variable $V2^{FTC}$ can be calculated using Eq. (2.9) if needed.

Until now, we have considered that every pair of adjacent components is separated. This leads to the calculation of the minimum vapor flow rates when we separate the feed

into pure components. However, in some cases, we may not know whether certain pairs of adjacent components should be separated from each other or not. For example, for crude oil distillation, many adjacent components do not have to be separated from each other as long as resulting products satisfy certain property specifications. To model this, binary variable $Z_{i'}^{NS}$ is introduced, changing Eq. (2.57) as follows:

$$\overline{S}_{i'} \leq \beta(2 - \sum_{i' \geq i \in \mathbf{I}} Y_i^L - \sum_{i' < i \in \mathbf{I}} Y_i^H + Z_{i'}^{NS}) \qquad i' \in \mathbf{I}^{\mathrm{R}} \qquad (2.58)$$

If $Z_{i'}^{NS} = 1$, $\overline{S}_{i'}$ can be positive, relaxing the impact of $\overline{V1}_{i',i'+1}$ on $V1^{FTC}$. For example, in **Figure 2.8B**, a system with four postulated components ($\mathbf{I} = \{\mathrm{A}, \mathrm{B}, \mathrm{C}, \mathrm{D}\}$) with positive flow rates is shown. If we only aim to separate the feed into AB/C/D, then we can set $Z_{\mathrm{A}}^{NS} = 1$ while setting others as 0. Then, $V1^{FTC}$ will be determined as the maximum among $\overline{V1}_{\mathrm{B,C}}$ and $\overline{V1}_{\mathrm{C,D}}$ except $\overline{V1}_{\mathrm{A,B}}$ because $\overline{S}_{\mathrm{A}}$ can be positive. Furthermore, we can let optimization to determine $Z_{i'}^{NS}$ depending on desired separation.

One thing to note is that when a pair of components are not separated, these components should behave like one component. For example, when components A and B are not separated, their split fractions to any other downstream units from the separation system should be identical. To enforce this, additional equations are introduced,

$$-(1 - Z_{i'}^{NS}) \leq E_{i',u} - E_{i'+1,u} \leq (1 - Z_{i'}^{NS}) \qquad i' \in \mathbf{I}^{\mathrm{R}}, u \in \mathbf{U} \qquad (2.59)$$

$$\sum_{u \in \mathbf{U}} E_{i',u} = 1 \qquad i' \in \mathbf{I} \qquad (2.60)$$

where set $\mathbf{U}$ denotes downstream units connected to the separation system; $E_{i',u}$ denotes the split fraction of component i' to unit u. If $Z_{i'}^{NS} = 1$, then $E_{i',u} = E_{i'+1,u}$ is enforced.

The separation energy targeting model, referred to as **M3**, can be formulated as follows:

Calculation of Underwood roots: **M1**

Separation energy targeting: Eqs. (2.51) $\sim$ (2.56), (2.57) or (2.58) (**M3**)

Enforcing split fraction if Eq. (2.58) is used: Eqs. (2.59), (2.60)

2.5 Utilization For Process Synthesis

The proposed column model (**M2**) can be adopted as a sub-module for distillation network synthesis [60]. Also, the separation energy targeting model (**M3**) can be adopted to estimate the energy target for the separation without designing the network. Notably, the proposed models can be readily integrated with reactor network synthesis models, where effluents can be undetermined due to reaction selections. The integrated model for combined reactor and separation network synthesis (**MT**) can be expressed as follows (See also **Figure 2.9**):

$$
\begin{aligned}
&\min \psi(\boldsymbol{x},\ \boldsymbol{y}) \\
&\boldsymbol{f}^R(\boldsymbol{x}^R, \boldsymbol{y}^R) = 0 \\
&\boldsymbol{f}^S(\boldsymbol{x}^S, \boldsymbol{y}^S) = 0 \\
&\boldsymbol{h}(\boldsymbol{x},\ \boldsymbol{y}) = 0 \qquad\qquad (\mathbf{MT}) \\
&[\boldsymbol{x}^R, \boldsymbol{x}^S, \boldsymbol{x}^{RS,W}] = \boldsymbol{x} \in \mathbf{X} \subset \mathbb{R}^p \\
&[\boldsymbol{y}^R, \boldsymbol{y}^S, \boldsymbol{y}^{RS,W}] = \boldsymbol{y} \in \mathbf{Y} \subset \{0,1\}^q
\end{aligned}
$$

Reaction information (e.g., conversions), separation information (e.g., vapor-liquid equilibrium constants), and cost information (e.g., material costs) need to be provided. Also,

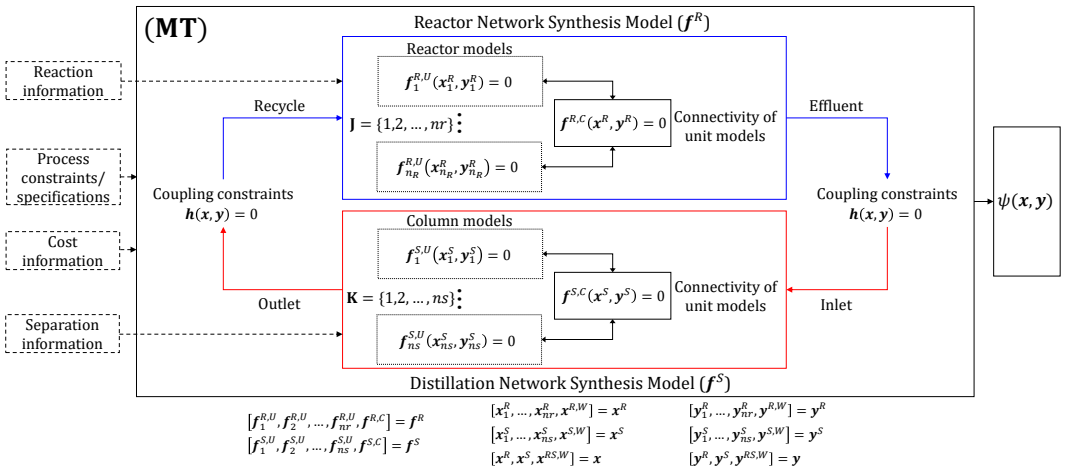

Figure 2.9: Integrated reaction-separation network synthesis model

process constraints and specifications (e.g., purity) can be enforced. The objective function ψ can be the total annualized cost or the negation of the total profit of the process. Vector $\boldsymbol{x}$ denotes continuous variables including those in reactor and distillation network synthesis models ($\boldsymbol{x}^R$ and $\boldsymbol{x}^S$, respectively); $\boldsymbol{y}$ denotes the vector of binary variables including those in reactor and distillation network synthesis models ($\boldsymbol{y}^R$ and $\boldsymbol{y}^S$); and $\boldsymbol{f}^R/\boldsymbol{f}^S$ denotes the vector of equality constraints in the reactor/distillation network synthesis model. We use an extent-based reaction model with a fixed conversion for reactor modeling, although more rigorous models (e.g., kinetics-based) can be also adopted. Only equality constraints are considered for a generic representation assuming that inequality constraints can be reformulated to equality constraints.

In **Figure 2.9**, there are two types of constraints in each network model: equations

for unit modeling (i.e., $\boldsymbol{f}_j^{R,U}$ and $\boldsymbol{f}_k^{S,U}$ for the reactor and distillation networks, respectively) and equations connecting the units (i.e., $\boldsymbol{f}^{R,C}$ and $\boldsymbol{f}^{S,C}$). The indexes j and k indicate the reactor unit and distillation column unit in the networks, respectively. The vectors of continuous and binary variables for the unit modeling of the reactor/distillation network are denoted as $\boldsymbol{x}_j^R/\boldsymbol{x}_k^S$ and $\boldsymbol{y}_j^R/\boldsymbol{y}_k^S$, respectively. For the connectivity constraints, vectors of auxiliary continuous ($\boldsymbol{x}^{R,W}/\boldsymbol{x}^{S,W}$) and binary ($\boldsymbol{y}^{R,W}/\boldsymbol{y}^{S,W}$) variables may be needed. Notably, the proposed column model (**M2**) can be used for unit modeling (i.e., $\boldsymbol{f}_k^{S,U}$), while the proposed separation energy targeting model (**M3**) can be used for the entire distillation network modeling (i.e., $\boldsymbol{f}^S$). Vector $\boldsymbol{h}$ denotes the constraints coupling the reactor and distillation network synthesis models; variables describing the effluents from the reactor network (e.g., temperatures, flow rates, etc.) are coupled with those describing the inlets into the distillation network. Also, variables describing the outlets from the distillation network can be coupled with those describing the recycle streams for the reactor network. In the coupling constraints, auxiliary continuous ($\boldsymbol{x}^{RS,W}$) and binary ($\boldsymbol{y}^{RS,W}$) variables may be needed. More information about the integrated model can be found in [81]. In the distillation network superstructure, columns can be deactivated; to model this, we need to reformulate **M2**. Binary variable Y_l^C is introduced to denote the activation of column l. Also, all variables and equations in **M2** are written for each column l. If a column is deactivated (i.e., $Y_l^C = 0$), the total molar flow rate of the feed into column l is enforced to be zero,

$$\underline{\delta}_l^T Y_l^C \leq \sum_{i \in \mathbf{I}} F_{l,i} \leq \overline{\delta}_l^T Y_l^C \qquad\qquad l \in \mathbf{L} \tag{2.61}$$

where $\underline{\delta}_l^T/\overline{\delta}_l^T$ denotes a lower/upper bound on the total molar flow rate. Eqs. (2.13) and

(2.14) are reformulated as follows,

$$\sum_{i \in \mathbf{I}} Y_{l,i}^{L} = Y_{l}^{\mathrm{C}} \qquad l \in \mathbf{L} \tag{2.62}$$

$$\sum_{i \in \mathbf{I}} Y_{l,i}^{H} = Y_{l}^{\mathrm{C}} \qquad l \in \mathbf{L} \tag{2.63}$$

and Eqs. (2.30) and (2.31) are reformulated as follows,

$$\sum_{i \in \mathbf{I}} Y_{l,i}^{LK} = Y_{l}^{\mathrm{C}} \qquad l \in \mathbf{L} \tag{2.64}$$

$$\sum_{i \in \mathbf{I}} Y_{l,i}^{HK} = Y_{l}^{\mathrm{C}} \qquad l \in \mathbf{L} \tag{2.65}$$

Finally, slack variable $S_{l,i}$ is enforced to be zero if the column is deactivated,

$$S_{l,i} \leq \beta Y_{l}^{\mathrm{C}} \qquad l \in \mathbf{L}, i \in \mathbf{I}^{\mathrm{R}} \tag{2.66}$$

When a column is deactivated, binary variables $Y_{l,i}^{L}/Y_{l,i}^{H}$ and $Y_{l,i}^{LK}/Y_{l,i}^{HK}$ are enforced to be zero, and only one distinct Underwood root in $(1, \alpha_{\mathrm{A}})$ is found due to Eq. (2.22).

2.6 Illustrative Examples

All examples are solved using solver BARON (19.12.7) [64] through GAMS (30.1.0) on a machine with AMD Ryzen 7 1700X processor 3.40 GHz and 16 GB memory. For the stopping criteria, the relative optimality gap is set to zero, and the resource limit is set to 1000 s.

2.6.1 Impact of Valid Constraints on Column Model

We study the impact of the proposed valid constraints (Eqs. (2.27) and (2.28)) on the solution time of the distillation column model (**M2**). Six problems with four

(**I**={A, B, C, D}) to nine (**I**={A, B, C, D, E, F, G, H, I}) components are solved with(out) the valid constraints (**M2**/**M2***, respectively) (See **Figure 2.10**). Feeds are assumed to be saturated liquids streams. The objective is to minimize the vapor flow rate in the top section of the column ($V1$), which is used as a surrogate variable for the cost. At least 95% of B/D should be recovered in the distillate/bottom stream, respectively.

Model/solution statistics of the resulting models are shown in **Table 2.1**. With **M2**, all the problems can be solved in less than or around 1 s; however, with **M2***, the solution times increase considerably (i.e., 1∼3 orders of magnitude); furthermore, when there are more than eight components, even a feasible solution cannot be found within the resource limit. This example shows a significant impact of the valid constraints on the computational performance of the proposed models.

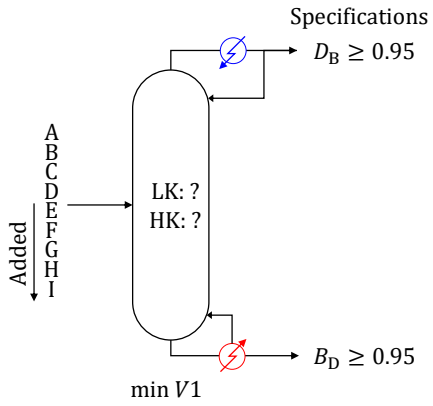

Figure 2.10: Schematic representation of problems in example 2.6.1

Table 2.1: Model/solution statistics of resulting models in example 2.6.1 with **M2*** and **M2**. Symbol † in the solution time denotes that the solver could not find a feasible solution within the resource limit (1000 s)

-	**M2***		**M2**	
Components	Eqs/vars(binary)	Times, s	Eqs/vars(binary)	Times, s
4	132/81 (24)	1.21	138/81 (24)	0.21
5	187/116 (30)	2.56	195/116 (30)	0.23
6	250/157 (36)	10.72	260/157 (36)	0.31
7	321/204 (42)	79.79	333/204 (42)	0.27
8	400/257 (48)	†	414/257 (48)	0.49
9	487/316 (54)	†	503/316 (54)	1.07

2.6.2 Application of Distillation Column Model in Distillation Network Synthesis

We consider a saturated liquid feed at 1 bar with seven components ($\mathbf{I} = \{$A: N-Hexane, B: 2,4-Dimethyl Pentane, C: N-Heptane, D: 2,2,3,3-Tetra Methyl Butane, E: N-Octane, F: N-Nonane, G: N-Decane$\}$) to produce four products which contain at least 90% of components A, C, E, and G, respectively. We consider a distillation network with three distillation columns (i.e., $\mathbf{L} = \{\text{H1}, \text{H2}, \text{H3}\}$) as shown in **Figure 2.11A**. The objective is to minimize the total vapor flow rate in the network (i.e., $\sum_{k \in \mathbf{K}} V1_k$). Note that we do not need to specify key components a priori.

The resulting model has 1243 equations and 484 variables with 126 of them being discrete variables. The optimal solution, which is obtained in 80.55 s, is shown in **Figure 2.11B**. The total vapor flow rate is 5.354. Component D/E is selected as the light/heavy key in column H1 while A/C and F/G are selected in columns H2 and H3, respectively.

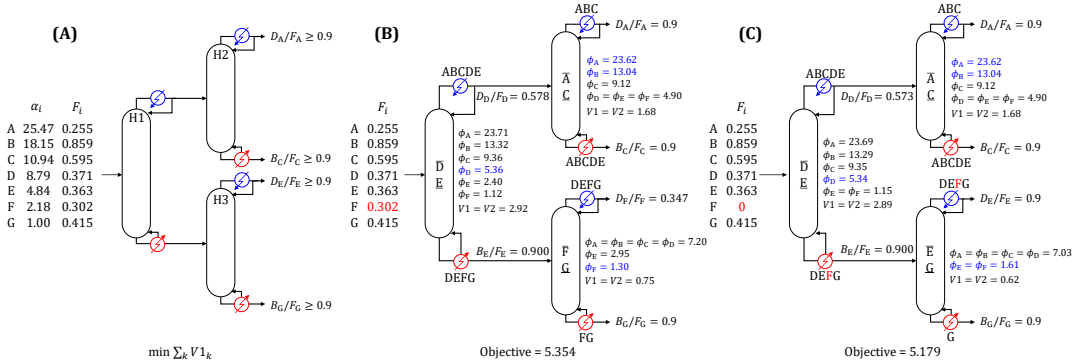

Figure 2.11: Utilization of the proposed column model as submodules for distillation network synthesis; (A): Problem setting; (B)/(C): Solution with $F_{\mathrm{F}} = 0.302/0$. Active roots are colored in blue.

Note that the recovery of the light key (i.e., D) in the distillate stream of column H1 is low ($D_{\mathrm{D}}/F_{\mathrm{D}} = 0.578$), denoting a non-sharp split. Thus, a considerable amount of component D is still present in the bottom stream of column H1, which is recovered as the distillate stream of column H3. The results from the proposed model are used for the rigorous simulation using the equilibrium mode of Radfrac module in Aspen Plus V11. Specifically, we use $V2$ and $\sum_i D_i$ obtained from the proposed model as the boilup and total distillate stream rate, respectively, in Radfrac modules with Peng-Robinson method for thermodynamic property calculation. The simulation results are in good agreement with the results from the proposed model (See **Table 2.2**).

In addition, to illustrate the capability of handling the undetermined feed, we change the molar flow rate of component F in the feed to column H1 to 0. The optimal solution, which is obtained in 18.55 s, is shown in **Figure 2.11C**. The total vapor flow rate is 5.179. Due to zero flow rate of component F, the key selection in column H1 is changed to E/G, and $\phi_{\mathrm{E}} = \phi_{\mathrm{F}}$ is enforced in all columns. The results are used for a rigorous

Table 2.2: Comparison of results between **M2** and rigorous simulation with $F_{\mathrm{F}} = 0.302$.

-	H1				H2				H3			
-	D_i		B_i		D_i		B_i		D_i		B_i	
-	**M2**	Aspen	**M2**	Aspen	**M2**	Aspen	**M2**	Aspen	**M2**	Aspen	**M2**	Aspen
A	0.255	0.255	-	0.000	0.229	0.228	0.026	0.027	-	0.000	-	0.000
B	0.859	0.859	-	0.000	0.428	0.433	0.431	0.426	-	0.000	-	0.000
C	0.595	0.595	-	0.000	0.060	0.055	0.535	0.540	-	0.000	-	0.000
D	0.214	0.227	0.157	0.144	-	0.000	0.214	0.227	0.157	0.144	-	0.000
E	0.036	0.023	0.327	0.340	-	0.000	0.036	0.023	0.327	0.298	-	0.042
F	-	0.000	0.302	0.302	-	0.000	-	0.000	0.105	0.120	0.197	0.182
G	-	0.000	0.415	0.415	-	0.000	-	0.000	0.041	0.068	0.374	0.347

simulation (See **Table 2.3**).

2.6.3 Synthesis of Reactor-Distillation Network

The synthesis of a reactor-distillation network is studied, where distillation columns in the network are modeled using **M2**. In the reactor network, there are seven alternative reactors carrying out different reactions to produce main product E; different reactions produce effluents with different components (ACE, ABCE, ADEF, ACEG, BCE, BCEF, and BCEG). Product specifications are given as at least 95% purity and 90% recovery of main product E.

We assume that product E can be separated by using at most two distillation columns; for example, if a feed with $\mathbf{I} = \{\mathrm{A}, \mathrm{C}, \mathrm{E}, \mathrm{F}\}$ is to be separated, we have two options. First, we can choose E as the light key (ACE/F) in the first distillation column and separate its distillate stream in the following column where E is selected as the heavy key (AC/E). In the second option, we can choose E as the heavy key first (AC/EF) and

Table 2.3: Comparison of results between **M2** and rigorous simulation with $F_{\mathrm{F}} = 0$.

-	H1				H2				H3			
-	D_i		B_i		D_i		B_i		D_i		B_i	
-	**M2**	Aspen	**M2**	Aspen	**M2**	Aspen	**M2**	Aspen	**M2**	Aspen	**M2**	Aspen
A	0.255	0.255	-	0.000	0.229	0.228	0.026	0.027	-	0.000	-	0.000
B	0.859	0.859	-	0.000	0.428	0.433	0.431	0.426	-	0.000	-	0.000
C	0.595	0.595	-	0.000	0.060	0.055	0.535	0.540	-	0.000	-	0.000
D	0.213	0.233	0.158	0.138	-	0.000	0.213	0.233	0.158	0.138	-	0.000
E	0.036	0.016	0.327	0.347	-	0.000	0.036	0.016	0.327	0.319	-	0.028
F	-	-	-	-	-	-	-	-	-	-	-	-
G	-	0.000	0.415	0.415	-	0.000	-	0.000	0.041	0.069	0.374	0.346

then separate the bottom stream while choosing E as the light key (E/F).

Thus, in the distillation network, three distillation columns ($\mathbf{L} = \{\mathrm{H1}, \mathrm{H2}, \mathrm{H3}\}$) are considered (See **Figure 2.12A**). In column H1, component E can be selected either as the light key or heavy key. If E is selected as the light key, then the distillate stream from column H1 can either be the main product or be sent to column H2 for further separation. If column H2 is active, component E should be selected as the heavy key in H2, and its bottom stream becomes the main product. On the other hand, if E is selected as the heavy key in H1, the bottom stream from H1 can either be the main product or be sent to column H3. In column H3, E is selected as the light key, and the main product is recovered as the distillate stream. The objective is to maximize profit which is equal to the revenue from the main product minus reactor and separation costs. The separation cost is calculated based on the summation of all vapor flow rates in the distillation network. More details can be found in the supporting information of the original work [83].

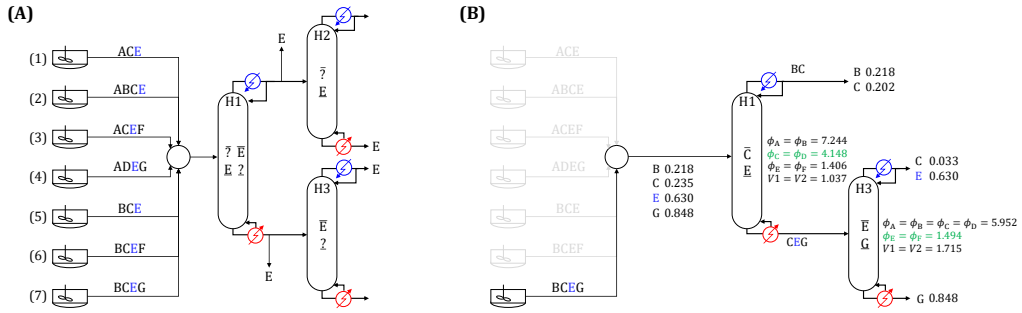

Figure 2.12: Integration of reactor network synthesis with distillation network synthesis utilizing the proposed distillation column model. In the optimal solution, reaction 7 is selected. Main product E is colored in blue, and active roots are colored in green.

The resulting model has 1241 equations and 497 variables with 136 of them being discrete variables. The optimal solution, which is obtained in 15.6 s, is shown in **Figure 2.12B**. The optimal profit is $\$2.44\times10^6$/yr. In the optimal solution, reaction (7) (producing components B, C, E, and G) is selected. Also, columns H1 and H3 are selected, where components C/E and E/G are selected as the light/heavy key, respectively. Note that component C is not perfectly recovered in the distillate stream in column H1, which, in turn, results in the increase of the total molar flow rate of the main product (i.e., the distillate stream of column H3) while satisfying the purity specification.

2.6.4 Optimal Reaction System Selection with Separation Energy Targeting

We consider effluents from high-throughput experiments where 30 reaction systems are studied. We seek to identify an optimal system (i.e., leading to the highest profit) while considering the separation cost for the effluent. Depending on the reaction selection,

components that are present in the effluent vary (See **Figure 2.13A**), leading to 15 postulated components (i.e., A to O). Rather than designing the separation network, we aim to calculate the energy requirement target to separate the effluent into pure components, so the proposed separation energy targeting model (**M3**) is utilized.

The resulting model has 1480 equations and 979 variables with 75 of them being discrete variables. The optimal solution, which is obtained in 69.25 s, is shown in **Figure 2.13B**. The optimal reaction is reaction 13, so the feed contains components A, B, C, D, E, F, I, K, L, M, and N. The split between components M and N (denoted as M/N) determines the energy target of the distillation network ($\overline{V1}_{\mathrm{M,N}} = 6.03$) while minimum vapor flow rates for other splits can be calculated from the optimal solution as shown in **Figure 2.13B**. The optimal profit is $\$17.84 \times 10^6$/yr while revenue is $\$51.20 \times 10^6$/yr, reaction system cost is $\$8.25 \times 10^6$/yr, and separation cost is $\$25.11 \times 10^6$/yr.

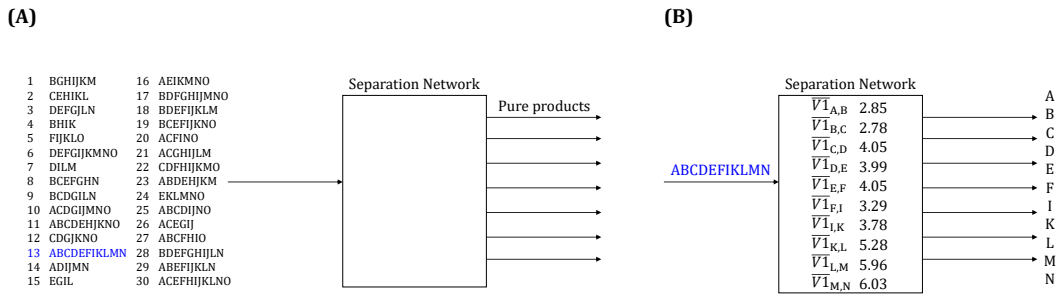

Figure 2.13: Separation energy targeting for optimal reaction selection; (A): Problem description; (B): Optimal solution. Reaction 13 is selected as the optimal reaction. The split between components M and N (M/N) determines the energy target of the separation.

2.6.5 Integrated Process Synthesis with Separation Energy Targeting

We seek to synthesize a multiple stage process using 13000 ton/yr of itaconic acid, adopted and modified from [62]. Four stages of reaction-separator networks (See **Figure 2.14A**) are considered based on the reaction network in [62]; in the first stage, itaconic acid (H), can be converted to 2-methylsuccinic acid (D), 3-methyl-dihydrofuran-2(3H)-one (C), or 3-methlyenedihydrofuran-2,5-dione (F) through RXN1, RXN2, or RXN3, respectively. Then, the outlet from the mixer is separated in the separator block (i.e., S1), which is modelled by **M3**. Components D and F are sent to the second stage or can be sold to the market; component H is recycled back to the reactor, while component C can be sold to the market or sent to the third stage. Then, in the second stage, component D can be converted to 4-hydroxy-3-methylbutanoic acid (G), C, or 3-methyldihydrofuran-2,5-dione (E) through RXN4, RXN5, or RXN6, respectively; also, component F can be converted to E through RXN 7. From the separation block (i.e., S2), components C and G can be sent to the third stage or be sold to the market while component E can only be sold to the market. Components D and F are recycled to the second stage. In the third stage, components G and C can be converted to B through RXN 8 and RXN9, respectively. From S3, components G and C are recycled to the third stage while component B can be sent to the fourth stage or sold to the market. In the fourth stage, component B is converted to 3-methyltetrahydrofuran (A) through RXN10. From S4, component B is recycled to the fourth stage, while component A is sold to the market. In each stage, only one reaction can be selected, while an entire stage can be deactivated. We assume that all reactions have fixed conversions (i.e., $\xi_j = 0.9$),

following [62].

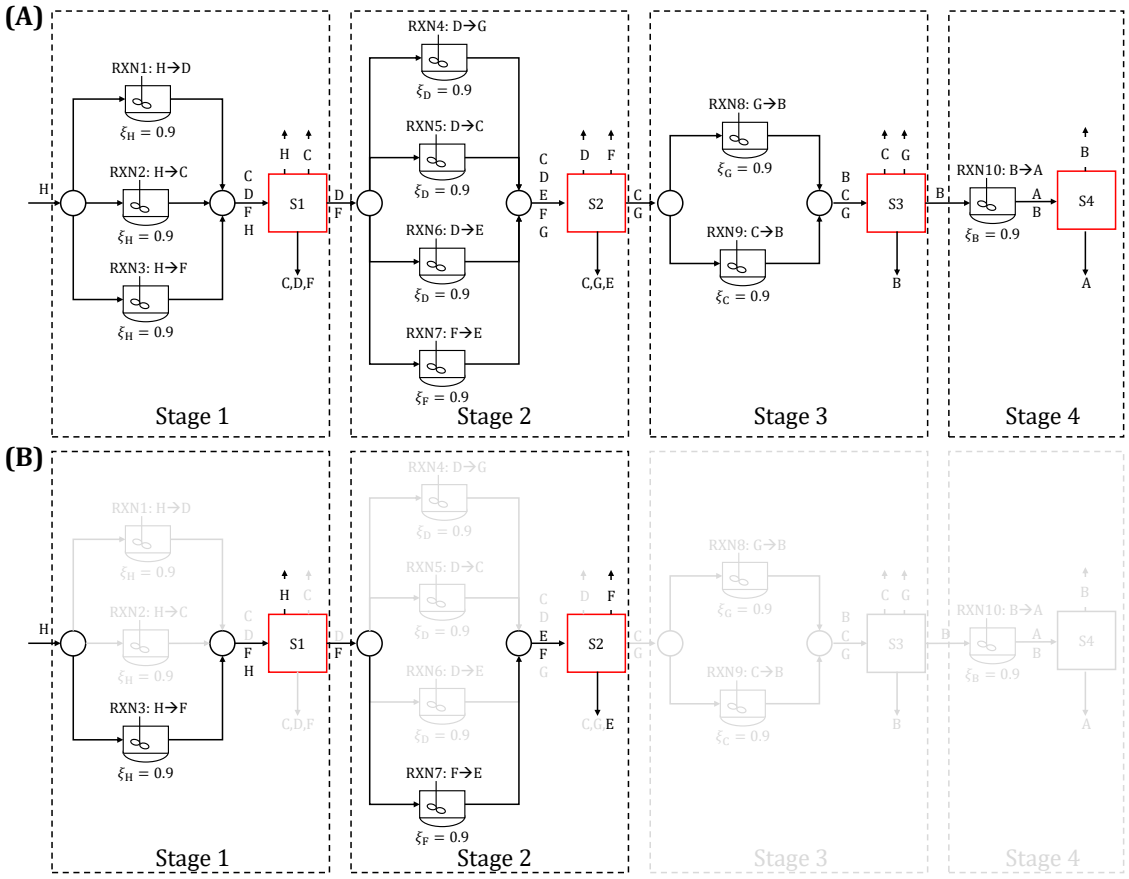

Figure 2.14: Integrated process synthesis with the proposed separation energy targeting model (**M3**), which can calculate the energy requirement target for the separation without designing the network; (A): Superstructure; (B): Optimal solution.

Notably, feeds into separation blocks can contain different components depending on decisions in upstream processes. For example, if RXN1 is selected, the feed into S1 contains only D and H while it contains F and H if RXN3 is selected. The objective is to maximize profit which is equal to the revenue from products (i.e., A, B, C, D, E, F, G) minus raw material cost, and separation cost.

The resulting model has 611 equations and 392 variables with 56 of them being discrete variables. The optimal solution, which is obtained in 2.23 s, is shown in **Figure 2.14B**. The optimal profit is $\$5.8 \times 10^6$/yr while revenue is $\$28.4 \times 10^6$/yr, raw material cost is $\$20.8 \times 10^6$/yr, and separation cost is $\$1.810^6$/yr. In the optimal solution, only the first and second stages are active, and RXN3 and RXN7 are selected, which are consistent with results from [62], although the separation cost is modelled in a different way. For the first distillation network (S1), $V1^{FTC}$ is calculated as 1.101, which is based on the split between components F and H. For the second distillation network (S2), $V1^{FTC}$ is calculated as 2.508, which is based on the split between components E and F.

2.6.6 Bio-refinery Optimization for Bioethanol Upgrading

Large-scale deployment of biofuels has the potential to mitigate the negative impacts of fossil fuel consumption. However, the most commonly available biofuels, i.e., ethanol and biodiesel, have maximum blending ratios with fossil-based fuels due to their properties. To achieve a higher market penetration of biofuels, upgrading ethanol into advanced biofuels is a promising way in three ways: first, existing infrastructure for ethanol manufacturing can be utilized; second, fuels in the whole distillation spectrum can be produced with ethanol upgrading; third, advancements in ethanol chemistry can be exploited to produce fuels with tailored properties. Although ethanol upgrading is promising, finding good strategies is not easy and requires system-level thinking. One of the reasons is that there are numerous candidate reactions and their combinations, whose evaluations are non-trivial. For example, there are more than twenty chemistries to upgrade ethanol, and they can be used in multiple serial and parallel arrangements. Furthermore,

each chemistry can be achieved by several different catalysts. Additionally, properties of product fuels need to be simultaneously considered. Due to these difficulties, researchers have mainly relied on their own understanding of chemistry, fuel properties, and process synthesis to design new upgrading strategies. However, this ad-hoc approach may miss novel opportunities and limit the system-level understanding. Therefore, a systematic framework to represent the ethanol upgrading problem is needed to systematically identify relevant trade-offs and novel upgrading strategies.

An effective framework should enable the simultaneous assessment of capital and operating costs. Accurate estimations of these costs for each option require extensive efforts, including extensive simulations and Techno-Economic Analysis (TEA). However, with thousands of alternatives, it is not possible to attain this level of detail; hence, it is necessary to find strategies to estimate these costs more efficiently. Accordingly, Lange correlation can be utilized to estimate the capital cost of a process based on the total amount of heat exchanged within the process,

$$C = \mu(Q^E)^{0.55} \tag{2.67}$$

where C denotes the capital cost; μ denotes the cost coefficient; Q^E denotes the amount of heat exchanged. To estimate the heat exchanged within separation systems, we use the separation energy targeting model (**M3**). Being combined with targeting-type models for the reactor system, we can survey a large number of alternatives without extensive simulation efforts to design the separation system for each candidate process.

Superstructure

We generate a superstructure embedding the state-of-the-art technologies for ethanol upgrading, including 22 different chemistries and 112 catalysts, upgrading ethanol to gasoline, jet fuel, and diesel (See **Figure 2.15**). The associated optimization model will be included in the future publication. Notably, the separation system should handle an undetermined feed because the components in the feed can vary depending on the selected catalyst.

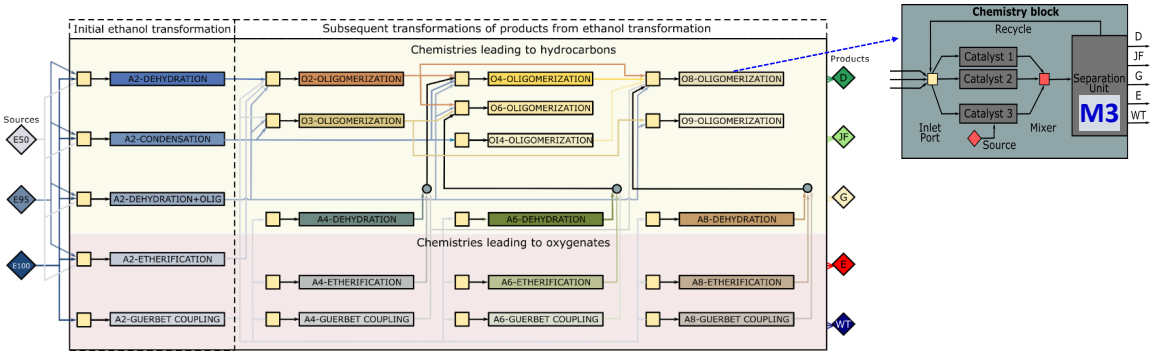

Figure 2.15: Superstructure of ethanol upgrading process. Three types of ethanol (i.e., 50%, 95%, and 100% weight percent ethanol) are considered. Each block is named after its primary reactant (A: Alcohols, O: Olefins; number denotes the number of carbons).

Results

By using the proposed framework, promising routes to produce gasoline, jet fuel, and diesel from ethanol can be identified (**Figure 2.16A**). Also, the minimum selling prices, fuel yields, and energy yields (**Figure 2.16B** and **2.16C**) can be assessed depending on the complexity of the biorefinery (i.e., the number of selected chemistries), which provides the system-level analysis of ethanol upgrading strategies.

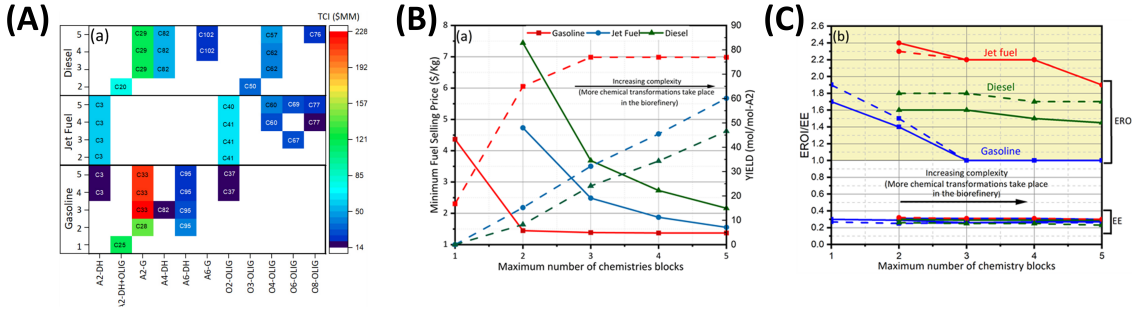

Figure 2.16: Results from optimal solutions; (A): Optimal chemistries and catalysts selected; (B): Minimum Fuel Selling Price (MFSP) and fuel yield; (C): Energy yield

Chapter 3

Generalized Distillation Network Synthesis[6]

3.1 Motivation

Although distillation network synthesis problem has been studied for several decades, most existing models are built upon several assumptions: 1) there is a single mixture to be separated (referred to as a *source* in this work); 2) components to be separated are known a priori; and 3) outgoing streams from the distillation network, referred to as *outlets*, are assumed to be almost pure components. However, if reactor network synthesis is considered with distillation network synthesis simultaneously, the number of sources and the components present in the sources can vary depending on decisions (e.g., reaction selection) in the network. Also, outlets can include products with multiple components as well as recycle streams, whose compositions are also decisions to be made in the synthesis problem. We refer to distillation network synthesis problems where aforementioned assumptions are relaxed as *generalized problems*.

Accordingly, we propose a superstructure-based distillation network synthesis model

[6]The contents of this chapter appear in Ryu and Maravelias, *Chem. Eng. Sci.* **2021**

to address generalized problems, thereby widening the scope of superstructure-based distillation network synthesis. The proposed model is applicable to systems with near-ideal mixtures as sources. It can handle multiple sources when components that are present in the sources can vary, while considering interactions between separation steps. Also, bypass streams are considered to avoid unnecessary separations with full consideration of thermal coupling, resulting in novel solutions. Due to its capabilities, the proposed model can be readily integrated with superstructure-based reactor network synthesis to formulate and solve an integrated synthesis problem for an entire process [81], realizing full benefit of the superstructure-based process synthesis approach.

3.2 Superstructure

We present the concepts and methods for the generation of the distillation network superstructure.

3.2.1 Superstructure Generation

We propose an extended version of the matrix method [89] combined with a network-based representation (i.e., we use the concepts of nodes and arcs). First, we define the set $\mathbf{N}$ to denote all nodes in the superstructure. We define source nodes $\mathbf{N}^{\mathrm{SO}}$ (yellow circle in **Figure 3.1**) which correspond to sources. Also, we define sink nodes $\mathbf{N}^{\mathrm{SI}}$ (blue circle in **Figure 3.1**), where each sink node has an outgoing stream denoting the outlet of the distillation network. Outlets include products as well as recycle streams. Then, we define the ordered set $\mathbf{I} = \{\mathrm{A}, \mathrm{B}, \mathrm{C}, ...\}$ ($|\mathbf{I}| = n$) to denote postulated components in sources in decreasing order of volatilities. We use index i to denote elements or orders

of elements (e.g., 1 or 2) in the set.

We introduce a matrix with n rows and n columns, where the set $\mathbf{J}/\mathbf{K}$ denotes its rows/columns. Elements in the upper triangular part $\{(j,k)|j \leq k\}$ of the matrix are referred to as *distillation nodes*, denoted as $\mathbf{N}^{\mathrm{D}}$. In **Figure 3.1**, a distillation network superstructure with four postulated components in the source ($\mathbf{I} = \{\mathrm{A}, \mathrm{B}, \mathrm{C}, \mathrm{D}\}$) is shown. We refer to distillation node (j,k) as an *upstream node* with respect to node (j',k') if $k < k'$ while as a *downstream node* if $k > k'$.

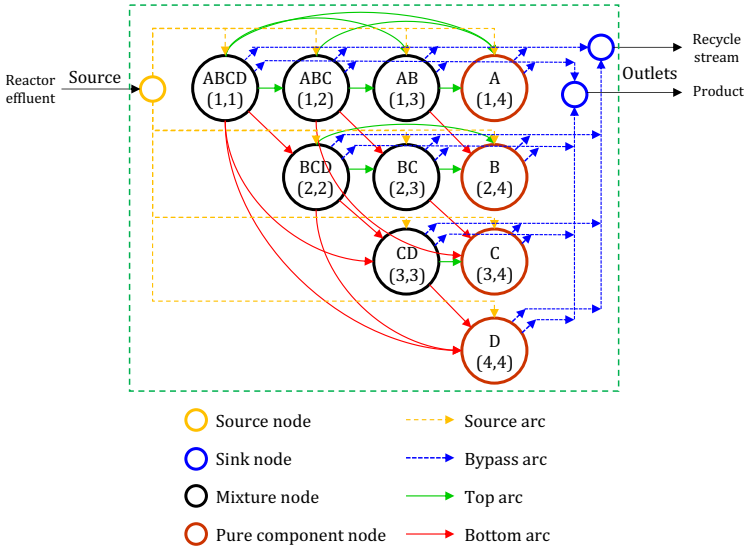

Figure 3.1: Distillation network superstructure to separate one source with postulated components $\{\mathrm{A}, \mathrm{B}, \mathrm{C}, \mathrm{D}\}$. Two sink nodes (blue circles) are shown for simplicity.

For each distillation node, the set of postulated components, $\mathbf{I}^{\mathrm{C}}_{jk}$, is defined as follows,

$$\mathbf{I}^{\mathrm{C}}_{jk} = \{i \in \mathbf{I} | j \leq i \leq n-k+j\} \qquad (j,k) \in \mathbf{N}^{\mathrm{D}} \tag{3.1}$$

where only these postulated components are considered to define potential separation tasks in each node; notably, postulated components can be different from components

that are present. We denote the lightest and heaviest postulated components as $i^L_{jk} = j$ and $i^H_{jk} = n - k + j$, respectively, and enforce them to be present in the sum of all inlets to node (j, k) while other postulated components may not be present. For example, in **Figure 3.1**, node (1,2) has $\mathbf{I}^{\mathrm{C}}_{12} = \{\mathrm{A}, \mathrm{B}, \mathrm{C}\}$ with $i^L_{12} = \mathrm{A}$ and $i^H_{12} = \mathrm{C}$. Thus, components A and C are enforced to be present in the sum of all inlets into node (1,2) while B is not necessary. Accordingly, splits AB/C, A/BC, AB/BC (i.e., split between A and C while B is distributed), and A/C (i.e., split between A and C without B) are considered as potential separation tasks. Notably, split A/C is considered due to undetermined sources, whereas it is ignored in the matrix method [89] which is based on the assumption that components ABC are always present. Note that component D, which is not included in $\mathbf{I}^{\mathrm{C}}_{12}$, can be present in inlets into node (1,2), but it is ignored when potential separation tasks are determined.

3.2.2 Distillation Nodes

There are two types of distillation nodes:

- Mixture node (black circle in **Figure 3.1**), $(j, k) \in \mathbf{N}^{\mathrm{DM}} = \{(j, k) \in \mathbf{N}^{\mathrm{D}} | k < n\}$, which consists of a mixer, a splitter, and a column (See **Figure 3.2A**).
- Pure component node (red circle in **Figure 3.1**), $(j, k) \in \mathbf{N}^{\mathrm{DP}} = \{(j, k) \in \mathbf{N}^{\mathrm{D}} | k = n\}$, which consists of only a mixer and a splitter (See **Figure 3.2B**).

The mixer in a distillation node has three origins of inlets: 1) top section, 2) bottom section of columns in upstream nodes, and 3) source nodes (See **Figure 3.2**). Then, the outlet from the mixer splits in the splitter, where a part of the outlet can be sent to sink nodes directly, termed as *bypass streams*. The consideration of the bypass stream

enables to avoid unnecessary separation, leading to novel solutions that cannot be found by previously proposed methods. In a pure component node, all streams are sent to sink nodes (See **Figure 3.2B**). In a mixture node, the rest of the stream is sent to the column (See **Figure 3.2A**), which has the top/bottom section where the distillate/bottom stream is recovered with the condenser/reboiler. Note that what we term columns in our representation can be stacked to form a single column; therefore, they are equivalent to pseudo-columns in the matrix method.

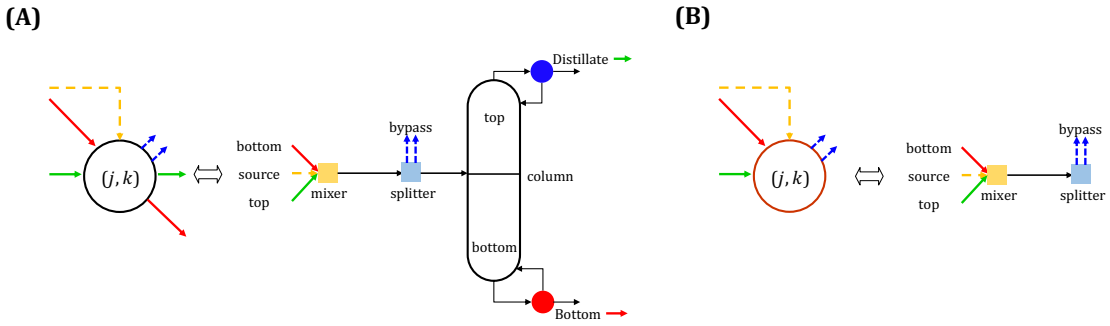

Figure 3.2: (A) Mixture node. (B) Pure component node.

3.2.3 Arcs

We define the set **A** to denote all arcs, which represent connections between nodes. Four types of arcs are defined (See **Figure 3.1**):

- Source arc (yellow dashed line), $\mathbf{A}^{\mathrm{S}}$, from a source node to a distillation node.
- Top arc (green solid line), $\mathbf{A}^{\mathrm{T}}$, from an upstream node to a downstream node, representing flow from the top section of the upstream column:

$$\mathbf{A}^{\mathrm{T}} = \{(j,k,j',k') | j' = j, k' > k, (j,k) \in \mathbf{N}^{\mathrm{DM}}, (j',k') \in \mathbf{N}^{\mathrm{D}}\} \tag{3.2}$$

- Bottom arc (red solid line), $\mathbf{A}^{\mathrm{B}}$, from an upstream node to a downstream node, representing flow from the bottom section of the upstream column:

$$\mathbf{A}^{\mathrm{B}} = \{(j,k,j',k') | k'-j' = k-j, k' > k, (j,k) \in \mathbf{N}^{\mathrm{DM}}, (j',k') \in \mathbf{N}^{\mathrm{D}}\} \tag{3.3}$$

- Bypass arc (blue dashed line), $\mathbf{A}^{\mathrm{P}}$, from a distillation node to a sink node.

In the matrix perspective, top arcs ($\mathbf{A}^{\mathrm{T}}$) represent the connections between two distillation nodes on the same row ($j = j'$), while bottom arcs ($\mathbf{A}^{\mathrm{B}}$) represent the connections between two distillation nodes on the same diagonal ($k' - j' = k - j$). Also, we refer to top arcs from node (j,k) as $\mathbf{A}^{\mathrm{TS}}_{jk}$, while top arcs toward node (j,k) as $\mathbf{A}^{\mathrm{TE}}_{jk}$. Bottom arcs from node (j,k) are denoted as $\mathbf{A}^{\mathrm{BS}}_{jk}$ while those toward node (j,k) as $\mathbf{A}^{\mathrm{BE}}_{jk}$.

3.2.4 Logic Rules and Connectivity

Here, it is assumed that there is only one source node to facilitate the presentation of the model, which will be relaxed later. We assume that the source and outlets are saturated liquid. We introduce $Y^0_{jk} \in \{0,1\}$ to denote the activation of the source arc to node (j,k) and enforce that only one source arc is active.

$$\sum_{(j,k)\in\mathbf{N}^{\mathrm{D}}} Y^0_{jk} = 1 \tag{3.4}$$

Also, we introduce $X_{jk} \in \{0,1\}$ to denote the activation of node (j,k). When $Y^0_{jk} = 1$, the corresponding distillation node should be also active,

$$Y^0_{jk} \leq X_{jk} \qquad\qquad (j,k) \in \mathbf{N}^{\mathrm{D}} \tag{3.5}$$

The activation of a top/bottom arc is denoted by $Y^T_{jkj'k'}/Y^B_{jkj'k'} \in \{0,1\}$, where $Y^T_{jkj'k'} = 1/Y^{\mathrm{B}}_{jkj'k'} = 1$ denotes that the top/bottom arc from node (j,k) to (j',k') is active. If

$X_{jk} = 1$, at least one arc toward node (j,k) should be active,

$$X_{jk} \leq Y^0_{jk} + \sum_{(j'k'jk)\in \mathbf{A}^{\mathrm{TE}}_{jk}} Y^T_{j'k'jk} + \sum_{(j'k'jk)\in \mathbf{A}^{\mathrm{BE}}_{jk}} Y^B_{j'k'jk} \qquad (j,k) \in \mathbf{N}^{\mathrm{D}} \tag{3.6}$$

which can be the source arc or top/bottom arcs. We enforce that no more than one top arc and one bottom arc toward the same node can be active at the same time,

$$\zeta_{jk} X_{jk} \geq \sum_{(j'k'jk)\in \mathbf{A}^{\mathrm{TE}}_{jk}} Y^T_{j'k'jk} + \sum_{(j'k'jk)\in \mathbf{A}^{\mathrm{BE}}_{jk}} Y^B_{j'k'jk} \qquad (j,k) \in \mathbf{N}^{\mathrm{D}} \tag{3.7}$$

based on the results from previous works [14, 72]. Eq. (3.7) cuts off some feasible solutions that are unlikely to be optimal. For distillation nodes that are located on the first row or the principal diagonal of the matrix (i.e., $\{(j,k) \in \mathbf{N}^{\mathrm{D}} | j = k \text{ or } j = 1\}$), only one arc can be active (i.e., $\zeta_{jk} = 1$); otherwise, $\zeta_{jk} = 2$.

We introduce $X^C_{jk} \in \{0,1\}$ to denote the activation of the column in a mixture node. If and only if column (j,k) is active, one top and one bottom arcs from (j,k) are active,

$$X^C_{jk} = \sum_{(j,k,j',k')\in \mathbf{A}^{\mathrm{TS}}_{jk}} Y^T_{jkj'k'} \qquad (j,k) \in \mathbf{N}^{\mathrm{DM}} \tag{3.8}$$

$$X^C_{jk} = \sum_{(j,k,j',k')\in \mathbf{A}^{\mathrm{BS}}_{jk}} Y^B_{jkj'k'} \qquad (j,k) \in \mathbf{N}^{\mathrm{DM}} \tag{3.9}$$

If a mixture node is active, at least one of the followings should hold: 1) the column inside is active or 2) at least one bypass arc from the node is active,

$$X_{jk} \leq X^C_{jk} + \sum_{s\in \mathbf{N}^{\mathrm{SI}}} Y^P_{jks} \qquad (j,k) \in \mathbf{N}^{\mathrm{DM}} \tag{3.10}$$

where $Y^P_{jks} \in \{0,1\}$ denotes the activation of the bypass arc from node (j,k) to sink node s. If node (j,k) is not active, then all arcs from the node (i.e., top/bottom arcs

and bypass arcs) cannot be active.

$$\sum_{(jkj'k')\in\mathbf{A}_{jk}^{\mathrm{TS}}} Y_{jkj'k'}^{T} + \sum_{(jkj'k')\in\mathbf{A}_{jk}^{\mathrm{BS}}} Y_{jkj'k'}^{B} \leq 2X_{jk} \qquad (j,k)\in\mathbf{N}^{\mathrm{DM}} \tag{3.11}$$

$$Y_{jks}^{P} \leq X_{jk} \qquad (j,k)\in\mathbf{N}^{\mathrm{D}}, s\in\mathbf{N}^{\mathrm{SI}} \tag{3.12}$$

3.3 Model Formulation

We present the formulation of the proposed model for distillation network synthesis based on the superstructure generated in section 3.2.

3.3.1 Distillation Network Sources

The component molar flow rate of the source (F_i^0) is disaggregated into $\widetilde{F}_{ijk}^0$,

$$F_i^0 = \sum_{(j,k)\in\mathbf{N}^{\mathrm{D}}} \widetilde{F}_{ijk}^0 \qquad i\in\mathbf{I} \tag{3.13}$$

$$\widetilde{F}_{ijk}^0 \leq \overline{\delta}_i^0 Y_{jk}^0 \qquad i\in\mathbf{I}, (j,k)\in\mathbf{N}^{\mathrm{D}} \tag{3.14}$$

where $\widetilde{F}_{ijk}^0 = F_i^0$ if $Y_{jk}^0 = 1$; otherwise $\widetilde{F}_{ijk}^0 = 0$. Parameter $\overline{\delta}_i^0$ denotes an upper bound on the molar flow rate of component i. Also, we introduce $Y_i \in \{0,1\}$ to denote whether the molar flow rate of component i in the source is greater than threshold value $\underline{\delta}_i^0$,

$$\underline{\delta}_i^0 Y_i \leq F_i^0 \leq \overline{\delta}_i^0 Y_i + \underline{\delta}_i^0 (1 - Y_i) \qquad i\in\mathbf{I} \tag{3.15}$$

If the molar flow rate of component i is greater than $\underline{\delta}_i^0$ (i.e, $Y_i = 1$), the component is considered to be *present*; if it is less than $\underline{\delta}_i^0$ (i.e., $Y_i = 0$), the component is considered to be not present, that is, it is not considered for task selection though material balances

for it are enforced. If needed, the presence of a component can be determined based on its molar fraction in the source,

$$-\overline{\delta}^{T}\gamma_i(1-Y_i) \le F_i^0 - \gamma_i \sum_{i\in\mathbf{I}} F_i^0 \le \overline{\delta}_i^0 Y_i \qquad i \in \mathbf{I} \tag{3.15a}$$

where $\overline{\delta}^{T}$ is an upper bound on the total molar flow rate of the source. If the molar fraction of component i is less than γ_i (i.e., $F_i^0 - \gamma_i \sum_{i\in\mathbf{I}} F_i^0 \le 0$), the component is considered to be not present. (i.e., $Y_i = 0$). Note that $\underline{\delta}_i^0$ and γ_i can be adjusted depending on the desired accuracy; if a component with a smaller molar flow rate or molar fraction should be considered, then $\underline{\delta}_i^0$ or γ_i can be adjusted to a smaller value. If component i' is not present, nodes with either $i_{jk}^L = i'$ or $i_{jk}^H = i'$ cannot be active

$$X_{jk} \le Y_i \qquad (j,k) \in \mathbf{N}^{\mathrm{D}}, i \in \{i_{jk}^L, i_{jk}^H\} \tag{3.16}$$

because the lightest/heaviest postulated components should be present (see section 3.2.1). For example, in **Figure 3.3**, a system with postulated components $\mathbf{I} = \{\mathrm{A}, \mathrm{B}, \mathrm{C}, \mathrm{D}\}$ is shown, where only A, B, and D are present in the source. Accordingly, nodes with $\mathbf{I}_{jk}^{\mathrm{C}} \in \{\{\mathrm{A}, \mathrm{B}, \mathrm{C}\}, \{\mathrm{B}, \mathrm{C}\}, \{\mathrm{C}, \mathrm{D}\}, \{\mathrm{C}\}\}$ cannot be active (See **Figure 3.3A**) due to Eq. (3.16) because component C is required for these nodes to be active. Also, only one top arc and one bottom arc originating from node (2,2) (i.e., (2,2,2,4) and (2,2,4,4)) can be active ($\mathbf{I}_{22}^{\mathrm{C}} = \{\mathrm{B}, \mathrm{C}, \mathrm{D}\}$). Two feasible distillation networks are shown in **Figure 3.3B** and **Figure 3.3C**.

3.3.2 Material Balances

We present material balances 1) inside each distillation node and 2) between distillation nodes.

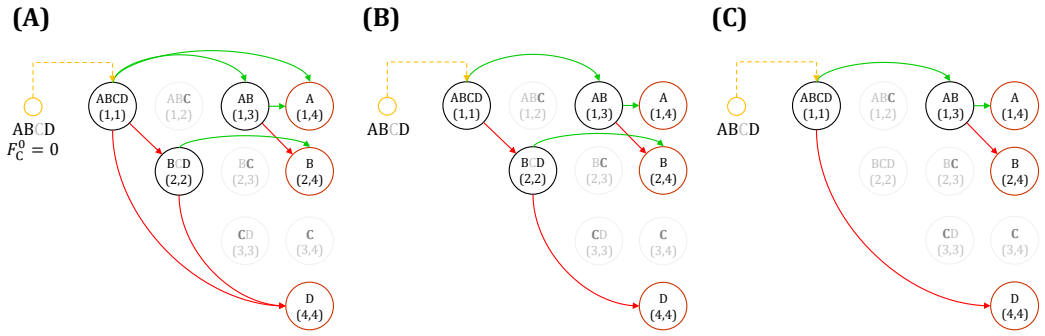

Figure 3.3: (A) Distillation network superstructure for the separation of the source with $\mathbf{I} = \{\mathrm{A}, \mathrm{B}, \mathrm{C}, \mathrm{D}\}$ and $F_{\mathrm{C}}^0 = 0$; nodes that cannot be active due to Eq. (3.16) are in gray with C in bold; (B, C) feasible distillation networks.

Distillation Nodes

The molar flow rate of component i in the sum of all inlets to node (j,k) is denoted as F_{ijk}. If node (j,k) is active, the lightest and heaviest postulated components (i.e., i_{jk}^L and i_{jk}^H) are enforced to be present in the inlets,

$$F_{ijk} \geq \delta_i^F X_{jk} \qquad i \in \{i_{jk}^L, i_{jk}^H\}, (j,k) \in \mathbf{N}^{\mathrm{D}} \tag{3.17}$$

In a mixture node, the sum of all inlets splits into the bypass stream (F_{ijks}^{P}) and the column feed stream (F_{ijk}^{C}),

$$F_{ijk} = \sum_{s \in \mathbf{N}^{\mathrm{SI}}} F_{ijks}^P + F_{ijk}^{\mathrm{C}} \qquad (j,k) \in \mathbf{N}^{\mathrm{DM}} \qquad i \in \mathbf{I} \tag{3.18}$$

while the sum of all inlets becomes the bypass stream in a pure component node:

$$F_{ijk} = \sum_{s \in \mathbf{N}^{\mathrm{SI}}} F_{ijks}^P \qquad (j,k) \in \mathbf{N}^{\mathrm{DP}} \qquad i \in \mathbf{I} \tag{3.19}$$

Bypass streams (F^{P}_{ijks}) are constrained as follows,

$$F^{P}_{ijks} = E_{jks} F_{ijk} \qquad i \in \mathbf{I}, (j,k) \in \mathbf{N}^{\mathrm{D}}, s \in \mathbf{N}^{\mathrm{SI}} \tag{3.20}$$

$$E_{jks} \leq Y^{P}_{jks} \qquad (j,k) \in \mathbf{N}^{\mathrm{D}}, s \in \mathbf{N}^{\mathrm{SI}} \tag{3.21}$$

where E_{jks} denotes the split fraction of the bypass stream to sink node s; if the bypass arc from node (j,k) to sink node s is not active ($Y^{P}_{jks} = 0$), then $E_{jks} = 0$. The material balance around a column is as follows,

$$F^{C}_{ijk} = D_{ijk} + B_{ijk} \qquad i \in \mathbf{I}, (j,k) \in \mathbf{N}^{\mathrm{DM}} \tag{3.22}$$

where D_{ijk} and B_{ijk} denote the molar flow rates of the distillate and bottom streams, respectively. The distillate and bottom streams are coupled with internal liquid/vapor streams (See **Figure 3.4A**),

$$\sum_{i \in \mathbf{I}} D_{ijk} = V1_{jk} - L1_{jk} \qquad (j,k) \in \mathbf{N}^{\mathrm{DM}} \tag{3.23}$$

$$\sum_{i \in \mathbf{I}} B_{ijk} = L2_{jk} - V2_{jk} \qquad (j,k) \in \mathbf{N}^{\mathrm{DM}} \tag{3.24}$$

where $V1_{jk}/V2_{jk}$ denotes the vapor molar flow rate in the top/bottom section and $L1_{jk}/L2_{jk}$ denotes the liquid molar flow rate in the top/bottom section.

Between Distillation Nodes

We introduce $\widetilde{D}_{ijkj'k'}/\widetilde{B}_{ijkj'k'}$ to denote the molar flow rate of component i from the top/bottom section of column (j,k) to node (j',k'). Variables $\widetilde{D}_{ijkj'k'}$ and $\widetilde{B}_{ijkj'k'}$ are

constrained as follows,

$$D_{ijk} - \delta^D_{ijk}(1 - Y^T_{jkj'k'}) \leq \widetilde{D}_{ijkj'k'} \leq D_{ijk} \qquad i \in \mathbf{I}, (j,k,j',k') \in \mathbf{A}^{\mathrm{T}} \tag{3.25}$$

$$\widetilde{D}_{ijkj'k} \leq \delta^D_{ijk} Y^T_{jkj'k'} \qquad i \in \mathbf{I}, (j,k,j',k') \in \mathbf{A}^{\mathrm{T}} \tag{3.26}$$

$$B_{ijk} - \delta^B_{ijk}(1 - Y^B_{jkj'k'}) \leq \widetilde{B}_{ijkj'k'} \leq B_{ijk} \qquad i \in \mathbf{I}, (j,k,j',k') \in \mathbf{A}^{\mathrm{B}} \tag{3.27}$$

$$\widetilde{B}_{ijkj'k} \leq \delta^B_{ijk} Y^B_{jkj'k'} \qquad i \in \mathbf{I}, (j,k,j',k') \in \mathbf{A}^{\mathrm{B}} \tag{3.28}$$

where $\delta^D_{ijk}/\delta^B_{ijk}$ is an upper bound on D_{ijk}/B_{ijk}. If the top arc from node (j,k) to (j',k')

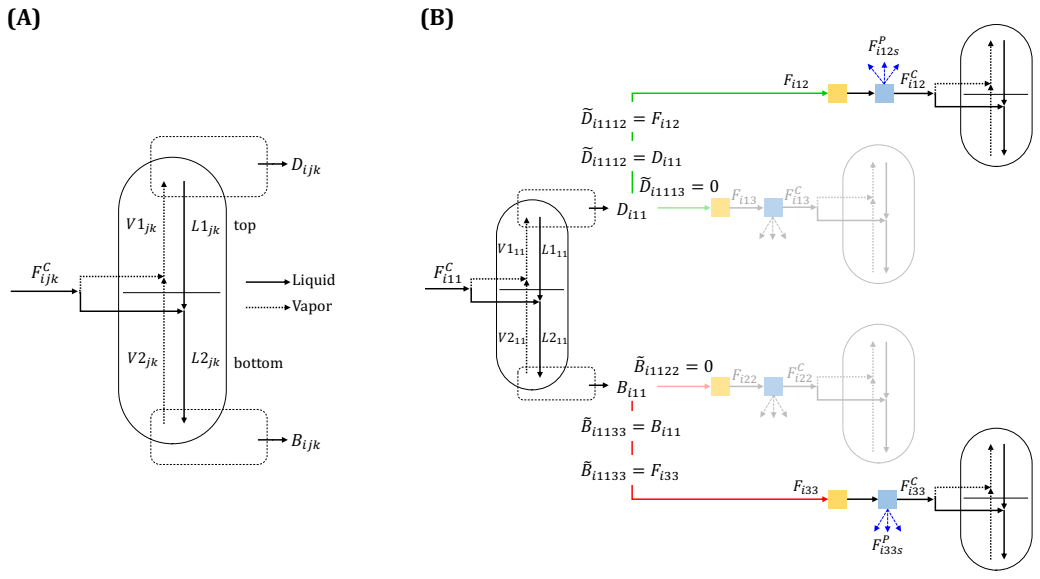

Figure 3.4: (A) Material flows inside distillation column in mixture node (j,k); (B) Material balance between different nodes with disaggregated distillate/bottom streams.

is active (i.e., $Y^T_{jkj'k'} = 1$), then $\widetilde{D}_{ijkj'k'} = D_{ijk}$ is enforced. Similarly, if the bottom arc from node (j,k) to (j',k') is active (i.e., $Y^B_{jkj'k'} = 1$), then $\widetilde{B}_{ijkj'k'} = B_{ijk}$ is enforced; otherwise, $\widetilde{D}_{ijkj'k'} = 0$ and $\widetilde{B}_{ijkj'k'} = 0$. For example, in **Figure 3.4B**, there are two top arcs (i.e., (1,1,1,2) and (1,1,1,3)) and two bottom arcs (i.e., (1,1,2,2) and (1,1,3,3))

from node (1,1), but only the top arc to node (1,2) and the bottom arc to node (3,3) are active; thus, $\widetilde{D}_{i,1112} = D_{i,11}$ and $\widetilde{B}_{i,1133} = B_{i,11}$ are enforced by Eqs. (3.25) and (3.27) respectively, whereas $\widetilde{D}_{i,1113} = 0$ and $\widetilde{B}_{i,1122} = 0$ are enforced by Eqs. (3.26) and (3.28), respectively.

Finally, F_{ijk} is constrained as follows,

$$F_{ijk} = \sum_{(j'k'jk)\in\mathbf{A}_{jk}^{\mathrm{TE}}} \widetilde{D}_{ij'k'jk} + \sum_{(j'k'jk)\in\mathbf{A}_{jk}^{\mathrm{BE}}} \widetilde{B}_{ij'k'jk} + F_{ijk}^{0} \qquad i \in \mathbf{I}, (j,k) \in \mathbf{N}^{\mathrm{D}} \tag{3.29}$$

3.3.3 Product Specifications

Product specifications such as purity (ρ_{is}^{P})

$$\textstyle\sum_{(j,k)\in\mathbf{N}^{\mathrm{D}}} F_{ijks}^{P} \geq \rho_{is}^{P} \sum_{(j,k)\in\mathbf{N}^{\mathrm{D}}} \sum_{i'\in\mathbf{I}} F_{i'jks}^{P} \quad i \in \mathbf{I}_{s}^{\mathrm{P}}, s \in \mathbf{N}^{\mathrm{SI}} \tag{3.30}$$

or recovery (ρ_{is}^{R})

$$\textstyle\sum_{(j,k)\in\mathbf{N}^{\mathrm{D}}} F_{ijks}^{P} \geq \rho_{is}^{R} F_{i}^{0} \quad i \in \mathbf{I}_{s}^{\mathrm{P}}, s \in \mathbf{N}^{\mathrm{SI}} \tag{3.31}$$

can be specified for sink nodes for products, where $\mathbf{I}_{s}^{\mathrm{P}}$ is the set of components with specifications in sink node s. If component i is not allowed in sink node s and present in the source (i.e., $Y_i = 1$), then the bypass arc from node (j,k) with $i \in \mathbf{I}_{jk}^{\mathrm{C}}$ to sink node s can be cut off:

$$Y_{jks}^{P} \leq 1 - Y_i \qquad (j,k) \in \mathbf{N}^{\mathrm{D}}, s \in \mathbf{N}^{\mathrm{SI}}, i \in \mathbf{I}_{s}^{\mathrm{N}} \cap \mathbf{I}_{jk}^{\mathrm{C}} \tag{3.32}$$

where $\mathbf{I}_{s}^{\mathrm{N}}$ denotes the set of components that are not allowed in sink node s. Note that if $Y_i = 0$, Eq. (3.32) is relaxed. For example, for a system with $\mathbf{I} = \{\mathrm{A}, \mathrm{B}, \mathrm{C}\}$, if sink node s does not allow component C while $Y_{\mathrm{C}} = 1$, bypass arcs from node (1,1) ($\mathbf{I}_{11}^{\mathrm{C}} = \{\mathrm{A}, \mathrm{B}, \mathrm{C}\}$), (2,2) ($\mathbf{I}_{22}^{\mathrm{C}} = \{\mathrm{B}, \mathrm{C}\}$), and (3,3) ($\mathbf{I}_{33}^{\mathrm{C}} = \{\mathrm{C}\}$) to s cannot be active because component C is present in bypass streams from these nodes.

3.3.4 Distillation Column Model

To handle undetermined sources into the distillation network, distillation column models need to be capable of handling an undetermined inlet and correctly calculate vapor/liquid flow rates for potential separation tasks. We employ the reformulated Underwood equations in appendix A.3 as unit models for the distillation column modeling. The unit model embeds all potential distillation tasks in each distillation node based on its postulated components, and feasible tasks are automatically selected depending on the components that are present in the inlet. We present only a part of the distillation column model while more details can be found in appendix B.1. Variable $Y_{ijk}^{LK}/Y_{ijk}^{HK} \in \{0,1\}$ denotes whether component i is selected as the light/heavy key in column (j,k). There are one light key and one heavy key if and only if the column is active.

$$X_{j,k}^{C} = \sum_{i \in \mathbf{I}} Y_{ijk}^{LK} \qquad (j,k) \in \mathbf{N}^{\mathrm{DM}} \tag{3.33}$$

$$X_{j,k}^{C} = \sum_{i \in \mathbf{I}} Y_{ijk}^{HK} \qquad (j,k) \in \mathbf{N}^{\mathrm{DM}} \tag{3.34}$$

Also, the key components must be present in the source:

$$Y_{ijk}^{LK} \leq Y_i \qquad i \in \mathbf{I}, (j,k) \in \mathbf{N}^{\mathrm{DM}} \tag{3.35}$$

$$Y_{ijk}^{HK} \leq Y_i \qquad i \in \mathbf{I}, (j,k) \in \mathbf{N}^{\mathrm{DM}} \tag{3.36}$$

Components between the light key and the heavy key are referred to as *distributed* components. Variable $Z_{ijk} \in \{0,1\}$ denotes whether component i is distributed,

$$Z_{ijk} = \sum_{i' \leq i-1} Y_{i'jk}^{LK} - \sum_{i' \leq i} Y_{i'jk}^{HK} \qquad i \in \mathbf{I}, (j,k) \in \mathbf{N}^{\mathrm{DM}} \tag{3.37}$$

For example, if a column separates a ABCD mixture with A/C as the light/heavy key, component B is distributed. We enforce that components lighter/heavier than the

light/heavy key are perfectly recovered in the distillate/bottom stream.

$$B_{ijk} \leq \delta^B_{ijk} \sum_{i' \leq i} Y^{LK}_{i'jk} \qquad i \in \mathbf{I}, (j,k) \in \mathbf{N}^{\mathrm{DM}} \tag{3.38}$$

$$D_{ijk} \leq \delta^D_{ijk} \sum_{i' \geq i} Y^{HK}_{i'jk} \qquad i \in \mathbf{I}, (j,k) \in \mathbf{N}^{\mathrm{DM}} \tag{3.39}$$

When a component is considered to be not present (i.e., $Y_i = 0$) but distributed (i.e., $Z_{ijk} = 1$), we assume that the component is evenly distributed between the distillate and bottom streams,

$$-\delta^B_{ijk}(1 + Y_i - Z_{ijk}) \leq D_{ijk} - B_{ijk} \leq \delta^D_{ijk}(1 + Y_i - Z_{ijk}) \quad i \in \mathbf{I}, (j,k) \in \mathbf{N}^{\mathrm{DM}} \tag{3.40}$$

3.3.5 Light/Heavy Key Selection

A separation task assigned to column (j,k) activates one top arc $(j,k,j',k') \in \mathbf{A}^{\mathrm{TS}}_{jk}$ and one bottom arc $(j,k,j'',k'') \in \mathbf{A}^{\mathrm{BS}}_{jk}$. We define the light key as the heaviest component that is *not* a postulated component in the bottom stream (i.e., $\mathbf{I}^{\mathrm{C}}_{j''k''}$), while the heavy key as the lightest component that is *not* a postulated component in the distillate stream (i.e., $\mathbf{I}^{\mathrm{C}}_{j'k'}$). Thus, the light/heavy key of a separation task can be identified by checking active top and bottom arcs. According to the definition of the key components, the set of light/heavy key *candidates* ($\mathbf{I}^{\mathrm{LK}}_{j'k'j''k''}$/$\mathbf{I}^{\mathrm{HK}}_{j'k'j''k''}$), for the separation task associated with top arc $(j,k,j',k') \in \mathbf{A}^{\mathrm{TS}}_{jk}$ and bottom arc $(j,k,j'',k'') \in \mathbf{A}^{\mathrm{BS}}_{jk}$, can be defined as follows,

$$\mathbf{I}^{\mathrm{LK}}_{j'k'j''k''} = \begin{cases} \{i | i^L_{j'k'} \leq i \leq i^L_{j''k''} - 1\} & \text{if } i^H_{j'k'} \geq i^L_{j''k''} \\ \{i | i = i^H_{j'k'}\} & \text{if } i^H_{j'k'} < i^L_{j''k''} \end{cases} \tag{3.41}$$

$$\mathbf{I}^{\mathrm{HK}}_{j'k'j''k''} = \begin{cases} \{i | i^H_{j'k'} + 1 \leq i \leq i^H_{j''k''}\} & \text{if } i^H_{j'k'} \geq i^L_{j''k''} \\ \{i | i = i^L_{j''k''}\} & \text{if } i^H_{j'k'} < i^L_{j''k''} \end{cases} \tag{3.42}$$

We present details on how to obtain these sets in appendix B.2. Then, we enforce key selections to be only within the light/heavy key candidates as follows,

$$\sum_{i \in \mathbf{I}^{\mathrm{LK}}_{j'k'j''k''}} Y^{LK}_{ijk} \geq Y^{T}_{jkj'k'} + Y^{B}_{jkj''k''} - X^{C}_{jk} \quad (j,k,j',k') \in \mathbf{A}^{\mathrm{T}}, (j,k,j'',k'') \in \mathbf{A}^{\mathrm{B}} \tag{3.43}$$

$$\sum_{i \in \mathbf{I}^{\mathrm{HK}}_{j'k'j''k''}} Y^{LK}_{ijk} \geq Y^{T}_{jkj'k'} + Y^{B}_{jkj''k''} - X^{C}_{jk} \quad (j,k,j',k') \in \mathbf{A}^{\mathrm{T}}, (j,k,j'',k'') \in \mathbf{A}^{\mathrm{B}} \tag{3.44}$$

where Eqs. (3.43) and (3.44) enforce that the light and heavy keys are selected in $\mathbf{I}^{\mathrm{LK}}_{j'k'j''k''}$ and $\mathbf{I}^{\mathrm{HK}}_{j'k'j''k''}$, respectively, if top arc (j,k,j',k') and bottom arc (j,k,j'',k'') are active.

Also, the light key should be the heaviest component among the light key candidates while the heavy key should be the lightest component among the heavy key candidates:

$$Y^{LK}_{ijk} \leq 1 - Y_{i'} + (2X^{C}_{jk} - Y^{T}_{jkj'k'} - Y^{B}_{jkj''k''}) \quad i', i \in \mathbf{I}^{\mathrm{LK}}_{j'k'j''k''}, i' > i, (j,k,j',k') \in \mathbf{A}^{\mathrm{T}}, (j,k,j'',k'') \in \mathbf{A}^{\mathrm{B}} \tag{3.45}$$

$$Y^{HK}_{ijk} \leq 1 - Y_{i'} + (2X^{C}_{jk} - Y^{T}_{jkj'k'} - Y^{B}_{jkj''k''}) \quad i', i \in \mathbf{I}^{\mathrm{HK}}_{j'k'j''k''}, i' < i, (j,k,j',k') \in \mathbf{A}^{\mathrm{T}}, (j,k,j'',k'') \in \mathbf{A}^{\mathrm{B}} \tag{3.46}$$

When component i is selected as the light key in column (j,k) with $Y^{T}_{jkj'k'} = 1$ and $Y^{B}_{jkj''k''} = 1$, then $1 \leq 1 - Y_{i'}$ holds in Eq (3.45), enforcing $Y_{i'} = 0, i' > i$ (i.e., there is no component that is heavier than component i in the light key candidates). Similarly, if component i is selected as the heavy key, then $Y_{i'} = 0, i' < i$ is enforced by Eq (3.46) (i.e., there is no component that is lighter than component i in the heavy key candidates).

3.3.6 Thermal Coupling

We introduce $W_{jk} \in \{0,1\}$, where $W_{jk} = 1$ denotes that there is no condenser/reboiler associated with distillate/bottom streams that are sent to node (j,k). This includes the case where column (j,k) is thermally coupled with upstream columns and the case where there is no active arc to node (j,k). Conversely, $W_{jk} = 0$ denotes that there are condensers/reboilers associated with distillate/bottom streams that are sent to node (j,k).

Vapor/Liquid Stream Exchange

When two columns are thermally coupled, they exchange both vapor and liquid streams. If $Y^B_{j',k',j,k} = 1$ and $W_{jk} = 1$ (See **Figure 3.5A**), the liquid stream is sent from column (j',k') to (j,k) while the vapor stream is sent from column (j,k) to (j',k'). We denote the flow rate of this liquid/vapor stream as $\widetilde{L2}_{j'k'jk}/\widetilde{V2}_{j'k'jk}$, and constrain it as follows,

$$L2_{j'k'} - \beta^L(1 - Y^B_{j'k'jk}) \leq \widetilde{L2}_{j'k'jk} \leq L2_{j'k'} \qquad (j',k',j,k) \in \mathbf{A}^{\mathrm{B}} \tag{3.47}$$

$$\widetilde{L2}_{j'k'jk} \leq \beta^L Y^B_{j'k'jk} \qquad (j',k',j,k) \in \mathbf{A}^{\mathrm{B}} \tag{3.48}$$

$$V2_{j'k'} - \beta^V(1 - Y^B_{j'k'jk}) \leq \widetilde{V2}_{j'k'jk} \leq V2_{j'k'} \qquad (j',k',j,k) \in \mathbf{A}^{\mathrm{B}} \tag{3.49}$$

$$\widetilde{V2}_{j'k'jk} \leq \beta^V Y^B_{j'k'jk} \qquad (j',k',j,k) \in \mathbf{A}^{\mathrm{B}} \tag{3.50}$$

where parameter β^V/β^L denotes an upper bound on the internal vapor/liquid flow rate. If $Y^B_{j'k'jk} = 1$, then $\widetilde{L2}_{j'k'jk} = L2_{j'k'}$ and $\widetilde{V2}_{j'k'jk} = V2_{j'k'}$ are enforced by Eqs. (3.47) and (3.49), respectively; otherwise, $\widetilde{L2}_{j'k'jk} = 0$ and $\widetilde{V2}_{j'k'jk} = 0$ are enforced by Eqs. (3.48) and (3.50).

Similarly, if $Y^T_{j',k',j,k} = 1$ and $W_{jk} = 1$ (See **Figure 3.5B**), the vapor stream is sent from column (j',k') to (j,k) while the liquid stream is sent from column (j,k) to (j',k').

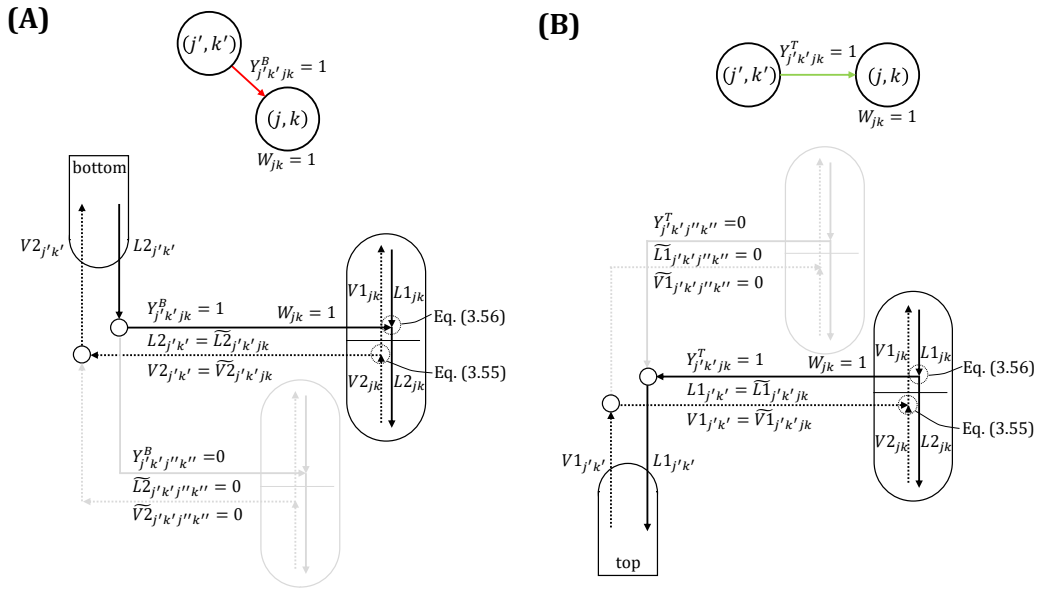

Figure 3.5: Material balances with thermal coupling. Solid lines denote liquid streams while dashed lines denote vapor streams; (A) Bottom section of column (j', k') is thermally coupled with column (j, k); (B) Top section of column (j', k') is thermally coupled with column (j, k).

We denote the flow rate of this vapor/liquid stream as $\widetilde{V1}_{j'k'jk}/\widetilde{L1}_{j'k'jk}$, and constrain it as follows:

$$V1_{j'k'} - \beta^V(1 - Y^T_{j'k'jk}) \le \widetilde{V1}_{j'k'jk} \le V1_{j'k'} \qquad (j', k', j, k) \in \mathbf{A}^{\mathrm{T}} \tag{3.51}$$

$$\widetilde{V1}_{j'k'jk} \le \beta^V Y^T_{j'k'jk} \qquad (j', k', j, k) \in \mathbf{A}^{\mathrm{T}} \tag{3.52}$$

$$L1_{j'k'} - \beta^L(1 - Y^T_{j'k'jk}) \le \widetilde{L1}_{j'k'jk} \le L1_{j'k'} \qquad (j', k', j, k) \in \mathbf{A}^{\mathrm{T}} \tag{3.53}$$

$$\widetilde{L1}_{j'k'jk} \le \beta^L Y^T_{j'k'jk} \qquad (j', k', j, k) \in \mathbf{A}^{\mathrm{T}} \tag{3.54}$$

If $Y^T_{j'k'jk} = 1$, then $\widetilde{V1}_{j'k'jk} = V1_{j'k'}$ and $\widetilde{L1}_{j'k'jk} = L1_{j'k'}$ are enforced by Eqs. (3.51) and (3.53), respectively; otherwise, $\widetilde{V1}_{j'k'jk} = 0$ and $\widetilde{L1}_{j'k'jk} = 0$ are enforced by Eqs (3.52) and (3.54).

Vapor/Liquid Flow Rate Balances

The material balance in a thermally coupled column (i.e., $W_{jk} = 1$) is as follows:

$$-2\beta^V(1 - W_{jk}) \le V1_{jk} \quad -V2_{jk} - \textstyle\sum_{(j'k'jk)\in\mathbf{A}^{\mathrm{TE}}_{jk}} \widetilde{V1}_{j'k'jk} + \sum_{(j'k'jk)\in\mathbf{A}^{\mathrm{BE}}_{jk}} \widetilde{V2}_{j'k'jk} \le 2\beta^V(1 - W_{jk}) \qquad (j, k) \in \mathbf{N}^{\mathrm{DM}} \tag{3.55}$$

$$-2\beta^L(1 - W_{jk}) \le L1_{jk} \quad -L2_{jk} - \textstyle\sum_{(j'k'jk)\in\mathbf{A}^{\mathrm{TE}}_{jk}} \widetilde{L1}_{j'k'jk} + \sum_{(j'k'jk)\in\mathbf{A}^{\mathrm{BE}}_{jk}} \widetilde{L2}_{j'k'jk} \le 2\beta^L(1 - W_{jk}) \qquad (j, k) \in \mathbf{N}^{\mathrm{DM}} \tag{3.56}$$

If $W_{jk} = 1$, then $V1_{jk} - V2_{jk} - \sum_{(j'k'jk)\in\mathbf{A}^{\mathrm{TE}}_{jk}} \widetilde{V1}_{j'k'jk} + \sum_{(j'k'jk)\in\mathbf{A}^{\mathrm{BE}}_{jk}} \widetilde{V2}_{j'k'jk} = 0$ and $L1_{jk} - L2_{jk} - \sum_{(j'k'jk)\in\mathbf{A}^{\mathrm{TE}}_{jk}} \widetilde{L1}_{j'k'jk} + \sum_{(j'k'jk)\in\mathbf{A}^{\mathrm{BE}}_{jk}} \widetilde{L2}_{j'k'jk} = 0$ are enforced by Eqs (3.55) and (3.56), respectively (See **Figure 3.5**); otherwise, the material balances are relaxed.

Conversely, if $W_{jk} = 0$, liquid stream is sent to column (j, k) but no vapor stream is sent to/from column (j, k) (See **Figure 3.6**). Thus, if $W_{j,k} = 0$,

$$-\beta^V W_{jk} \leq V1_{jk} - V2_{jk} \leq \beta^V W_{jk} \qquad (j,k) \in \mathbf{N}^{\mathrm{DM}} \qquad (3.57)$$

$V1_{jk} - V2_{jk} = 0$ is enforced by Eq (3.57), denoting there is no vapor stream sent to/from column (j, k).

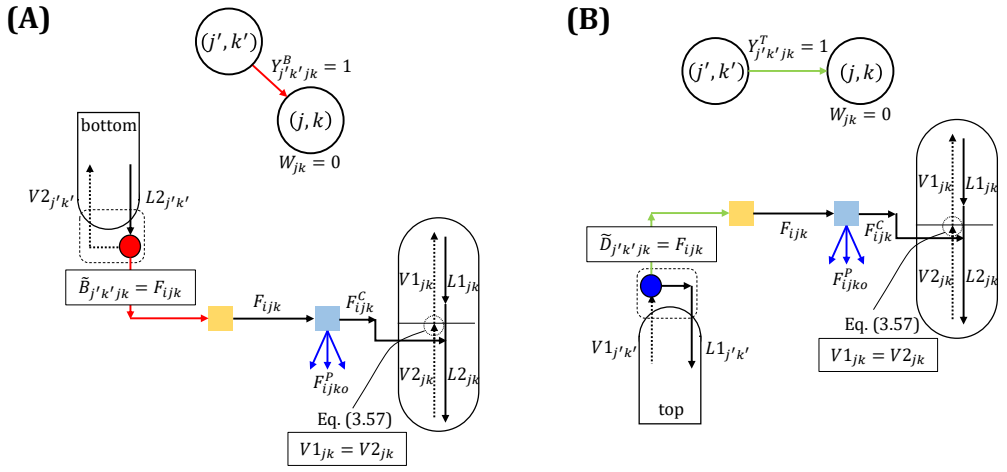

Figure 3.6: Material balances without thermal coupling. Solid lines denote liquid streams while dashed lines denote vapor streams; (A) Bottom section of upstream column (j', k') with reboiler is connected to downstream column (j, k). The bottom stream from column (j', k') is liquid, so it does not change the internal vapor flow rate in column (j, k); (B) Top section of upstream column (j', k') with condenser is connected to downstream column (j, k). The distillate stream is liquid, so it does not change the internal vapor flow rate in column (j, k)

Notably, if two arcs headed to node (j, k) (i.e., one bottom arc $(j', k', j, k) \in \mathbf{A}^{\mathrm{BE}}_{jk}$ and one top arc $(j'', k'', j, k) \in \mathbf{A}^{\mathrm{TE}}_{jk}$) are active and $W_{jk} = 0$ (See **Figure 3.7A**), then there is a reboiler at the bottom section of column (j', k') and there is a condenser at the top

section of column (j'', k''). However, these reboiler and condenser can be removed (i.e., $W_{jk} = 1$) by stacking columns as shown in **Figure 3.7B**, so that capital and operating

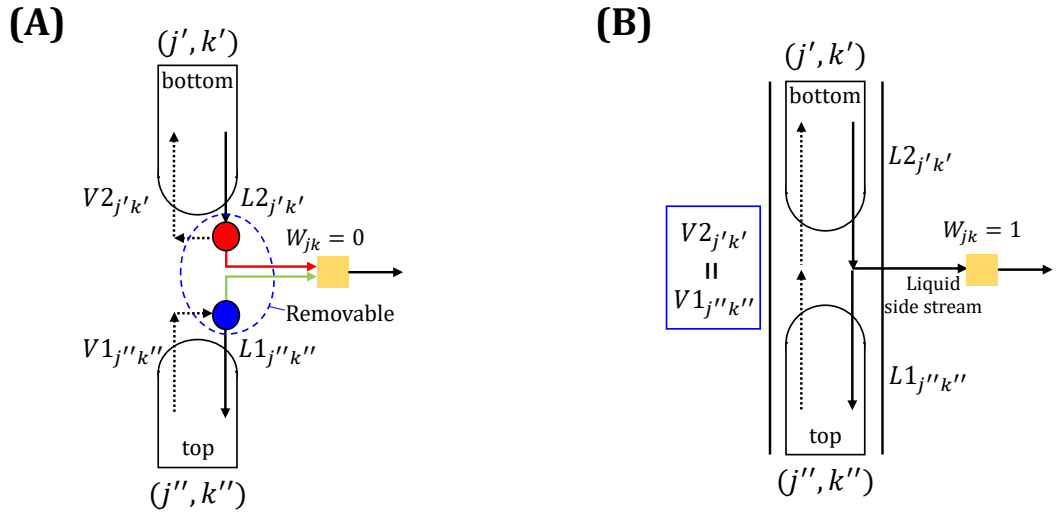

Figure 3.7: Cases where bottom arc (j', k', j, k) and top arc (j'', k'', j, k) are active; (A) Downstream column (j, k) is not thermally coupled with upstream columns ($W_{jk} = 0$). Due to the condenser and the reboiler, both cooling and heating are needed; (B) Upstream columns are stacked into a single column. The condenser and reboiler are removed ($W_{jk} = 1$), so there is no cooling/heating duty. Only liquid side stream is sent to column (j, k), so internal vapor flow rates in the stacked column should not be changed by the side stream.

costs can be reduced. Thus, we enforce $W_{jk} = 1$ if two arcs headed to node (j, k) are active.

$$W_{jk} \geq \sum_{(j'k'jk) \in \mathbf{A}^{\mathrm{TE}}_{jk}} Y^{T}_{j'k'jk} + \sum_{(j'k'jk) \in \mathbf{A}^{\mathrm{BE}}_{jk}} Y^{B}_{j'k'jk} - 1 \qquad (j, k) \in \mathbf{N}^{\mathrm{D}} \tag{3.58}$$

When columns (j', k') and (j'', k'') are stacked, we only consider a liquid side stream, which is sent to node (j, k). Thus, the internal vapor flow rates in the stacked column

should not be changed by the side stream (i.e., $V2_{j'k'} = V1_{j''k''}$ if $Y^B_{j'k'jk} = 1$ and $Y^T_{j''k''jk} = 1$, See **Figure 3.7B**). When $Y^B_{j'k'jk} = 1$, then $\sum_{(j''k''jk)\in \mathbf{A}^{\mathrm{BE}}_{jk}} \widetilde{V2}_{j''k''jk} = V2_{j'k'}$ holds due to Eqs. (3.49) and (3.50). Also, when $Y^T_{j''k''jk} = 1$, then $\sum_{(j'k'jk)\in \mathbf{A}^{\mathrm{TE}}_{jk}} \widetilde{V1}_{j'k'jk} = V1_{j''k''}$ holds due to Eqs. (3.51) and (3.52). Thus, we can introduce the following,

$$-\beta^V \psi_{jk} \leq \sum_{(j'k'jk)\in \mathbf{A}^{\mathrm{TE}}_{jk}} \widetilde{V1}_{j'k'jk} - \sum_{(j'k'jk)\in \mathbf{A}^{\mathrm{BE}}_{jk}} \widetilde{V2}_{j'k'jk} \leq \beta^V \psi_{jk} \quad (j,k) \in \mathbf{N}^{\mathrm{D}} \tag{3.59}$$

$$\psi_{jk} = 2 - \sum_{(j'k'jk)\in \mathbf{A}^{\mathrm{TE}}_{jk}} Y^T_{j'k'jk} - \sum_{(j'k'jk)\in \mathbf{A}^{\mathrm{TE}}_{jk}} Y^B_{j'k'jk} \qquad (j,k) \in \mathbf{N}^{\mathrm{D}} \tag{3.60}$$

where $\sum_{(j'k'jk)\in \mathbf{A}^{\mathrm{TE}}_{jk}} \widetilde{V1}_{j'k'jk} - \sum_{(j'k'jk)\in \mathbf{A}^{\mathrm{BE}}_{jk}} \widetilde{V2}_{j'k'jk} = 0$ is enforced by Eqs. (3.59) and (3.60) if two arcs to node (j,k) are active.

When two columns are stacked and operated with the same internal vapor flow rate, one column may not be operated at its minimum vapor flow rate [14]. If needed, configurations where each column is operated at its minimum internal vapor flow rates can be found if Eqs. (3.59) and (3.60) are excluded.

Thermal Coupling vs. Bypass

Notably, if $W_{jk} = 1$, no bypass arc from node (j,k) can be active due to Eqs. (3.47) and (3.51). This is because if there is an active bypass arc, a part of the liquid/vapor stream sent from upstream column (j',k') to downstream column (j,k) should be utilized for the bypass stream, resulting in $\widetilde{L2}_{j'k'jk} < L2_{j'k'}$ or $\widetilde{V1}_{j'k'jk} < V1_{j'k'}$. However, when $Y^T_{j'k'jk} = 1$, then $\widetilde{L2}_{j'k'jk} = L2_{j'k'}$ is enforced by Eq. (3.47), so no bypass arc can be active. Similarly, when $Y^B_{j'k'jk} = 1$, then $\widetilde{V1}_{j'k'jk} = V1_{j'k'}$ is enforced by Eq. (3.51), so no bypass arc can be active. Thus, thermal coupling "competes" with bypass streams.

If a mixture, instead of an almost pure component, is allowed for an outlet, bypass

streams can be chosen because separation loads in all downstream columns can be reduced. However, when the benefit of bypass streams is not sufficient, thermal coupling can be selected. One key aspect of the proposed model is that it can automatically consider trade-offs between the selection of bypass streams and thermal coupling depending on outlet compositions. If needed, it is also possible to allow bypass streams and thermal coupling at the same time, illustrated in section 3.4.1.

3.3.7 Heat Duty Calculation

We introduce Q^T_{jk}/Q^B_{jk} to denote the cooling/heating duty in the condenser/reboiler associated with the distillate/bottom stream sent to node (j,k),

$$\sum_{(j'k'jk)\in\mathbf{A}^{\mathrm{TE}}_{jk}} \widetilde{V1}_{j'k'jk} - \beta^V W_{jk} \leq \frac{Q^T_{jk}}{\lambda_{jk}} \leq \sum_{(j'k'jk)\in\mathbf{A}^{\mathrm{TE}}_{jk}} \widetilde{V1}_{j'k'jk} \qquad (j,k)\in\mathbf{N}^{\mathrm{D}} \qquad (3.61)$$

$$\sum_{(j'k'jk)\in\mathbf{A}^{\mathrm{BE}}_{jk}} \widetilde{V2}_{j'k'jk} - \beta^V W_{jk} \leq \frac{Q^B_{jk}}{\lambda_{jk}} \leq \sum_{(j'k'jk)\in\mathbf{A}^{\mathrm{BE}}_{jk}} \widetilde{V2}_{j'k'jk} \qquad (j,k)\in\mathbf{N}^{\mathrm{D}} \qquad (3.62)$$

where λ_{jk} denotes an average molar heat of vaporization of the inlet into node (j,k). If $W_{jk}=0$, then $Q^T_{jk}/\lambda_{jk} = \sum_{(j'k'jk)\in\mathbf{A}^{\mathrm{TE}}_{jk}} \widetilde{V1}_{j'k'jk}$ and $Q^B_{jk}/\lambda_{jk} = \sum_{(j'k'jk)\in\mathbf{A}^{\mathrm{BE}}_{jk}} \widetilde{V2}_{j'k'jk}$ are enforced by Eqs. (3.61) and (3.62); otherwise, the equalities are relaxed. Conversely, if $W_{jk}=1$, the cooling/heating duty is set to zero,

$$Q^T_{jk} \leq \beta^T(1-W_{jk}) \qquad (j,k)\in\mathbf{N}^{\mathrm{D}} \qquad (3.63)$$

$$Q^B_{jk} \leq \beta^B(1-W_{jk}) \qquad (j,k)\in\mathbf{N}^{\mathrm{D}} \qquad (3.64)$$

3.3.8 Terminal Nodes

If node (j,k) is active (i.e., $X_{jk}=1$) but the corresponding column is inactive (i.e., $X^C_{jk}=0$), then all inlets into node (j,k) are sent to sink nodes (i.e., there is no further

separation). Thus, these nodes are termed as *terminal nodes*. Note that all active pure component nodes are terminal nodes while an active mixture node can also be a terminal node. For example, in **Figure 3.8A**, a distillation network where the source with components A, B, C, and D is separated into three outlets (i.e., three sink nodes: P1, P2, and P3) is shown; notably, sink node P1 allows a mixture of A and B. Also, the corresponding column configuration is shown in **Figure 3.8B**. If the inlet into mixture

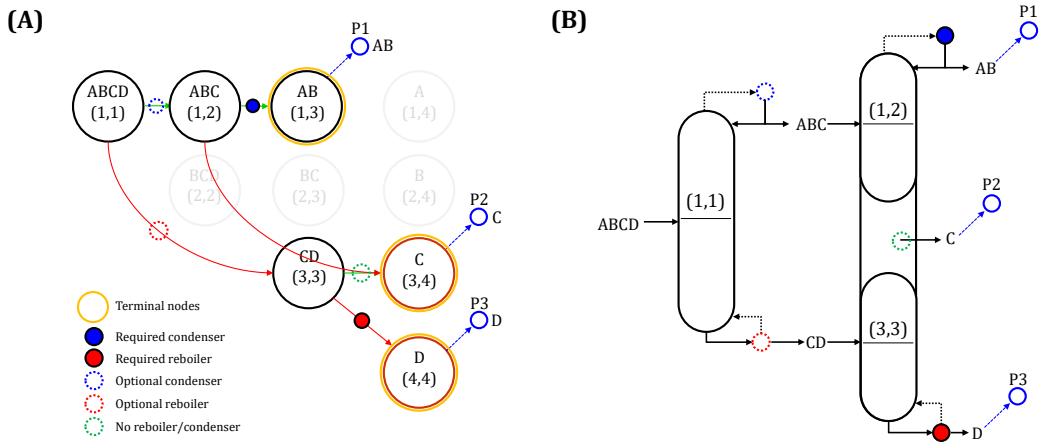

Figure 3.8: (A): A distillation network to separate the source with A, B, C, and D. Sink node P1 allows AB mixture, so mixture node (1,3) is selected as a terminal node. Reboilers/condensers that can be removed by thermal coupling is represented with red/blue dashed-circle, while reboilers/condensers that should be present are represented with red/blue filled circle. When there should be no condenser/reboiler, it is represented as green dashed-circle; (B): Corresponding column configuration.

node (1,3) can be directly sent to sink node P1 without any further separations between A and B (i.e., column (1,3) is inactive), then node (1,3) becomes a terminal node (See **Figure 3.8A**). Also, nodes (3,4) and (4,4) are also terminal nodes because they are active pure component nodes.

Notably, for a terminal node, if only one arc toward the terminal node is active, then there should be a condenser/reboiler associated with the stream sent to the terminal node (See **Figure 3.8B**). For example, since node (1,3) is a terminal node and only one arc to (1,3) is active (i.e., top arc (1,2,1,3)), a condenser is needed in column (1,2). Similarly, since node (4,4) is a terminal node and only one arc toward it is active (i.e., bottom arc (3,3,4,4)), a reboiler is needed in column (3,3). Notably, even though node (3,4) is a terminal node, no reboiler/condenser is needed because there are two active arcs toward node (3,4) (i.e., bottom arc (1,2,3,4) and top arc (3,3,3,4)). This requirement is enforced as follows:

$$1 - W_{jk} \geq \begin{cases} -\sum_{(j''k''jk)\in \mathbf{A}_{jk}^{\mathrm{TE}}} Y_{j''k''jk}^{T} + \sum_{(j''k''jk)\in \mathbf{A}_{jk}^{\mathrm{BE}}} Y_{j''k''jk}^{B} - X_{jk}^{C} & (j,k) \in \mathbf{N}^{\mathrm{DM}} \\ -\sum_{(j''k''jk)\in \mathbf{A}_{jk}^{\mathrm{TE}}} Y_{j''k''jk}^{T} + \sum_{(j''k''jk)\in \mathbf{A}_{jk}^{\mathrm{BE}}} Y_{j''k''jk}^{B} & (j,k) \in \mathbf{N}^{\mathrm{DP}} \end{cases} \tag{3.65}$$

$$1 - W_{jk} \geq \begin{cases} \sum_{(j''k''jk)\in \mathbf{A}_{jk}^{\mathrm{TE}}} Y_{j''k''jk}^{T} - \sum_{(j''k''jk)\in \mathbf{A}_{jk}^{\mathrm{BE}}} Y_{j''k''jk}^{B} - X_{jk}^{C} & (j,k) \in \mathbf{N}^{\mathrm{DM}} \\ \sum_{(j''k''jk)\in \mathbf{A}_{jk}^{\mathrm{TE}}} Y_{j''k''jk}^{T} - \sum_{(j''k''jk)\in \mathbf{A}_{jk}^{\mathrm{BE}}} Y_{j''k''jk}^{B} & (j,k) \in \mathbf{N}^{\mathrm{DP}} \end{cases} \tag{3.66}$$

The right-hand side of Eq. (3.65) becomes 1 when there is only one active *bottom* arc headed to terminal node (j,k), enforcing $W_{jk} = 0$; otherwise, it is relaxed. For pure component nodes, there is no column, so Eq. (3.65) is defined without X_{jk}^{C}. Similarly, the right-hand side of Eq. (3.66) becomes 1 when there is only one active *top* arc headed to terminal node (j,k), enforcing $W_{jk} = 0$; otherwise, relaxed.

3.3.9 Objective Function

If the operating cost for the energy is dominant in the total annualized cost, the objective function can be defined as the cost for total heating/cooling duty for the distillation network (i.e., $\sum_{(j,k)\in\mathbf{N}^{\mathrm{D}}}(\mu^C Q^T_{jk} + \mu^H Q^B_{jk})$), where μ^C/μ^H denotes the cost parameter for cooling/heating. If the capital cost needs to be considered, we can include the internal vapor flow rates in the objective function (i.e., $\sum_{(j,k)\in\mathbf{N}^{\mathrm{D}}}(\mu^C Q^T_{jk} + \mu^H Q^B_{jk}) + \sum_{(j,k)\in\mathbf{N}^{\mathrm{DM}}}\mu^V(V1_{jk} + V2_{jk})$), which can serve as surrogate variables for the column diameter and height; μ^V denotes the cost parameter for the capital cost.

3.4 Extensions

3.4.1 Bypass with Thermal Coupling

The proposed model can be extended to allow bypass streams between thermally coupled columns. When a bypass stream is active between thermally coupled columns (See **Figure 3.9**), the flow rate of the vapor/liquid stream sent to the downstream column (i.e., $\widetilde{V1}_{j'k'jk}/\widetilde{L2}_{j'k'jk}$) should be strictly less than that in the upstream column (i.e., $V1_{j'k'}/L2_{j'k'}$). For example, if a fraction of the vapor stream from the top section of the upstream column is sent to a sink node, $V1_{j'k'} > \widetilde{V1}_{j'k'jk}$ should hold (See **Figure 3.9A**). To allow this, Eq. (3.51) is reformulated as follows,

$$V1_{j'k'} - \beta^V(1 - Y^T_{j'k'jk} + \sum_{s\in\mathbf{N}^{\mathrm{SI}}} Y^P_{jks}) \le \widetilde{V1}_{j'k'jk} \le V1_{j'k'} \quad (j',k',j,k)\in\mathbf{A}^{\mathrm{T}}, (j,k)\in\mathbf{N}^{\mathrm{D}} \tag{3.51a}$$

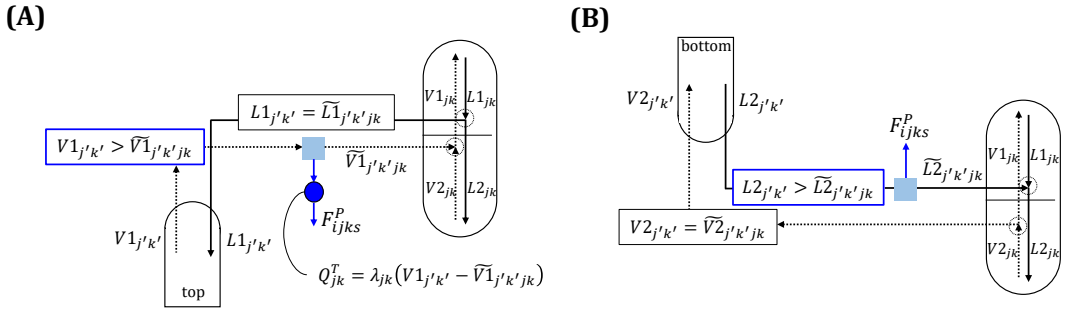

Figure 3.9: Bypass stream between thermally coupled columns; (A): The top section of the upstream column is thermally coupled with the downstream column. Only vapor stream is allowed to bypass. As outlets are liquid, bypass stream needs to be condensed; (B): The bottom section of the upstream column is thermally coupled with the downstream column. Only liquid stream is allowed to bypass.

where $\widetilde{V1}_{j'k'jk} < V1_{j'k'}$ is allowed if at least one bypass arc is active (i.e., $\sum_{s\in\mathbf{N}^{\mathrm{SI}}} Y^P_{jks} \geq 1$). Similarly, Eq. (3.47) is reformulated as follows,

$$L2_{j'k'} - \beta^L(1 - Y^B_{j'k'jk} + \sum_{s\in\mathbf{N}^{\mathrm{SI}}} Y^P_{jks}) \leq \widetilde{L2}_{j'k'jk} \leq L2_{j'k'} \quad (j',k',j,k) \in \mathbf{A}^{\mathrm{B}}, (j,k) \in \mathbf{N}^{\mathrm{D}} \tag{3.47a}$$

where $\widetilde{L2}_{j'k'jk} < L2_{j'k'}$ is allowed when at least one bypass arc is active (See **Figure 3.9B**). When columns are not thermally coupled (i.e., $W_{jk} = 0$ for downstream node), $\widetilde{V1}_{j'k'jk} = V1_{j'k'}$ and $\widetilde{L2}_{j'k'jk} = L2_{j'k'}$ are enforced again by the following constraints,

$$V1_{j'k'} - \beta^V(1 - Y^T_{j'k'jk} + W_{jk}) \leq \widetilde{V1}_{j'k'jk} \quad (j',k',j,k) \in \mathbf{A}^{\mathrm{T}}, (j,k) \in \mathbf{N}^{\mathrm{D}} \tag{3.67}$$

$$L2_{j'k'} - \beta^L(1 - Y^B_{j'k'jk} + W_{jk}) \leq \widetilde{L2}_{j'k'jk} \quad (j',k',j,k) \in \mathbf{A}^{\mathrm{T}}, (j,k) \in \mathbf{N}^{\mathrm{D}} \tag{3.68}$$

If a fraction of the vapor stream from the top section is directly sent to a sink node, it needs to be condensed to make liquid products (See **Figure 3.9A**). To calculate this

condenser duty, Eq. (3.63) is reformulated as follows,

$$Q^T_{jk}/\lambda_{jk} \geq (V1_{j'k'} - \widetilde{V1}_{j'k'jk}) - \beta^V(2 - Y^T_{j'k'jk} - W_{jk}) \qquad (j,k,j',k') \in \mathbf{A}^{\mathrm{T}} \tag{3.63a}$$

$$Q^T_{jk}/\lambda_{jk} \leq (V1_{j'k'} - \widetilde{V1}_{j'k'jk}) + \beta^V(2 - Y^T_{j'k'jk} - W_{jk}) \qquad (j,k,j',k') \in \mathbf{A}^{\mathrm{T}} \tag{3.63b}$$

where $Q^T_{jk}/\lambda_{jk} = V1_{j'k'} - \widetilde{V1}_{j'k'jk}$ is enforced if the top section of the upstream column is thermally coupled with the downstream column (i.e., $Y^T_{j'k'jk} = 1$ and $W_{jk} = 1$).

3.4.2 Multiple Sources

When there are multiple sources, $Y^0_{sjk} \in \{0,1\}$ is introduced instead of Y^0_{jk}. Also, $F^0_{si}/\widetilde{F}^0_{sijk} \in \mathbb{R}^+$ is introduced to replace $F^0_i/\widetilde{F}^0_{ijk}$. Then, Eqs. (3.4), (3.5), (3.6), (3.13), (3.14), and (3.31) are reformulated as follows:

$$\sum_{(j,k)\in\mathbf{N}^{\mathrm{D}}} Y^0_{sjk} = 1 \qquad s \in \mathbf{N}^{\mathrm{SO}} \tag{3.4a}$$

$$Y^0_{sjk} \leq X_{jk} \qquad s \in \mathbf{N}^{\mathrm{SO}}, (j,k) \in \mathbf{N}^{\mathrm{D}} \tag{3.5a}$$

$$X_{jk} \leq \sum_{s\in\mathbf{N}^{\mathrm{SO}}} Y^0_{sjk} + \sum_{(j'k'jk)\in\mathbf{A}^{\mathrm{TE}}_{jk}} Y^T_{j'k'jk} + \sum_{(j'k'jk)\in\mathbf{A}^{\mathrm{BE}}_{jk}} Y^B_{j'k'jk} \quad (j,k) \in \mathbf{N}^{\mathrm{D}} \tag{3.6a}$$

$$F^0_{si} = \sum_{(j,k)\in\mathbf{N}^{\mathrm{D}}} \widetilde{F}^0_{sijk} \qquad s \in \mathbf{N}^{\mathrm{SO}}, i \in \mathbf{I} \tag{3.13a}$$

$$\widetilde{F}^0_{sijk} \leq \overline{\delta}^0_{si} Y^0_{sjk} \qquad s \in \mathbf{N}^{\mathrm{SO}}, i \in \mathbf{I}, (j,k) \in \mathbf{N}^{\mathrm{D}} \tag{3.14a}$$

$$\sum_{(j,k)\in\mathbf{N}^{\mathrm{D}}} F^P_{ijks} \geq \rho^R_{is} \sum_{s'\in\mathbf{N}^{\mathrm{SO}}} F^0_{s'i} \qquad i \in \mathbf{I}^{\mathrm{P}}_s, s \in \mathbf{N}^{\mathrm{SI}} \tag{3.31a}$$

Furthermore, $Y_{ijk} \in \{0,1\}$ is introduced, instead of Y_i, to denote whether component i is present in the sum of all inlets to node (j,k). Accordingly, Eqs. (3.15), (3.16), (3.32),

(3.35), (3.36), and (3.40) are reformulated as follows:

$$\underline{\delta}_{ijk} Y_{ijk} \leq F_{ijk} \leq \overline{\delta}_{ijk} Y_{ijk} + \underline{\delta}_{ijk}(1 - Y_{ijk}) \quad i \in \mathbf{I}^{\mathrm{C}}_{jk}, (j,k) \in \mathbf{N}^{\mathrm{D}} \tag{3.15b}$$

$$X_{jk} \leq Y_{ijk} \qquad i \in \{i^L_{jk}, i^H_{jk}\}, (j,k) \in \mathbf{N}^{\mathrm{D}} \tag{3.16a}$$

$$Y^P_{jks} \leq 1 - Y_{ijk} \qquad (j,k) \in \mathbf{N}^{\mathrm{D}}, s \in \mathbf{N}^{\mathrm{SI}}, i \in \mathbf{I}^{\mathrm{N}}_s \cap \mathbf{I}^{\mathrm{C}}_{jk} \tag{3.32a}$$

$$Y^{LK}_{ijk} \leq Y_{ijk} \qquad i \in \mathbf{I}^{\mathrm{C}}_{jk}, (j,k) \in \mathbf{N}^{\mathrm{DM}} \tag{3.35a}$$

$$Y^{HK}_{ijk} \leq Y_{ijk} \qquad i \in \mathbf{I}^{\mathrm{C}}_{jk}, (j,k) \in \mathbf{N}^{\mathrm{DM}} \tag{3.36a}$$

$$-\delta^B_{ijk}(1 + Y_{ijk} - Z_{ijk}) \leq D_{ijk} - B_{ijk} \leq \delta^D_{ijk}(1 + Y_{ijk} - Z_{ijk}) \quad i \in \mathbf{I}^{\mathrm{C}}_{jk}, (j,k) \in \mathbf{N}^{\mathrm{DM}} \tag{3.40a}$$

Note that in Eqs. (3.15b), (3.35a), (3.36a), and (3.40a), postulated components in each node (i.e., $\mathbf{I}^{\mathrm{C}}_{jk}$) are considered. Lastly, Eqs. (3.45) and (3.46) are reformulated as follows:

$$Y^{LK}_{ijk} \leq 1 - Y_{i'jk} + (2X^C_{jk} - Y^T_{jkj'k'} - Y^B_{jkj''k''}) \qquad i', i \in \mathbf{I}^{\mathrm{LK}}_{j'k'j''k''}, i' > i, (j,k,j',k') \in \mathbf{A}^{\mathrm{T}}, (j,k,j'',k'') \in \mathbf{A}^{\mathrm{B}} \tag{3.45a}$$

$$Y^{HK}_{ijk} \leq 1 - Y_{i'jk} + (2X^C_{jk} - Y^T_{jkj'k'} - Y^B_{jkj''k''}) \qquad i', i \in \mathbf{I}^{\mathrm{HK}}_{j'k'j''k''}, i' < i, (j,k,j',k') \in \mathbf{A}^{\mathrm{T}}, (j,k,j'',k'') \in \mathbf{A}^{\mathrm{B}} \tag{3.46a}$$

3.5 Examples

All examples are solved using solver BARON (20.10.16) [55] through GAMS (33.1.0) on a machine with Intel Xeon E5520 processor 2.26 GHz and 16 GB memory. For the stopping criteria, the relative optimality gap is set to 10^{-3}.

3.5.1 Reactor-Distillation Network Synthesis without Recycle

We study an integrated reactor-distillation network synthesis problem. In the reactor network, three alternative reactors carrying out different reactions (i.e., A→B+C, A→C+D, and A→2D) are considered (See **Figure 3.10A**). The postulated components in the distillation network are $\mathbf{I} = \{\mathrm{A}, \mathrm{B}, \mathrm{C}, \mathrm{D}\}$. The source should be separated into pure components (components A∼D are recovered from sink nodes P1∼P4, respectively); thus, bypass streams are not considered. The objective function is to maximize the annualized net profit of the process which is equal to the revenue from products minus the costs of the raw material, reactor, and distillation network. The cost of the distillation network is calculated using total cooling/heating duties (for operational cost) and vapor flow rates (for capital cost). More details (e.g., relative volatilities, cost parameters, objective function, etc.) can be found in the supporting information of the original work [85]. Note that selecting the third reaction can lead to a simpler distillation network because there are only two components to separate (A/D); however, component C, which is a product of the first and second reactors, has a higher price than component D. Therefore, this example illustrates the trade-off between the revenue from products and the separation cost.

The model has 2117 equations and 883 variables with 179 of them being discrete variables. In the optimal solution, which is obtained in 19.84 s, the second reactor (A→C+D) is selected (See **Figure 3.10B**). The optimal profit is $\$1.437 \times 10^6$/yr, where the revenue is $\$3.962 \times 10^6$/yr; the material cost is $\$0.922 \times 10^6$/yr; the reactor cost is $\$0.836 \times 10^6$/yr; and the separation cost is $\$0.767 \times 10^6$/yr. The source is assigned to node (1,1) ($\mathbf{I}_{11}^{\mathrm{C}} = \{\mathrm{A}, \mathrm{B}, \mathrm{C}, \mathrm{D}\}$). Column (1,1) is thermally coupled with column (3,3)

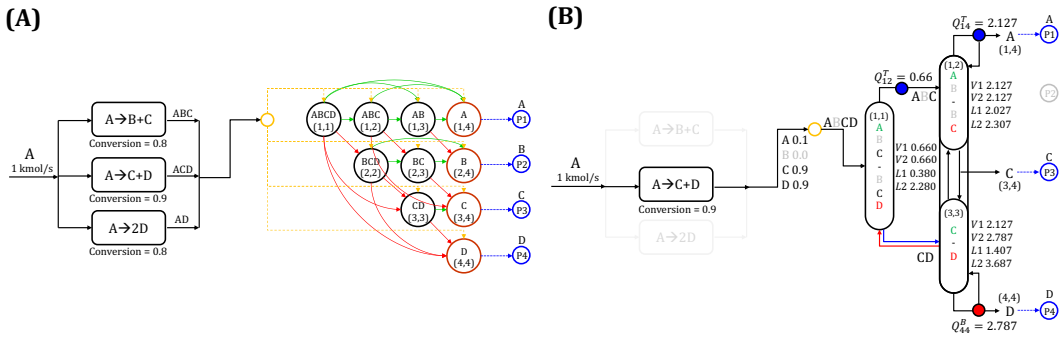

Figure 3.10: (A): Superstructure of example 3.5.1; bypass arcs that cannot be active due to Eq. (3.32) are not shown for clarity; (B): Optimal solution: light/heavy key is represented in green/red; inactive reactors, streams, and components are represented in gray; column (1,1) is thermally coupled with column (3,3) but not with column (1,2); this is because installing the condenser at column (1,1) can reduce the vapor flow rate in the top section (i.e., $V1$) of column (1,2), reducing the capital cost.

but not with column (1,2). Because of the condenser in column (1,1), the vapor flow rate in the top section of column (1,2) can be reduced, reducing the capital cost of column (1,2). If the capital cost is not considered in the objective function, a fully thermally coupled configuration is obtained in the optimal solution. Also, the internal vapor flow rate at the bottom section of column (1,2) is equal to that at the top section of column (3,3) because they are stacked to form a single column.

3.5.2 Reactor-Distillation Network Synthesis with Recycle

We study the synthesis of a process where a feedstock of 0.5 kmol/s of C is used to produce component A or B through three alternative reactions (See **Figure 3.11A**). All reactions require additional reactant D with different feed ratios. Also, the recycle

of components is considered. Notably, to produce the recycle stream, the separation between components C and D might be avoided because they are both reactants. Four postulated components are considered (i.e., $\mathbf{I} = \{\mathrm{A}, \mathrm{B}, \mathrm{C}, \mathrm{D}\}$) with five sink nodes (i.e., P1∼P5). Sink node P5 is assigned to the recycle stream while P1∼P4 are assigned to pure components A∼D, respectively. Also, bypass with thermal coupling is allowed. The objective is to maximize the annualized profit which is equal to the revenue from products minus the costs for raw materials, reactors, and distillation network.

The model has 2227 equations and 933 variables with 189 of them being discrete. The optimal solution, obtained in 1183.9 s, is shown in **Figure 3.11B**. The optimal

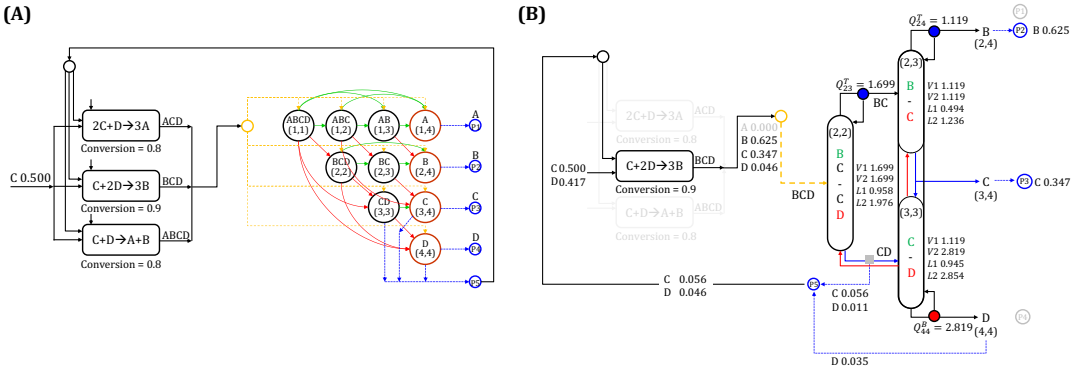

Figure 3.11: (A): Superstructure of example 3.5.2; bypass arcs that cannot be active due to Eq. (3.32) are not shown for clarity; (B): Optimal solution: light/heavy key is represented in green/red; inactive reactors, streams, and nodes are represented in gray; multiple condensers are selected while only one reboiler is selected; recycle stream (i.e., outlet from P5) is produced by mixing the bottom stream from the column in node (2,2) (where sloppy split BC/CD is performed) and pure D; bypass with thermal coupling occurs between columns in node (2,2) and (3,3).

profit is $\$0.703 \times 10^6$/yr, where the revenue is $\$2.206 \times 10^6$/yr; the material cost is

$\$1.059 \times 10^6$/yr; the reactor cost is $\$0.170 \times 10^6$/yr; and the distillation network cost is $\$0.274 \times 10^6$/yr. In the optimal solution, the second reactor is selected, so component A is not present in the source into the distillation network. Accordingly, the source node is assigned to node (2,2) where $\mathbf{I}_{22}^{\mathrm{C}} = \{\mathrm{B}, \mathrm{C}, \mathrm{D}\}$. Notably, a fraction of the bottom stream from column (2,2), which is produced by BC/CD split, is directly sent to final node P5 to produce the recycle stream while columns (2,2) and (3,3) are thermally coupled; this solution is allowed by the extension discussed in section 3.4.1.

3.5.3 Distillation Network Synthesis with Multiple Sources

We study a system with two sources containing hydrocarbon components (See **Figure 3.12A**): {A: 2,4-Dimethyl Pentane, B: 2,2,3,3-Tetra Methyl Butane, C: N-Octane} and {C: N-Octane, D: N-Nonane, E: N-Decane}. The set of postulated components is $\mathbf{I} = \{\mathrm{A}, \mathrm{B}, \mathrm{C}, \mathrm{D}, \mathrm{E}\}$. Sources should be separated into pure components, so five sink nodes (i.e., P1∼P5) are considered. The objective is to minimize the annualized cost.

The resulting model has 3581 equations and 1422 variables with 310 of them being discrete variables. The optimal solution, obtained in 1203.5 s, is shown in **Figure 3.12B** and has an annualized cost of $\$0.339 \times 10^6$/yr. Two sources are assigned to different columns and share the final complex column; the first source with components ABC is separated into AB and BC, which are then sent to the final complex column. The second source, with components CDE, is separated into CD and E, and only the distillate stream (i.e., CD) is sent to the final complex column. When we enforce that the two sources are first mixed, the annualized cost increases significantly (i.e., $\$0.451 \times 10^6$/yr). Thus, this example illustrates the advantage of considering multiple sources.

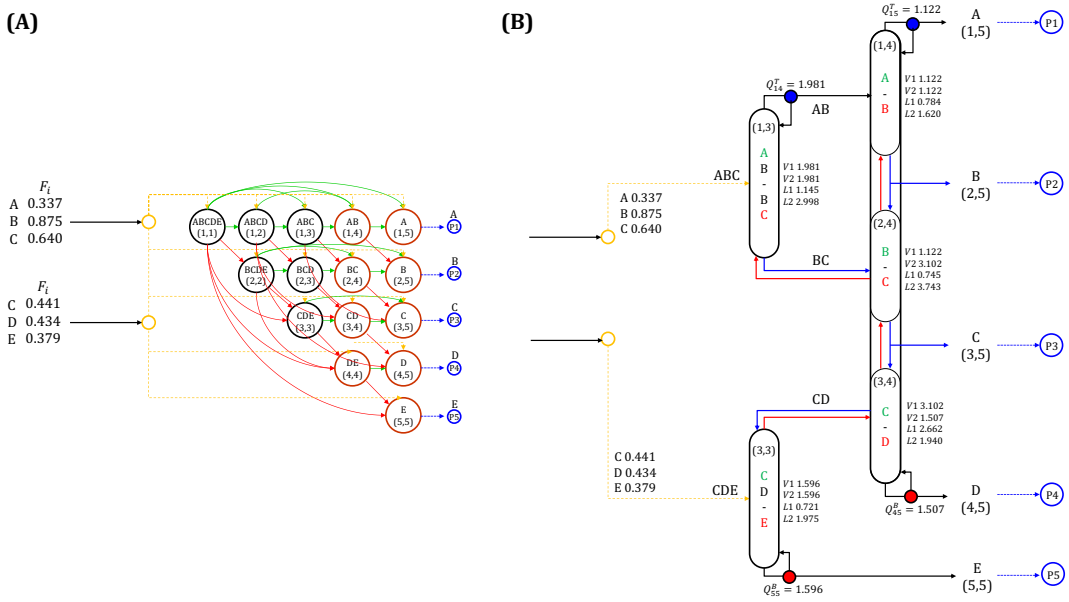

Figure 3.12: (A): Superstructure of example 3.5.3; bypass arcs that cannot be active due to Eq. (3.32) are not shown for clarity; (B): Optimal solution: light/heavy key is represented in green/red; the source with components ABC is separated into AB and BC first and sent to the complex column; the source with components CDE is separated into CD and E, and only the distillate stream (i.e., CD) is sent to the complex column.

3.5.4 Reactor-Distillation Network Synthesis with Multiple Sources

We study the synthesis of a reactor-separation network with a given feedstock (i.e., 1 kmol/s of A and 1 kmol/s of B), where there are two sources into the distillation network from two different reactor networks (See **Figure 3.13**). In the first reactor network, three reactors carrying out alternative reactions (i.e., RXN1: 2A+B→3C, RXN2: A+3B→4D, RXN3: A+B→C+D) are considered, where components C or D can be produced. In the second reactor network, component C can be converted to product D

through two reactors carrying out alternative reactions (i.e., RXN4: 2C→D+E, RXN5: C→D). Notably, adopting RXN5 instead of RXN4 can avoid the production of byproduct E and can achieve a higher conversion ($0.7 > 0.5$), whereas a more expensive catalyst is needed. Thus, between RXN4 and RXN5, there is a trade-off between the separation cost for byproduct E and the catalyst cost. Component C can be produced from the first reactor network via RXN1 and RXN3, or can be purchased with a limited availability ($C \leq 1$ kmol/s). Five postulated components are considered ($\mathbf{I} = \{A, B, C, D, E\}$) with

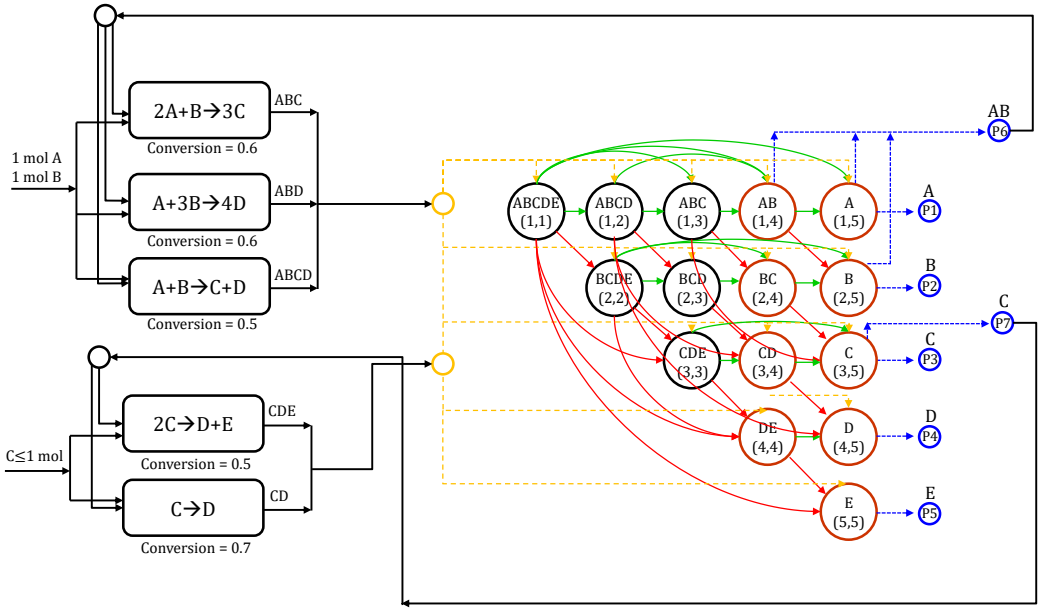

Figure 3.13: Superstructure of example 3.5.4; bypass arcs that cannot be active due to Eq. (3.32) are not shown for clarity.

two source nodes and seven sink nodes (i.e., P1∼P7); sink nodes P1∼P5 are assigned for pure components (i.e., A, B, C, D, and E, respectively) while P6 and P7 are assigned for the recycle streams into the first and the second reactor network, respectively. Notably, for the recycle stream into the first reactor network, the separation between components

A and B might be avoided because they are both reactants. The objective is to maximize the total annualized profit which is equal to the revenue minus the costs for raw materials, reactors, and distillation network.

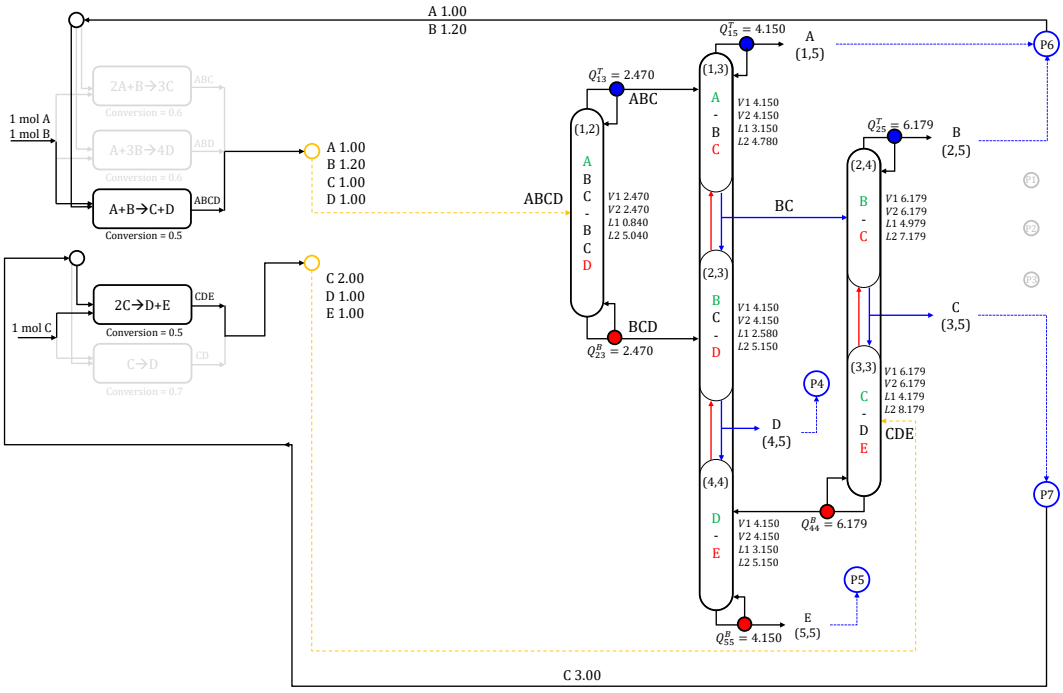

Figure 3.14: Best solution in 72000 s for example 3.5.4. RXN3 and RXN4 are selected, so the effluents contain $\{A, B, C, D\}$ and $\{C, D, E\}$, respectively. The effluent from the first reactor network is sent to node (1,2) while that from the second reactor network is sent to node (3,3).

The model has 3698 equations and 1535 variables with 319 of them being discrete. The model is solved to 6.63% optimality in 72000 s. The best solution (See **Figure 3.14**) is found after 522.64 s. The profit is $\$1.718 \times 10^6$/yr while the revenue is $\$8.855 \times 10^6$/yr; the material cost is $\$3.848 \times 10^6$/yr; the reactor cost is $\$1.979 \times 10^6$/yr; and the separation cost is $\$1.297 \times 10^6$/yr. In the first reactor network, RXN3 is selected, producing the

effluent with components A, B, C, and D. Also, the effluent is sent to node (1,2). In the second reactor network, RXN4 is selected, producing the effluent with components C, D, and E. The effluent is sent to node (3,3). Notably, the effluents from different reactor networks are not mixed because their compositions are vastly different; however, they do share some columns (i.e., column for C/D split) while utilizing thermal couplings, illustrating the advantage of considering multiple sources into the distillation network, which is neglected in most existing works. Note that in this solution, the bypass stream from node (1,4) to sink node P6 is not active because the separation between A/B can be done freely by the vapor flow rates generated for D/E split.

Chapter 4

Distillation Network Synthesis with Graphical Insights[7]

4.1 Motivation

Graphical approaches, where feasible distillation columns (i.e., columns carrying out separation tasks that meet thermodynamics-based constraints) and distillation networks (consisting of distillation columns, mixers, etc.) are represented in a ternary or quaternary diagram [22, 30, 90], have been proposed to solve distillation network synthesis problems. Graphical approaches allow the identification of feasible distillation networks without considering complex mathematical equations. However, they cannot be readily used for optimization because metrics (e.g., total cost) and/or process constraints are not easily representable. Furthermore, systems with more than four components cannot be readily handled.

Simulation- and optimization-based approaches, which rely on models that contain equations describing thermodynamic constraints and unit material/energy balances, have also been proposed. In simulation-based approaches, promising network configurations are simulated and the best configuration is selected [65]. In optimization-based

[7]The contents of this chapter appear in Ryu and Maravelias, *AIChE J.* **2022**

approaches and, in particular, superstructure-based approaches, the optimal network configuration and major operating decisions are identified using an optimization model [38, 51, 52, 60]. Superstructure-based models have not been typically combined with rigorous unit models because the resulting integrated models would be computationally expensive. One potential research avenue therefore is the use of models that can cheaply calculate the cost of a column combined with methods that ensure feasibility of the corresponding separation task. Towards this goal, we propose an approach where graphically-inspired feasibility constraints are combined with simplified surrogate cost models.

4.2 Model Formulation

We outline mathematical models for the distillation column and distillation network.

4.2.1 Distillation Column

We define ordered set $\mathbf{I} = \{\mathrm{A}, \mathrm{B}, ...\}$ to denote components in decreasing order of volatility and set $\mathbf{L}$ to denote distillation columns. For a given feed composition, a composition of the distillate/bottom stream of a column is said to be contained in the feasible region of distillation if it can be achieved by the column. One common approximation to represent feasible regions, usually used in graphical approaches, is based on the fact that a more volatile component is more concentrated in the distillate stream while less concentrated in the bottom stream. Mathematically, this assumption can be compactly

represented as follows,

$$\frac{x^D_{l,i-1}}{x^D_{l,i}} \geq \frac{x^F_{l,i-1}}{x^F_{l,i}} \geq \frac{x^B_{l,i-1}}{x^B_{l,i}} \qquad l \in \mathbf{L}, i \in \mathbf{I} \setminus \{\mathrm{A}\} \tag{4.1}$$

where $x^F_{l,i}/x^D_{l,i}/x^B_{l,i}$ denotes the molar fraction in the feed/distillate/bottom stream. For a

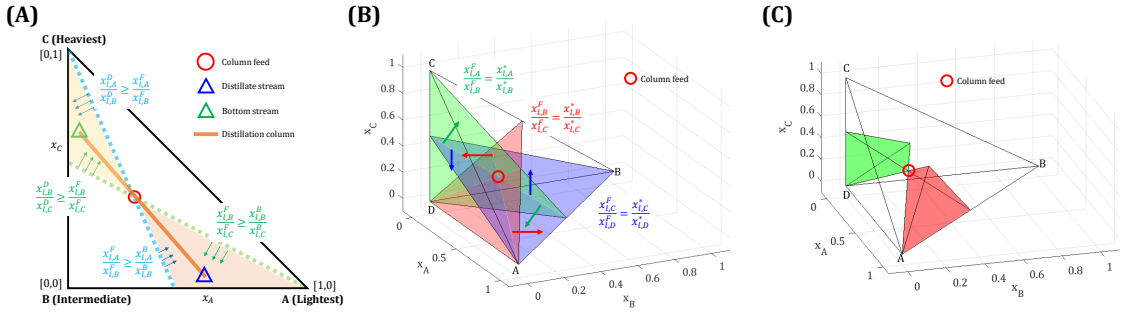

Figure 4.1: Feasible regions for distillate and bottom streams (A): ternary mixture; (B): three hyperplanes associated with Eq. (1) in quaternary mixture; (C): feasible polytopes determined by Eq. (4.1) in quaternary mixture.

ternary mixture, Eq. (4.1) represents four inequalities, resulting in two 2-D polytopes in the ternary diagram. These polytopes approximate feasible regions for the distillate and bottom streams, respectively (See **Figure 4.1A**). This approximation can be generalized for n-component mixtures. For a quaternary mixture, six inequalities from Eq. (4.1) result in two 3-D polytopes in the quaternary diagram (See **Figure 4.1B** and **4.1C**). A special case of Eq. (4.1) was proposed for a subset of pairs of consecutive components depending on pre-defined distillation tasks to improve computational performance [72]. Eq. (4.1) is more general in that it is used for all pairs of consecutive components to enforce feasibility when distillation tasks are not predefined. Additionally, the material balance should be met for each column,

$$F_{l,i} = D_{l,i} + B_{l,i} \qquad l \in \mathbf{L}, i \in \mathbf{I} \tag{4.2}$$

where $F_{l,i}/D_{l,i}/B_{l,i}$ denotes the molar flow rate of the feed/distillate/bottom stream. Molar fractions of components in the streams are calculated as follows:

$$x^F_{l,i} = \frac{F_{l,i}}{\sum_{i' \in \mathbf{I}} F_{l,i'}} \qquad l \in \mathbf{L}, i \in \mathbf{I} \tag{4.3}$$

$$x^D_{l,i} = \frac{D_{l,i}}{\sum_{i' \in \mathbf{I}} D_{l,i'}} \qquad l \in \mathbf{L}, i \in \mathbf{I} \tag{4.4}$$

$$x^B_{l,i} = \frac{B_{l,i}}{\sum_{i' \in \mathbf{I}} B_{l,i'}} \qquad l \in \mathbf{L}, i \in \mathbf{I} \tag{4.5}$$

Next, to calculate the cost, we use a modified version of the Underwood equation [103, 83] to calculate energy demand, which is used as a proxy of the cost.

$$(\sum_{i \in \mathbf{I}} F_{l,i})(1-q) = \sum_{i \in \mathbf{I}} \frac{\alpha_i F_{l,i}}{\alpha_i - \phi_{l,i'-1}} \qquad l \in \mathbf{L}, i' \in \mathbf{I} \setminus \{\mathrm{A}\} \tag{4.6}$$

$$V^D_l \geq \sum_{i \in \mathbf{I}} \frac{\alpha_i D_{l,i}}{\alpha_i - \phi_{l,i'-1}} \qquad l \in \mathbf{L}, i' \in \mathbf{I} \setminus \{\mathrm{A}\} \tag{4.7}$$

$$V^B_l \geq -\sum_{i \in \mathbf{I}} \frac{\alpha_i B_{l,i}}{\alpha_i - \phi_{l,i'-1}} \qquad l \in \mathbf{L}, i' \in \mathbf{I} \setminus \{\mathrm{A}\} \tag{4.8}$$

Parameter q denotes the thermal state of the feed, which we assume as 1 (i.e., saturated liquid); α_i denotes the relative volatility, which can be calculated by the ratio of K-value with respect to the least volatile (i.e., heaviest) component in the feed (i.e., $\alpha_i = K_i/K_{\text{heaviest}}$); $\phi_{l,i}$ denotes the Underwood root satisfying Eq. (4.6); and V^D_l/V^B_l denotes the molar vapor flow rates in the top and bottom sections, respectively. Eq. (4.6) has $|\mathbf{I}| - 1$ roots, and each root is bounded between α_{i-1} and α_i (i.e., $\alpha_{i-1} > \phi_{l,i-1} > \alpha_i, i \in \mathbf{I} \setminus \{\mathrm{A}\}$). We calculate the cost of a distillation column using the vapor flow rate,

$$C^C_l = \mu^H V^B_l + \mu^C V^D_l \qquad l \in \mathbf{L} \tag{4.9}$$

where μ^H and μ^C include both capital and operating costs assuming that: (1) the number of trays (indicative of the difficulty of the separation) and column diameter

increase with the vapor flow rate; (2) the operational costs, which depend primarily on utilities, are proportional to the vapor flow rates. More complex objective functions can be readily considered. Eqs. (4.2)-(4.8) do not enforce thermodynamic constraints on product compositions, so Eq. (4.1) is needed to enforce feasibility.

4.2.2 Distillation Network

An example distillation superstructure is shown in **Figure 4.2**. We briefly present the corresponding model here while details can be found in appendix C (i.e., Eqs. (C.1)-(C.22)). We define set $\mathbf{S}^{\text{IN}}$ to denote inlets into the distillation network, represented as

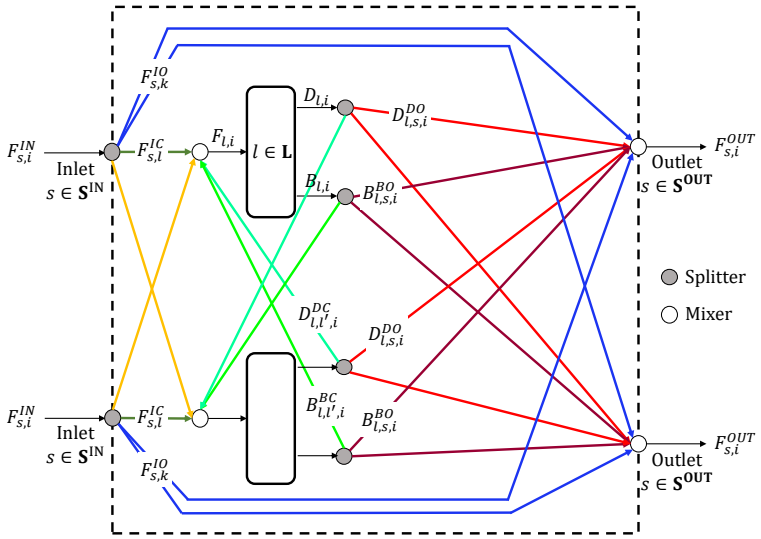

Figure 4.2: Distillation network superstructure with 2 inlet streams and 2 outlet streams. Inlet streams can be sent to columns (orange) or outlets (blue). The distillate and bottom streams of a column can be sent to other columns (green and light green) or outlets (red and dark red). Splitters are represented as gray circle while mixers as white circles.

splitters with incoming flow $F^{IN}_{s,i}$. We define set $\mathbf{S}^{\text{OUT}}$ to denote outlets, represented

as mixers whose outgoing stream, with flow $F_{s,i}^{OUT}$, can go to a final product sink as well as be a recycle or purge stream. Inlet streams can be sent to columns or outlets. We introduce $Y_l \in \{0,1\}$ to denote whether column l is selected. When the column is not selected (i.e., $Y_l = 0$), stream flow rates associated with the column are set to 0. The distillate/bottom stream of a column can be sent to other columns or outlets. For each connection between two units (i.e., inlet-column, inlet-outlet, column-column, and column-outlet), we introduce a binary variable to represent its selection in the optimal solution (See appendix C). The objective is to maximize the profit of the system,

$$Profit = \sum_{s \in \mathbf{S}^{\mathrm{OUT}}} \mu_s^P (\sum_{i \in \mathbf{I}} F_{s,i}^{OUT}) - (\sum_{i \in \mathbf{I}} \mu_i^M \psi_{r,i}^{R,IT}) - \sum_{l \in \mathbf{L}} C_l^C - \tilde{C}^O \tag{4.10}$$

where μ_s^P denotes the price of outlet stream s; $\mu_i^M/\psi_{r,i}^{R,IT}$ denotes the cost/molar flow rate of the raw material; and $\tilde{C}^O$ denotes the total cost of units other than distillation columns (e.g., reactors).

4.3 Illustrative Examples

We use two case studies to show the applicability of the proposed approach. Synthesis models are formulated using Eqs. (4.1)-(4.9) for distillation columns, Eqs. (C.1)-(C.22) for the distillation network, Eqs. (C.23)-(C.25) for the reactor network, and Eq. (4.10) for the objective function. All examples are solved using global optimization solver BARON (21.1.13) [64] through GAMS (34.3.0) on a machine with an Intel i7-9700 processor 3.00 GHz and 16 GB memory. We set the resource limits as 1000 s and 7200 s for the first and the second examples, respectively.

4.3.1 Ternary Mixture

We present the synthesis of a reactor-distillation system. Two reactors carry out different reactions (i.e., R1: A+D→B and R2: A+2D→C), where component D is the limiting reactant, and can be completely converted, in both reactions. The reactor effluents are sent to a two-column distillation network to be separated into recycle streams (A > 80% purity), final products (i.e., B and C with > 95% purity), and a purge stream. The first reactor requires an A:D ratio of 1.1∼1.3 whereas the second reactor requires this ratio to be between 1.3∼1.5. We present two solutions obtained with and without the

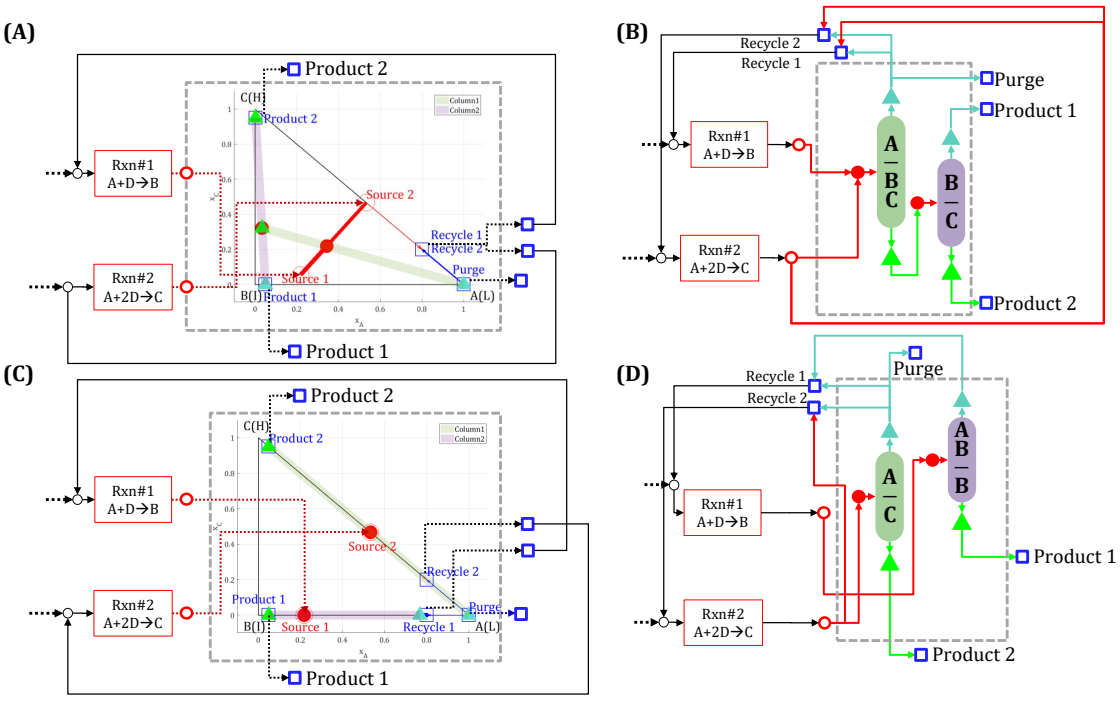

Figure 4.3: (A), (B): best solution with the constraint to enforce reactor outlets to be mixed before distillation network; (C), (D): best solution without the constraint. (red empty circle: inlet stream (i.e., source); red filled circle: column feed; dark green triangle: distillate stream; bright green triangle: bottom stream; blue square: outlet stream)

constraint enforcing reactor effluents to be mixed before the distillation network. The former is what has been typically proposed in the literature, whereas the latter allows the identification of solutions where unnecessary mixing is avoided. The objective is to maximize the profit. In the best solution, with profit/distillation cost of 7.60/13.64, the two effluents are mixed, and the sharp splits between A and BC (i.e., split A/BC) and B and C (i.e., split B/C) are selected, (See **Figure 4.3A** and **4.3B**). In terms of recycle streams, the reactor effluent from the second reactor (for R2) is mixed with the distillate stream of the column carrying out the A/BC split. When the mixing constraint is not used, each inlet is assigned to a different column; the split between components A and B becomes non-sharp (AB/B) (See **Figure 4.3C** and **4.3D**); and component C is separated from A (A/C split) not from B (B/C split), resulting in an easier separation. Thus, the cost is reduced significantly.

4.3.2 Quaternary Mixture

We study the synthesis of a reactor-distillation system potentially resulting in a quaternary mixture to be separated using three columns. Two reactors carry out different reactions (i.e., R1: A+B→C and R2: A+2B→D) with component B being the limiting reactant in both reactions. The conversion of component B is 80% in both reactions. Final products C and D have to meet 95% purity specifications. The first reactor requires the A:B ratio to be between 1.1∼1.3 whereas the second reactor requires this ratio to be between 1.3∼1.5. We start the solution process from a feasible solution with a conventional direct sequence (See appendix C) for the distillation network.

In the best solution (See **Figure 4.4A** and **4.4B**), reactor effluents are split: a

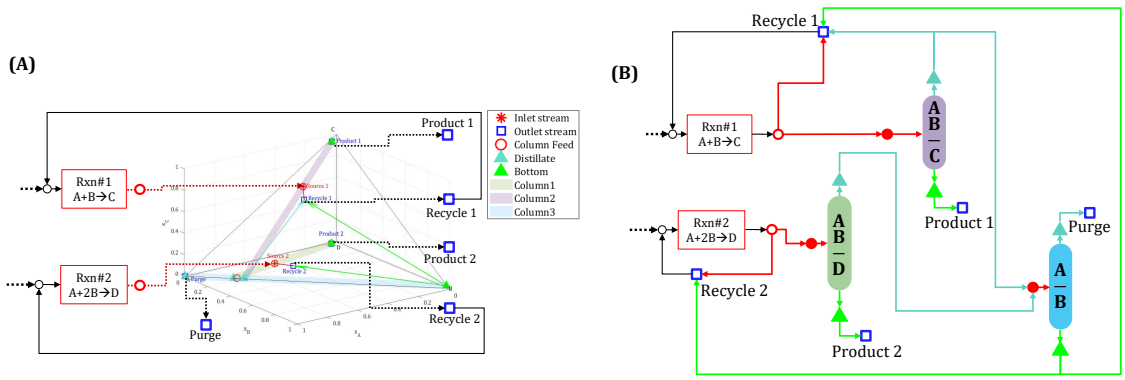

Figure 4.4: (A): best solution in quaternary diagram (B): process configuration of the best solution; red empty circle: inlet stream (i.e., source); red filled circle: column feed; dark green triangle: distillate stream; bright green triangle: bottom stream; blue square: outlet stream

fraction is directly recycled and the remaining fraction is sent to the distillation network. In the distillation network, each reactor effluent is assigned to a different column to obtain the final products in the bottom stream (i.e., C and D, respectively), whereas the distillate streams are sent to the next column to be separated into A, to be purged, and B, to be recycled. To generate recycle streams to the first reactor, the effluent from the first reactor, the distillate stream of the AB/C split column, and the bottom stream of the A/B split column are mixed. This solution would not be readily found using the graphical approach.

Chapter 5

Heat Integration[8]

5.1 Motivation

The area of heat integration has received renewed attention over the last few years due to an emphasis on the design of energy efficient and sustainable processes. Simultaneous synthesis of the process and heat exchanger network can lead to a more energy efficient and sustainable process because the potential benefit from heat integration can be incorporated when determining optimal unit processes and their designs/operations. However, in the process synthesis problem, temperatures, flow rates and even stream classifications can vary depending on the structure of the optimal process, which violate assumptions in most existing Heat Exchanger Network Synthesis (HENS) models. Thus, existing HENS models cannot be readily used for simultaneous synthesis of the process and heat exchanger network.

Accordingly, in this work, we propose mixed-integer linear programming (MILP) models for utility targeting and HENS, building upon some of the concepts introduced in the transportation/transshipment model, addressing the aforementioned limitations. Specifically, the proposed models can handle variable stream flow rates and temperatures, as well as unclassified streams, hence facilitating its integration with process

[8]The contents of this chapter appear in Ryu and Maravelias, *Ind. Eng. Chem. Res.* **2019**

synthesis models. On top of that, with discrete temperature grids, the models remain linear, leading to significantly more effective integrated synthesis-HENS models. Furthermore, the proposed HENS model yields a detailed HEN configuration, which is not available in targeting models.

5.2 Model Formulation

The proposed models are formulated based on a discrete temperature grid framework [6, 47]. The problem statement is as follows.

1. A set of process streams to be heated or cooled is given.
2. Process streams have *variable* inlet/outlet temperatures and flow rates. Also, the classification of the streams may be *undefined*.
3. A range of stream inlet/outlet temperatures and flow rates are given.
4. Temperatures and costs of utilities are fixed and known.
5. Minimum temperature difference (ΔT^{min}) is given.

The objective for utility targeting is to calculate minimum utility cost, and the objective for HENS is to find the optimal HEN that minimizes the total annualized cost (i.e., operating + investment cost).

5.2.1 Projection of Temperature to Discrete Grid

First, the temperature grid needs to be constructed. For the base case, we consider an *uniform grid* with the same length of intervals. After finding the highest temperature

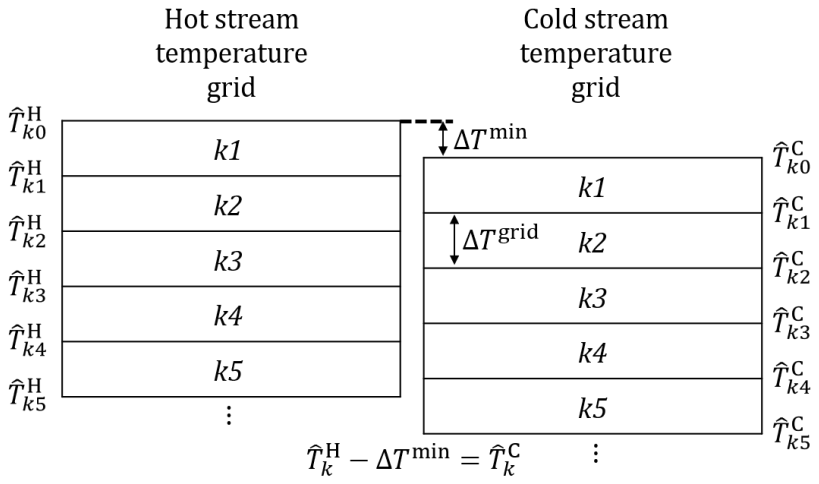

Figure 5.1: Hot/cold stream temperature grids

(e.g., high pressure steam), we can determine the temperature difference in each interval (ΔT^{grid}) and the number of intervals so that all stream inlet/outlet temperatures can be mapped onto the grid. The cold stream temperature grid is adjusted by the minimum temperature difference (ΔT^{min}) to guarantee thermodynamic feasibility of heat exchanges. Since the selection of number, and secondarily size, of intervals affects solution quality due to the projection of stream temperatures onto the discrete grid, it is important to carefully determine the size/number of intervals to achieve accurate mapping. If this leads to a large number of intervals, a non-uniform grid, discussed later, can be used. The temperature grids are illustrated in **Figure 5.1**. The set of interval boundaries is defined as $\mathbf{K}$, and the set of intervals as $\mathbf{K}^{\mathrm{I}}$. The temperature of each interval boundary ($\hat{T}^H_k, \hat{T}^C_k$) is given depending on the classification of the grid. Since each interval boundary has its corresponding temperature, we use boundary and boundary temperature interchangeably. Next, we project stream data onto the grid so that feasibility is ensured. We define the set of streams as $\mathbf{S}$. For each stream, we introduce

twelve parameters for the projection. These parameters, at the end of this step, will be used to generate subsets of interval boundaries onto which the inlet/outlet temperature of a stream can be assigned to.

Six parameters are used for inlet temperatures. First, $\phi_{s,k}^{H,IN,UP}$ is set to 1 when $\hat{T}_k^H$ is the feasible boundary temperature closest to the upper bound on the inlet temperature of stream s ($T_s^{IN,UP}$) as shown in Eq. (5.1). Similarly, $\phi_{s,k}^{H,IN,LO}$ is set to 1 if $\hat{T}_k^H$ is the closest temperature to the lower bound on the inlet temperature of stream s ($T_s^{IN,LO}$) as shown in Eq. (5.2). Note that the direction of the inequality is opposite for the upper bound and the lower bound.

$$\phi_{s,k}^{H,IN,UP} = \begin{cases} 1 & \text{if } k = \arg\min_{k'} \|\hat{T}_{k'}^H - T_s^{IN,UP}\| \\ & \quad \text{s.t.} \hat{T}_{k'}^H \leq T_s^{IN,UP} \qquad s \in \mathbf{S}, k \in \mathbf{K} \\ 0 & \text{otherwise} \end{cases} \tag{5.1}$$

$$\phi_{s,k}^{H,IN,LO} = \begin{cases} 1 & \text{if } k = \arg\min_{k'} \|\hat{T}_{k'}^H - T_s^{IN,LO}\| \\ & \quad \text{s.t.} \hat{T}_{k'}^H \geq T_s^{IN,LO} \qquad s \in \mathbf{S}, k \in \mathbf{K} \\ 0 & \text{otherwise} \end{cases} \tag{5.2}$$

Parameter $\psi_{s,k}^{H,IN}$ is used to represent the feasibility of the assignment of the inlet temperature of stream s onto the hot stream grid interval boundary k. The assignment is possible only to the boundaries between the boundary with $\psi_{s,k}^{H,IN,UP} = 1$ and that with $\psi_{s,k}^{H,IN,LO} = 1$. Then, parameter $\psi_{s,k}^{H,IN}$ is calculated as follows:

$$\psi_{s,k}^{H,IN} = \phi_{s,k}^{H,IN,UP} + \psi_{s,k-1}^{H,IN} - \phi_{s,k-1}^{H,IN,LO} \quad s \in \mathbf{S}, k \in \mathbf{K} \tag{5.3}$$

In **Figure 5.2**, the inlet data of stream s are projected onto the grid, and ($\phi_{s,\mathrm{k3}}^{H,IN,UP}$,

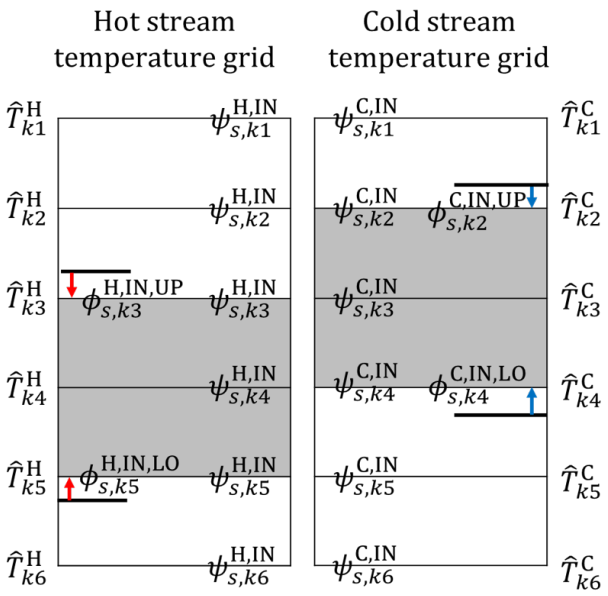

Hot temperature grid assignment	k1	k2	k3	k4	k5	k6
$\phi^{H,IN,UP}_{s,k}$	-	-	1	-	-	
$\phi^{H,IN,LO}_{s,k}$	-	-	-	-	1	
$\psi^{H,IN}_{s,k}$	-	-	1	1	1	

Hot temperature grid assignment	k1	k2	k3	k4	k5	k6
$\phi^{C,IN,UP}_{s,k}$	-	1	-	-	-	
$\phi^{C,IN,LO}_{s,k}$	-	-	-	1	-	
$\psi^{C,IN}_{s,k}$	-	1	1	1	-	

Figure 5.2: Projection of stream data onto the grids (5 intervals are selected for illustration purposes.

$\phi^{H,IN,LO}_{s,\mathrm{k5}}$), ($\phi^{C,IN,UP}_{s,\mathrm{k2}}, \phi^{C,IN,LO}_{s,\mathrm{k4}}$) are activated. Thus, interval boundaries ($\mathrm{k3}, \mathrm{k4}, \mathrm{k5}$) are available for the inlet temperature of stream s as a hot stream, and ($\mathrm{k2}, \mathrm{k3}, \mathrm{k4}$) as a cold stream, where $\psi^{H,IN}_{s,k}, \psi^{C,IN}_{s,k}$ are activated. Remaining parameters for the cold stream grid and outlet temperatures are determined similarly. The assignment onto the cold stream grid is exactly the same, except $\hat{T}^C_k$ is used instead of $\hat{T}^H_k$ (See **Appendix D.1** for more information). After the projection step, subsets of interval boundary that the inlet/outlet temperature of each stream can be assigned to (i.e., $\mathbf{K}^{\mathrm{F,H,IN}}_s, \mathbf{K}^{\mathrm{F,H,OUT}}_s, \mathbf{K}^{\mathrm{F,C,IN}}_s, \mathbf{K}^{\mathrm{F,C,OUT}}_s$) are obtained, referred to as *feasible mapping set*

$$\mathbf{K}^{\mathrm{F,H,IN}}_s = \{k | \psi^{H,IN}_{s,k} = 1, k \in \mathbf{K}\} \quad s \in \mathbf{S} \tag{5.4}$$

$$\mathbf{K}^{\mathrm{F,H,OUT}}_s = \{k | \psi^{H,OUT}_{s,k} = 1, k \in \mathbf{K}\} \quad s \in \mathbf{S} \tag{5.5}$$

$$\mathbf{K}^{\mathrm{F,C,IN}}_s = \{k | \psi^{C,IN}_{s,k} = 1, k \in \mathbf{K}\} \quad s \in \mathbf{S} \tag{5.6}$$

$$\mathbf{K}_s^{\mathrm{F,C,OUT}} = \{k|\psi_{s,k}^{C,OUT} = 1, k \in \mathbf{K}\} \quad s \in \mathbf{S} \tag{5.7}$$

5.2.2 Utility Targeting Model

Assignment of inlet/outlet temperature onto grid

For a simple analysis, utility targeting can be a powerful tool for the design of the plant. The utility targeting model that we will propose below can be readily used to find the minimum utility demand when there are unclassified streams and/or streams that have variable temperatures and flow rates.

We introduce binary variables (U_s^H, U_s^C) for stream classification (hot, cold). In the superstructure process synthesis problem, streams that are connected to a process unit $u \in \mathbf{U}$, are activated and classified if and only if the process unit is selected. We define subset $\mathbf{S}_u^{\mathrm{U}}$ which includes the streams connected to unit u. If Y_u^U denotes the selection of process unit u, we have:

$$U_s^H + U_s^C = Y_u^U \quad s \in \mathbf{S}_u^{\mathrm{U}}, u \in \mathbf{U} \tag{5.8}$$

We introduce binary variables $(Y_{s,k}^{IN,H}, Y_{s,k}^{OUT,H}, Y_{s,k}^{IN,C}, Y_{s,k}^{OUT,C})$, which are set to 1 when the inlet/outlet temperature of stream s is assigned to interval boundary k. We enforce that the inlet/outlet temperature of a stream can be only assigned to a temperature boundary in the feasible mapping set,

$$\sum_{k\in\mathbf{K}} Y_{s,k}^{IN,H} = \begin{cases} U_s^H & k \in \mathbf{K}_s^{\mathrm{F,H,IN}} \\ 0 & \text{otherwise} \end{cases} \quad s \in \mathbf{S} \tag{5.9}$$

$$\sum_{k\in\mathbf{K}} Y_{s,k}^{IN,C} = \begin{cases} U_s^C & k \in \mathbf{K}_s^{\mathrm{F,H,IN}} \\ 0 & \text{otherwise} \end{cases} \quad s \in \mathbf{S} \tag{5.10}$$

$$\sum_{k\in\mathbf{K}} Y_{s,k}^{OUT,H} = \begin{cases} U_s^H & k \in \mathbf{K}_s^{\mathrm{F,H,OUT}} \\ 0 & \text{otherwise} \end{cases} \quad s \in \mathbf{S} \tag{5.11}$$

$$\sum_{k\in\mathbf{K}} Y_{s,k}^{OUT,C} = \begin{cases} U_s^C & k \in \mathbf{K}_s^{\mathrm{F,C,OUT}} \\ 0 & \text{otherwise} \end{cases} \quad s \in \mathbf{S} \tag{5.12}$$

where the summation of the binary variables in the feasible mapping set is equal to the classification variable (U_s^H/U_s^C), otherwise 0. Then, we can calculate the inlet/outlet temperature as follows:

$$T_s^{IN} = \sum_{k\in\mathbf{K}} (Y_{s,k}^{IN,H}\hat{T}_k^H + Y_{s,k}^{IN,C}\hat{T}_k^C) \quad s \in \mathbf{S} \tag{5.13}$$

$$T_s^{OUT} = \sum_{k\in\mathbf{K}} (Y_{s,k}^{OUT,H}\hat{T}_k^H + Y_{s,k}^{OUT,C}\hat{T}_k^C) \quad s \in \mathbf{S} \tag{5.14}$$

For the unclassified streams, the sign of the difference between the inlet and outlet temperatures is determined by the classification of the stream,

$$T_s^{IN} - T_s^{OUT} \leq \frac{\Delta T_s^{max}}{2}(1 - U_s^C + U_s^H) \quad s \in \mathbf{S} \tag{5.15}$$

$$T_s^{IN} - T_s^{OUT} \geq \frac{\Delta T_s^{max}}{2}(-1 - U_s^C + U_s^H) \quad s \in \mathbf{S} \tag{5.16}$$

where parameter ΔT_s^{max} is the maximum absolute difference between the inlet and outlet temperatures of stream s.

Binary variable $Z_{s,k}^H/Z_{s,k}^C$ represents which temperature intervals are spanned by the stream; they are activated when interval $k \in \mathbf{K}^{\mathrm{I}}$ is between boundaries that are selected

Figure 5.3: Assignment of binary variables for inlet/outlet temperature and corresponding spanned intervals

for the inlet and outlet temperature of stream s, which is illustrated in **Figure 5.3**.

$$Z^{H}_{s,k} = Y^{IN,H}_{s,k-1} + Z^{H}_{s,k-1} - Y^{OUT,H}_{s,k-1} \quad s \in \mathbf{S}, k \in \mathbf{K}^{\mathrm{I}} \tag{5.17}$$

$$Z^{C}_{s,k} = -Y^{IN,C}_{s,k-1} + Z^{C}_{s,k-1} + Y^{OUT,C}_{s,k-1} \quad s \in \mathbf{S}, k \in \mathbf{K}^{\mathrm{I}} \tag{5.18}$$

In the left side of **Figure 5.3**, stream s is determined as a hot stream with $T^{H}_{\mathrm{k2}}/T^{H}_{\mathrm{k4}}$ as its inlet/outlet temperature, so $Z^{H}_{s,\mathrm{k3}}$ and $Z^{H}_{s,\mathrm{k4}}$ are activated, meaning that interval k3 and k4 are spanned by the stream. In the left side of **Figure 5.3**, stream s becomes a cold stream and span intervals k2, k3, and k4.

Calculation of flow rate, surplus heat, and heat requirement

We define a subset of process streams, $\mathbf{S}^{\mathrm{P}}$, not including utility streams. The flow rate of each process stream is disaggregated into three components $(F^{H}_{s,k}, F^{C}_{s,k}, \tilde{F}_{s,k})$, where $F^{H}_{s,k}/F^{C}_{s,k}$ denotes the flow rate of process stream s as a hot/cold stream in the interval k while $\tilde{F}_{s,k}$ is a slack variable. Note that we use flow rate and heat capacity of a stream interchangeably because, in many cases, heat capacity is given for chemical plant stream.

$$F_s = F^{H}_{s,k} + F^{C}_{s,k} + \tilde{F}_{s,k} \quad s \in \mathbf{S}^{\mathrm{P}}, k \in \mathbf{K}^{\mathrm{I}} \tag{5.19}$$

When stream s spans interval k of the hot/cold stream grid, variables $F^H_{s,k}/F^C_{s,k}$ can be nonzero (Eq. (5.20)/(5.21)), while $\tilde{F}_{s,k}$ is deactivated by Eq. (5.22)/(5.23).

$$F^H_{s,k} \leq \overline{\delta}_s Z^H_{s,k} \quad s \in \mathbf{S}^{\mathrm{P}}, k \in \mathbf{K}^{\mathrm{I}} \tag{5.20}$$

$$F^C_{s,k} \leq \overline{\delta}_s Z^C_{s,k} \quad s \in \mathbf{S}^{\mathrm{P}}, k \in \mathbf{K}^{\mathrm{I}} \tag{5.21}$$

$$\tilde{F}_{s,k} \leq \overline{\delta}_s (1 - Z^H_{s,k}) \quad s \in \mathbf{S}^{\mathrm{P}}, k \in \mathbf{K}^{\mathrm{I}} \tag{5.22}$$

$$\tilde{F}_{s,k} \leq \overline{\delta}_s (1 - Z^C_{s,k}) \quad s \in \mathbf{S}^{\mathrm{P}}, k \in \mathbf{K}^{\mathrm{I}} \tag{5.23}$$

Thus, the flow rate of stream s (i.e., F_s) becomes identical with either $F^H_{s,k}$ or $F^C_{s,k}$ due to Eq. (5.19). On the other hand, if stream s does not span interval k, $F_s = \tilde{F}_{s,k}$ holds. Parameters $\overline{\delta}_s$ denotes the upper bound on flow rate of stream s. The heating/cooling duty in each interval (i.e., Q^H_k/Q^C_k) is calculated using the specific heat capacity (λ_s), disaggregated flow rate ($F^H_{s,k}/F^C_{s,k}$), and temperature change within the interval:

$$Q^H_k = \textstyle\sum_{s \in \mathbf{S}^{\mathrm{P}}} [(\hat{T}^H_{k-1} - T^H_k) F^H_{s,k} \lambda_s] + Q^{HU}_k \quad k \in \mathbf{K}^{\mathrm{I}} \tag{5.24}$$

$$Q^C_k = \textstyle\sum_{s \in \mathbf{S}^{\mathrm{P}}} [(\hat{T}^C_{k-1} - T^C_k) F^C_{s,k} \lambda_s] + Q^{CU}_k \quad k \in \mathbf{K}^{\mathrm{I}} \tag{5.25}$$

where Q^{HU}_k/Q^{CU}_k is hot/cold utility at each interval. Notably, with the discrete temperature grid, Eqs. (5.24) and (5.25) are linear even when flow rates are variable.

Finally, the residual heat in each interval is calculated,

$$R_k = R_{k-1} + Q^H_k - Q^C_k \quad k \in \mathbf{K}^{\mathrm{I}} \tag{5.26}$$

The first interval does not have any residual heat from the interval above (i.e., $R_0 = 0$), and the last interval does not have any residual heat into the interval below (i.e., $R_{\|\mathbf{K}\|} = 0$).

$$R_k = 0 \quad k = 0, \|\mathbf{K}\| \tag{5.27}$$

The objective for utility targeting is to minimize the cost of utility usage,

$$C = \mu^{HU} \sum_{k \in \mathbf{K}^{\mathrm{I}}} Q_k^{HU} + \mu^{CU} \sum_{k \in \mathbf{K}^{\mathrm{I}}} Q_k^{CU} \tag{5.28}$$

where μ^{HU}/μ^{CU} is the parameter cost for the hot/cold utility.

5.2.3 Heat Exchanger Network Synthesis Model

Map heat exchange onto grid

The proposed framework can be extended to HENS in the presence of unclassified streams with variable flow rates/temperatures. In HENS, temperatures at which streams enter/exit heat exchangers need to be determined. We refer to the entry/exit of a stream as the start/end of a heat exchanger. Binary variables $V_{s,k,s'}^{S,H}/V_{s',k',s}^{S,C}$ are introduced to denote the start of a heat exchanger; $V_{s,k,s'}^{S,H} = 1$ if a heat exchanger between hot stream s and cold s' starts at interval k for the hot stream. Similarly, $V_{s',k',s}^{S,C} = 1$ if a heat exchanger between cold stream s' and hot s starts at interval k' for the cold stream. Binary variables $V_{s,k,s'}^{S,H}/V_{s',k',s}^{S,C}$ are also introduced to denote the end of a heat exchanger.

To denote intervals spanned by a heat exchanger, binary variables $X_{s,k,s'}^{H}/X_{s',k',s}^{C}$ are introduced,

$$X_{s,k,s'}^{H} = X_{s,k-1,s'}^{H} + V_{s,k,s'}^{S,H} - V_{s,k-1,s'}^{E,H} \quad s, s' \in \mathbf{S}, k \in \mathbf{K}^{\mathrm{I}} \tag{5.29}$$

$$X_{s',k'-1,s}^{C} = X_{s',k',s}^{C} + V_{s',k'-1,s}^{S,C} - V_{s',k',s}^{E,C} \quad s, s' \in \mathbf{S}, k \in \mathbf{K}^{\mathrm{I}} \tag{5.30}$$

where $X_{s,k,s'}^{H}/X_{s',k',s}^{C}$ is set to 1 when the exchanger between hot stream s and cold stream s' spans interval k/k' of the hot/cold stream. For example, in **Figure 5.3**, a heat exchanger starts at interval k2 and ends at interval k3 of the hot stream grid, denoted by $X_{s,\mathrm{k2},s'}^{H} = 1$ and $X_{s,\mathrm{k3},s'}^{H} = 1$. Likewise, in the cold stream side, $X_{s',k',s}^{C} = 1$ at

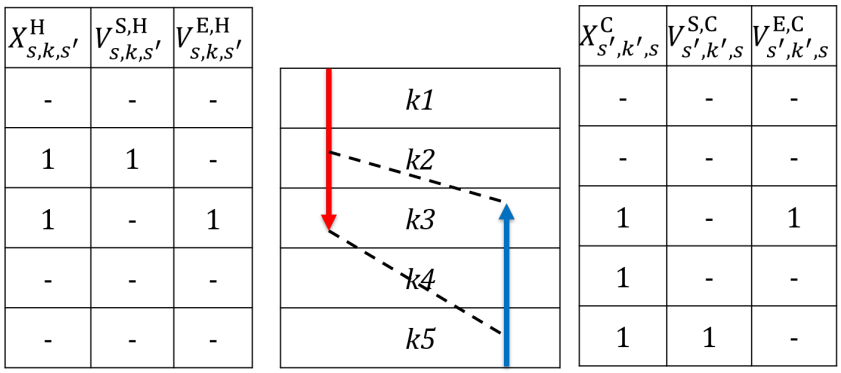

Figure 5.4: Start, end, and spanning of heat exchanger

intervals k3, k4, and k5 because the exchanger starts at k5 and ends at k3. We ensure that the number of matches between a pair of hot and cold streams are the same in both sides,

$$\sum_{k\in\mathbf{K}^{\mathrm{I}}} V^{S,H}_{s,k,s'} = \sum_{k'\in\mathbf{K}^{\mathrm{I}}} V^{S,C}_{s',k',s} \quad s,s' \in \mathbf{S} \tag{5.31}$$

and that no heat exchanger starts and ends at the same interval.

$$V^{S,H}_{s,k,s'} + V^{E,H}_{s,k,s'} \leq 1 \quad s,s' \in \mathbf{S}^{\mathrm{P}}, k \in \mathbf{K}^{\mathrm{I}} \tag{5.32}$$

$$V^{S,C}_{s',k',s} + V^{E,C}_{s',k',s} \leq 1 \quad s,s' \in \mathbf{S}^{\mathrm{P}}, k \in \mathbf{K}^{\mathrm{I}} \tag{5.33}$$

Eqs. (5.32) and (5.33) are needed to ensure thermodynamic feasibility of heat exchange. For utilities, these constraints are not needed because the start/end temperature is already known.

Heat duty calculation

For HENS, instead of residual heat, we introduce *available enthalpy* ($H^{H}_{s,k}$) and *required enthalpy* ($H^{C}_{s,k}$), and replace Eqs. (5.24) - (5.27) to Eqs. (5.34) and (5.35),

$$H^{H}_{s,k} = (\hat{T}^{H}_{k-1} - \hat{T}^{H}_{k})\lambda_s F^{H}_{s,k} = \Delta T^{grid}\lambda_s F^{H}_{s,k} \quad s \in \mathbf{S}^{\mathrm{P}}, k \in \mathbf{K}^{\mathrm{I}} \tag{5.34}$$

$$H^C_{s',k'} = (\hat{T}^C_{k'-1} - \hat{T}^C_{k'})\lambda_{s'} F^C_{s',k'} = \Delta T^{grid}\lambda_{s'} F^C_{s',k'} \quad s' \in \mathbf{S}^{\mathrm{P}}, k' \in \mathbf{K}^{\mathrm{I}} \tag{5.35}$$

where λ_s denotes the specific heat capacity of stream s; $Q^{EX}_{s,k,s',k'}$ denotes the amount of heat exchanged between stream s at interval k and stream s' at interval k'. We define the cumulative transferred heat $\bar{Q}^H_{s,k,s'}$ and cumulative received heat $\bar{Q}^C_{s',k',s}$,

$$\bar{Q}^H_{s,k,s'} = \textstyle\sum_{k' \geq k} Q^{EX}_{s,k,s',k'} \quad s, s' \in \mathbf{S}, k \in \mathbf{K}^{\mathrm{I}} \tag{5.36}$$

$$\bar{Q}^C_{s',k',s} = \textstyle\sum_{k \leq k'} Q^{EX}_{s,k,s',k'} \quad s, s' \in \mathbf{S}, k \in \mathbf{K}^{\mathrm{I}} \tag{5.37}$$

where $\bar{Q}^H_{s,k,s'}$ is the total amount of heat transferred from hot stream s at interval k to cold stream s'; $\bar{Q}^C_{s',k',s}$ is the total amount of heat received by cold stream s' in interval k' from hot stream s. Note that heat should be sent to the same interval or intervals below while heat should be received from the same interval or intervals above. For unclassified streams, additional constraints are imposed to prevent heat exchange hot-hot and cold-cold streams (See section 5.2.3).

The cumulative transferred/received heat is (de)activated by binary variables for interval spanning (i.e., $X^H_{s,k,s'}/X^C_{s',k',s}$),

$$\underline{\epsilon} X^H_{s,k,s'} \leq \bar{Q}^H_{s,k,s'} \leq \lambda_s \overline{\delta}_s (\hat{T}^H_{k-1} - \hat{T}^H_k) X^H_{s,k,s'} \quad s, s' \in \mathbf{S}, k \in \mathbf{K}^{\mathrm{I}} \tag{5.38}$$

$$\underline{\epsilon} X^C_{s',k',s} \leq \bar{Q}^C_{s',k',s} \leq \lambda_{s'} \overline{\delta}_{s'} (\hat{T}^C_{k'-1} - \hat{T}^C_{k'}) X^C_{s',k',s} \quad s, s' \in \mathbf{S}, k \in \mathbf{K}^{\mathrm{I}} \tag{5.39}$$

where $\underline{\epsilon}$ is a lower bound on the cumulative heat. Eq. (5.38)/(5.39) enforces that cumulative transferred/received heat is deactivated when the corresponding interval is not spanned by the heat exchanger between hot stream s and cold stream s', denoted by $X^H_{s,k,s'} = 0/X^C_{s',k,s} = 0$. Finally, available/required enthalpy is satisfied through heat exchange with process streams or utilities,

$$H^H_{s,k} = \textstyle\sum_{s' \neq s} \bar{Q}^H_{s,k,s'} \quad s \in \mathbf{S}, k \in \mathbf{K}^{\mathrm{I}} \tag{5.40}$$

$$H^C_{s',k'} = \sum_{s \neq s'} \bar{Q}^C_{s',k',s} \quad s' \in \mathbf{S}, k' \in \mathbf{K}^{\mathrm{I}} \tag{5.41}$$

Forbidden matches

We ensure that heat exchange between hot-hot or cold-cold is forbidden. Stream s can transfer heat from interval k to stream s' only if stream s spans interval k as a hot stream (i.e., $Z^H_{s,k} = 1$) and stream s' is a cold stream (i.e., $U^C_{s'} = 1$).

$$X^H_{s,k,s'} \leq Z^H_{s,k} \quad s, s' \in \mathbf{S}, k \in \mathbf{K}^{\mathrm{I}} \tag{5.42}$$

$$X^H_{s,k,s'} \leq U^C_{s'} \quad s, s' \in \mathbf{S}, k \in \mathbf{K}^{\mathrm{I}} \tag{5.43}$$

Similarly, stream s' can receive heat at interval k' from stream s only if stream s' spans interval k' as a cold stream (i.e., $Z^C_{s',k'} = 1$) and stream s is a hot stream (i.e., $Z^H_s = 1$),

$$X^C_{s',k',s} \leq Z^C_{s',k'} \quad s, s' \in \mathbf{S}, k' \in \mathbf{K}^{\mathrm{I}} \tag{5.44}$$

$$X^C_{s',k',s} \leq U^H_s \quad s, s' \in \mathbf{S}, k \in \mathbf{K}^{\mathrm{I}} \tag{5.45}$$

Flow rates

Flow rates of streams in each heat exchanger need to be tracked if *stream split*, meaning that a stream is split into multiple sub-streams and sent to different heat exchangers, is considered. We introduce binary variables $W^H_{s,k,s'}/W^C_{s',k',s}$ to model stream split; when hot stream s at interval k exchanges heat with multiple streams s' and s'', then $W^H_{s,k,s'}$ and $W^H_{s,k,s''}$ are set to 1. Stream split can occur only when the stream spans the corresponding interval,

$$W^H_{s,k,s'} \leq X^H_{s,k,s'} \quad s, s' \in \mathbf{S}^{\mathrm{P}}, k \in \mathbf{K}^{\mathrm{I}} \tag{5.46}$$

$$W^C_{s',k',s} \leq X^C_{s',k',s} \quad s, s' \in \mathbf{S}^{\mathrm{P}}, k' \in \mathbf{K}^{\mathrm{I}} \tag{5.47}$$

Then, we further decompose the disaggregated flow rate ($F^{H}_{s,k}/F^{C}_{s',k'}$) into the flow rate of the stream in each heat exchanger ($F^{I,H}_{s,k,s'}/F^{I,C}_{s',k',s}$) and the slack variable ($\tilde{F}^{SP,H}_{s,k,s'}/\tilde{F}^{SP,C}_{s',k',s}$),

$$F^{H}_{s,k} = F^{I,H}_{s,k,s'} + \tilde{F}^{SP,H}_{s,k,s'} \quad s, s' \in \mathbf{S}^{\mathrm{P}}, k \in \mathbf{K}^{\mathrm{I}} \tag{5.48}$$

$$F^{C}_{s',k'} = F^{I,C}_{s',k',s} + \tilde{F}^{SP,C}_{s',k',s} \quad s, s' \in \mathbf{S}^{\mathrm{P}}, k' \in \mathbf{K}^{\mathrm{I}} \tag{5.49}$$

where the flow rate in the heat exchanger can have a non-zero value when there is a heat exchanger (i.e., $X^{H}_{s,k,s'} = 1/X^{C}_{s',k',s} = 1$) and the slack variable is deactivated if the stream is not split (i.e., $W^{H}_{s,k,s'} = 0/W^{C}_{s',k',s} = 0$).

$$F^{I,H}_{s,k,s'} \leq \overline{\delta}_{s} X^{H}_{s,k,s'} \quad s, s' \in \mathbf{S}^{\mathrm{P}}, k \in \mathbf{K}^{\mathrm{I}} \tag{5.50}$$

$$F^{I,C}_{s',k',s} \leq \overline{\delta}_{s'} X^{C}_{s',k',s} \quad s, s' \in \mathbf{S}^{\mathrm{P}}, k' \in \mathbf{K}^{\mathrm{I}} \tag{5.51}$$

$$\underline{\delta}_{s} W^{H}_{s,k,s'} \leq \tilde{F}^{SP,H}_{s,k,s'} \leq \overline{\delta}_{s}(1 - X^{H}_{s,k,s'} + W^{H}_{s,k,s'}) \quad s, s' \in \mathbf{S}^{\mathrm{P}}, k \in \mathbf{K}^{\mathrm{I}} \tag{5.52}$$

$$\underline{\delta}_{s'} W^{C}_{s',k',s} \leq \tilde{F}^{SP,C}_{s',k',s} \leq \overline{\delta}_{s'}(1 - X^{C}_{s',k',s} + W^{C}_{s',k',s}) \quad s, s' \in \mathbf{S}^{\mathrm{P}}, k' \in \mathbf{K}^{\mathrm{I}} \tag{5.53}$$

Parameter $\underline{\delta}_{s}$ denotes a lower bound on the flow rate in the heat exchanger. When the hot stream s has only one heat exchanger at interval k, which exchanges heat with cold stream s' (i.e., $X^{H}_{s,k,s'} = 1$ and $W^{H}_{s,k,s'} = 0$), the flow rate in the heat exchanger is equal to the disaggregated flow rate (i.e., $F^{H}_{s,k} = F^{I,H}_{s,k,s'}$). On the other hand, if the stream splits, the slack variable is enforced to be positive, making the flow rate in each heat exchanger less than the disaggregated flow rate. When there is no heat exchanger (i.e., $X^{H}_{s,k,s'}/X^{C}_{s',k',s} = 0$), then the slack variable is equal to the disaggregated flow rate.

We enforce flow rate balances between consecutive intervals,

$$F^{I,H}_{s,k,s'} = F^{I,H}_{s,k-1,s'} + \tilde{F}^{S,H}_{s,k,s'} - \tilde{F}^{E,H}_{s,k-1,s'} \quad s, s' \in \mathbf{S}^{\mathrm{P}}, k \in \mathbf{K}^{\mathrm{I}} \tag{5.54}$$

$$F^{I,C}_{s',k'-1,s} = F^{I,C}_{s',k',s} + \tilde{F}^{S,C}_{s',k'-1,s} - \tilde{F}^{E,C}_{s',k',s} \quad s, s' \in \mathbf{S}^{\mathrm{P}}, k' \in \mathbf{K}^{\mathrm{I}} \tag{5.55}$$

where slack variables (i.e., $\tilde{F}^{S,H}_{s,k,s'}, \tilde{F}^{E,H}_{s,k,s'}, \tilde{F}^{S,C}_{s',k',s}, \tilde{F}^{E,C}_{s',k',s}$) can have non-zero values when there is a start/end of a heat exchanger.

$$\tilde{F}^{S,H}_{s,k,s'} \leq \overline{\delta}_s V^{S,H}_{s,k,s'} \quad s, s' \in \mathbf{S}^{\mathrm{P}}, k \in \mathbf{K}^{\mathrm{I}} \tag{5.56}$$

$$\tilde{F}^{E,H}_{s,k,s'} \leq \overline{\delta}_s V^{E,H}_{s,k,s'} \quad s, s' \in \mathbf{S}^{\mathrm{P}}, k \in \mathbf{K}^{\mathrm{I}} \tag{5.57}$$

$$\tilde{F}^{S,C}_{s',k',s} \leq \overline{\delta}_{s'} V^{S,C}_{s',k',s} \quad s, s' \in \mathbf{S}^{\mathrm{P}}, k' \in \mathbf{K}^{\mathrm{I}} \tag{5.58}$$

$$\tilde{F}^{E,C}_{s',k',s} \leq \overline{\delta}_{s'} V^{E,C}_{s',k',s} \quad s, s' \in \mathbf{S}^{\mathrm{P}}, k' \in \mathbf{K}^{\mathrm{I}} \tag{5.59}$$

When there is no change of the heat exchanger along the consecutive intervals (i.e., no start/end of heat exchanger), then slack variables are deactivated, and flow rates are consistent through intervals (i.e,. $F^{I,H}_{s,k,s'} = F^{I,H}_{s,k-1,s'}$); otherwise, flow rates can change because slack variables can have non-zero values. In **Figure 5.5**, hot stream s exchanges

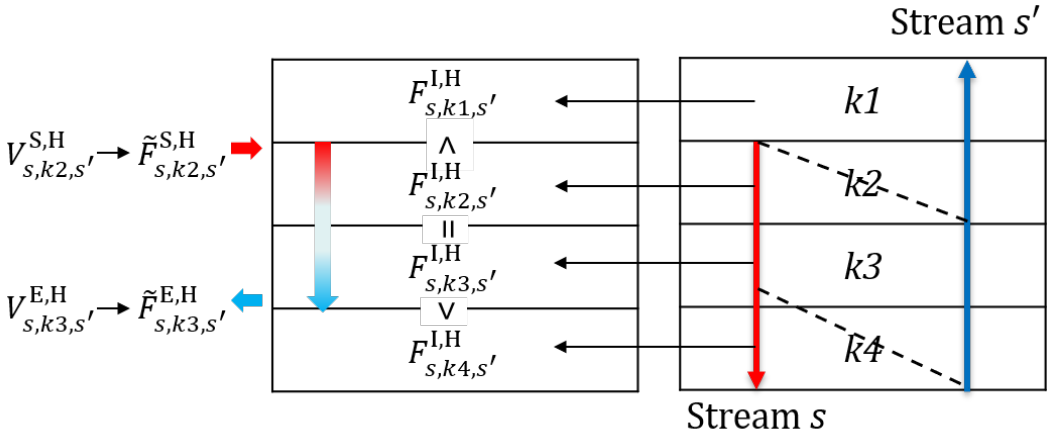

Figure 5.5: Flow rate balance due to start/end of heat exchanger

heat with cold stream s' at interval k2 and k3. The start of the heat exchanger at interval k2 relaxes the equality between flow rates at intervals k1 and k2, so $F^{I,H}_{s,\mathrm{k2},s'}$ can have a greater value than $F^{I,H}_{s,\mathrm{k1},s'}$ to start heat exchange. At interval k3, since there

is no start/end of the heat exchanger, flow rates in the heat exchanger at k2 and k3 are consistent. Finally, due to the end of the heat exchanger at interval k4, $F^{I,H}_{s,\mathrm{k4},s'}$ can have a smaller value than $F^{I,H}_{s,\mathrm{k3},s'}$ to end the heat exchanger. The same argument can be applied to cold streams.

The flow rate balance in each interval can be expressed as follows:

$$F^{H}_{s,k} + \tilde{F}^{tot,H}_{s,k} = \textstyle\sum_{s' \in \mathbf{S}} F^{I,H}_{s,k,s'} \quad s \in \mathbf{S}^{\mathrm{P}}, k \in \mathbf{K}^{\mathrm{I}} \tag{5.60}$$

$$F^{C}_{s',k'} + \tilde{F}^{tot,C}_{s',k'} = \textstyle\sum_{s \in \mathbf{S}} F^{I,C}_{s',k',s} \quad s' \in \mathbf{S}^{\mathrm{P}}, k' \in \mathbf{K}^{\mathrm{I}} \tag{5.61}$$

where dummy variables ($\tilde{F}^{tot,H}_{s,k}/\tilde{F}^{tot,C}_{s,k}$) can have non-zero values when stream s ends one heat exchanger and starts a new one in the same interval k.

$$\tilde{F}^{tot,H}_{s,k} \leq \overline{\delta}_s \textstyle\sum_{s' \in \mathbf{S}} V^{S,H}_{s,k,s'} \quad s \in \mathbf{S}^{\mathrm{P}}, k \in \mathbf{K}^{\mathrm{I}} \tag{5.62}$$

$$\tilde{F}^{tot,H}_{s,k} \leq \overline{\delta}_s \textstyle\sum_{s' \in \mathbf{S}} V^{E,H}_{s,k,s'} \quad s \in \mathbf{S}^{\mathrm{P}}, k \in \mathbf{K}^{\mathrm{I}} \tag{5.63}$$

$$\tilde{F}^{tot,C}_{s',k'} \leq \overline{\delta}_{s'} \textstyle\sum_{s \in \mathbf{S}} V^{S,C}_{s',k',s} \quad s' \in \mathbf{S}^{\mathrm{P}}, k' \in \mathbf{K}^{\mathrm{I}} \tag{5.64}$$

$$\tilde{F}^{tot,C}_{s',k'} \leq \overline{\delta}_{s'} \textstyle\sum_{s \in \mathbf{S}} V^{E,C}_{s',k',s} \quad s' \in \mathbf{S}^{\mathrm{P}}, k' \in \mathbf{K}^{\mathrm{I}} \tag{5.65}$$

For example, in **Figure 5.6A**, hot stream s ends one heat exchanger with stream s1 at interval $k+1$ and starts a new one with stream s2 in the same interval. Then, the summation in the right hand side of the Eq. (5.60) becomes twice of $F^{H}_{s,k}$. In this case, dummy variable $\tilde{F}^{tot,H}_{s,k}$ can have a non-zero value to satisfy the flow rate balance.

Notably, we enforce that these dummy variables are deactivated when the stream is split in an interval,

$$\tilde{F}^{tot,H}_{s,k} \leq \overline{\delta}_s (1 - W^{H}_{s,k,s'}) \quad s \in \mathbf{S}^{\mathrm{P}}, k \in \mathbf{K}^{\mathrm{I}} \tag{5.66}$$

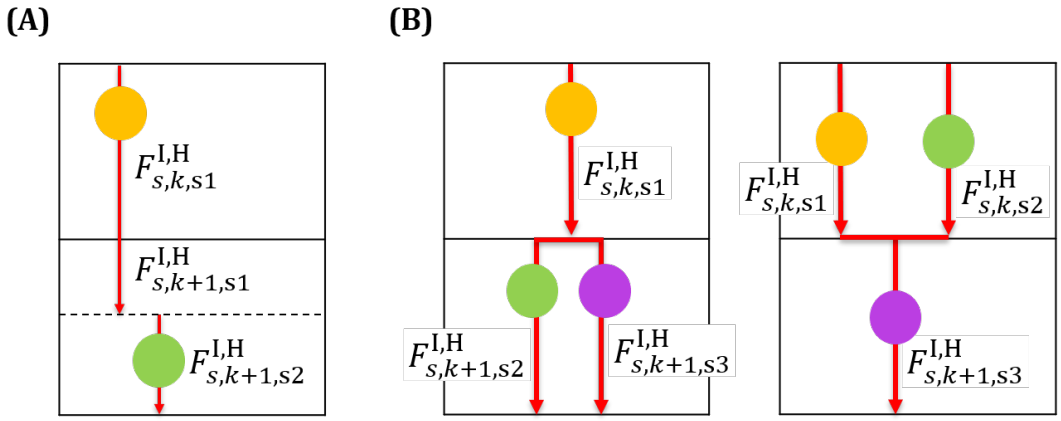

Figure 5.6: (A): when a stream ends a heat exchanger and starts a new one with a different stream in the same interval; (B): Feasible configurations without extension

$$\tilde{F}^{tot,C}_{s',k'} \leq \overline{\delta}_{s'}(1 - W^{C}_{s',k',s}) \quad s' \in \mathbf{S}^{\mathrm{P}}, k' \in \mathbf{K}^{\mathrm{I}} \tag{5.67}$$

which excludes several configurations (See section 5.2.4). Eqs. (5.66) - (5.67) enforce that stream splitting/mixing can only occur at the interval boundary as shown in **Figure 5.6B**, enforcing isothermal mixing. However, the model can be extended to consider constrained non-isothermal mixing between split streams (See Section 5.2.4).

Next, the cumulative heat ($\bar{Q}^{H}_{s,k,s'}/\bar{Q}^{C}_{s',k',s}$) can be calculated using the flow rate in each heat exchanger,

$$\bar{Q}^{H}_{s,k,s'} = \lambda_s F^{I,H}_{s,k,s'}(\hat{T}^{H}_{k-1} - \hat{T}^{H}_{k}) - \tilde{Q}^{D,H}_{s,k,s'} \quad s, s' \in \mathbf{S}^{\mathrm{P}}, k \in \mathbf{K}^{\mathrm{I}} \tag{5.68}$$

$$\bar{Q}^{C}_{s',k',s} = \lambda_{s'} F^{I,C}_{s',k',s}(\hat{T}^{C}_{k'-1} - \hat{C}^{H}_{k'}) - \tilde{Q}^{D,C}_{s',k',s} \quad s, s' \in \mathbf{S}^{\mathrm{P}}, k' \in \mathbf{K}^{\mathrm{I}} \tag{5.69}$$

where slack variables $\tilde{Q}^{D,H}_{s,k,s'}$ and $\tilde{Q}^{D,C}_{s',k',s}$ can have non-zero values when there is a start or an end of a heat exchanger in interval k and k', respectively,

$$\tilde{Q}^{D,H}_{s,k,s'} \leq \overline{\epsilon}_s(V^{S,H}_{s,k,s'} + V^{E,H}_{s,k,s'}) \quad s, s' \in \mathbf{S}^{\mathrm{P}}, k \in \mathbf{K}^{\mathrm{I}} \tag{5.70}$$

$$\tilde{Q}^{D,C}_{s',k',s} \leq \bar{\epsilon}_{s'}(V^{S,C}_{s',k',s} + V^{E,C}_{s',k',s}) \quad s, s' \in \mathbf{S}^{\mathrm{P}}, k' \in \mathbf{K}^{\mathrm{I}} \tag{5.71}$$

Parameter $\bar{\epsilon}_s$ denotes an upper bound on the cumulative heat of stream s. When slack variables have non-zero values, the temperature change in the heat exchanger can be less than the size of the interval; otherwise, the temperature change should be the same as the size of the interval that the heat exchanger spans.

Temperature feasibility on the boundary interval

Temperature grids are shifted to introduce the minimum temperature difference (ΔT^{min}) between hot and cold streams, which can ensure enough thermodynamic driving force for heat exchange. However, if hot and cold streams exchange heat in the same interval, the minimum temperature difference might not be guaranteed within the heat exchanger. For example, in **Figure 5.7**, hot stream s and cold stream s' exchange heat in intervals k2∼k4. The heat exchanger starts at interval k2 in the hot stream grid and ends at the interval k2, the same interval, in the cold stream grid. In this case, there is a range of the outlet temperature of the cold stream that may violate the minimum temperature difference. Likewise, at interval k4, the hot stream ends the heat exchange while the cold stream starts, resulting in a range of the outlet temperature for the hot stream that may violate the minimum temperature difference. To prevent these cases, the inlet/outlet temperature of a stream in a heat exchanger can be calculated as follows,

$$T^{IN,H}_{s,k,s'} = \hat{T}^{H}_{k} + \frac{\bar{Q}^{H}_{s,k,s'}}{\lambda_s F^{I,H}_{s,k,s'}} \quad s, s' \in \mathbf{S}^{\mathrm{P}}, k \in \mathbf{K}^{\mathrm{I}} \tag{5.72}$$

$$T^{OUT,H}_{s,k,s'} = \hat{T}^{H}_{k-1} - \frac{\bar{Q}^{H}_{s,k,s'}}{\lambda_s F^{I,H}_{s,k,s'}} \quad s, s' \in \mathbf{S}^{\mathrm{P}}, k \in \mathbf{K}^{\mathrm{I}} \tag{5.73}$$

$$T^{IN,C}_{s',k,s} = \hat{T}^{C}_{k-1} - \frac{\bar{Q}^{C}_{s',k,s}}{\lambda_{s'} F^{I,C}_{s',k,s}} \quad s, s' \in \mathbf{S}^{\mathrm{P}}, k \in \mathbf{K}^{\mathrm{I}} \tag{5.74}$$

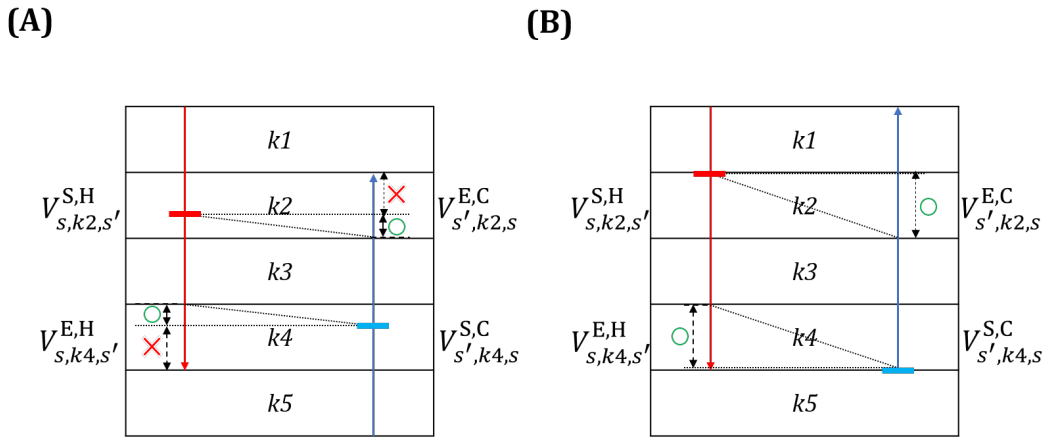

Figure 5.7: (A): Range of outlet temperature that violates minimum temperature difference; (B): Guaranteed minimum temperature difference with Eqs. (5.84) and (5.85)

$$T^{OUT,C}_{s',k,s} = \hat{T}^{C}_{k} + \frac{\bar{Q}^{C}_{s',k,s}}{\lambda_{s'} F^{I,C}_{s',k,s}} \quad s, s' \in \mathbf{S}^{\mathrm{P}}, k \in \mathbf{K}^{\mathrm{I}} \tag{5.75}$$

and used in constraints to enforce the feasibility.

$$T^{IN,H}_{s,k,s'} \geq T^{OUT,C}_{s',k,s} + \Delta T^{min} \quad s, s' \in \mathbf{S}^{\mathrm{P}}, k \in \mathbf{K}^{\mathrm{I}} \tag{5.76}$$

$$T^{OUT,H}_{s,k,s'} \geq T^{IN,C}_{s',k,s} + \Delta T^{min} \quad s, s' \in \mathbf{S}^{\mathrm{P}}, k \in \mathbf{K}^{\mathrm{I}} \tag{5.77}$$

However, Eqs. (5.72) - (5.75) are nonlinear, increasing computational complexity of the model significantly. By rearranging Eqs. (5.76) and (5.77) using Eqs. (5.72) - (5.75), we can obtain Eqs. (5.78) and (5.79), respectively,

$$\frac{\bar{Q}^{H}_{s,k,s'}}{\lambda_{s} F^{I,H}_{s,k,s'}} \geq \frac{\bar{Q}^{C}_{s',k,s}}{\lambda_{s'} F^{I,C}_{s',k,s}} \quad s, s' \in \mathbf{S}^{\mathrm{P}}, k \in \mathbf{K}^{\mathrm{I}} \tag{5.78}$$

$$\frac{\bar{Q}^{H}_{s,k,s'}}{\lambda_{s} F^{I,H}_{s,k,s'}} \leq \frac{\bar{Q}^{C}_{s',k,s}}{\lambda_{s'} F^{I,C}_{s',k,s}} \quad s, s' \in \mathbf{S}^{\mathrm{P}}, k \in \mathbf{K}^{\mathrm{I}} \tag{5.79}$$

Notably, the term in the right hand side of Eq. (5.78) is upper bounded by the size of the interval (i.e., $T^{grid}_{k} = (T^{H}_{k-1} - T^{H}_{k}) = (T^{C}_{k-1} - T^{C}_{k})$) because it represents the temperature

change in an interval; thus, if the term in the left hand side is greater than T_k^{grid}, Eq. (5.78) will hold. Similarly, the term in the left hand side of Eq. (5.79) is upper bounded by T_k^{grid}, so if the term in the right hand side is greater than T_k^{grid}, Eq. (5.79) will hold.

$$\text{If } \frac{\bar{Q}^H_{s,k,s'}}{\lambda_s F^{I,H}_{s,k,s'}} \geq T_k^{grid} \rightarrow \frac{\bar{Q}^H_{s,k,s'}}{\lambda_s F^{I,H}_{s,k,s'}} \geq \frac{\bar{Q}^C_{s',k',s}}{\lambda_s F^{I,C}_{s',k',s}} \tag{5.80}$$

$$\text{If } \frac{\bar{Q}^C_{s',k',s}}{\lambda_{s'} F^{I,C}_{s',k',s}} \geq T_k^{grid} \rightarrow \frac{\bar{Q}^H_{s,k,s'}}{\lambda_s F^{I,H}_{s,k,s'}} \leq \frac{\bar{Q}^C_{s',k',s}}{\lambda_{s'} F^{I,C}_{s',k',s}} \tag{5.81}$$

As a result, we can derive the following linear constraints,

$$\lambda_{s'} T_k^{grid} F^{I,C}_{s',k,s} \leq \bar{Q}^C_{s',k,s} \quad s, s' \in \mathbf{S}^{\mathrm{P}}, k \in \mathbf{K}^{\mathrm{I}} \tag{5.82}$$

$$\lambda_s T_k^{grid} F^{I,H}_{s,k,s'} \leq \bar{Q}^H_{s,k,s'} \quad s, s' \in \mathbf{S}^{\mathrm{P}}, k \in \mathbf{K}^{\mathrm{I}} \tag{5.83}$$

Finally, using binary variables, we enforce the above inequalities to be active only when a heat exchanger ends and starts at the same interval,

$$\lambda_{s'} F^{I,C}_{s',k,s} T_k^{grid} \leq \bar{Q}^C_{s',k,s} + \zeta(2 - V^{E,H}_{s,k,s'} - V^{S,C}_{s',k,s}) \quad s, s' \in \mathbf{S}^{\mathrm{P}}, k \in \mathbf{K}^{\mathrm{I}} \tag{5.84}$$

$$\lambda_s F^{I,H}_{s,k,s'} T_k^{grid} \leq \bar{Q}^H_{s,k,s'} + \zeta(2 - V^{S,H}_{s,k,s'} - V^{E,C}_{s',k,s}) \quad s, s' \in \mathbf{S}^{\mathrm{P}}, k \in \mathbf{K}^{\mathrm{I}} \tag{5.85}$$

where ζ is a parameter that relaxes inequalities when any of binary variables is 0. When hot stream s ends a heat exchanger with stream s' at interval k (i.e., $V^{E,H}_{s,k,s'} = 1$) while cold stream s' starts a heat exchanger with stream s at the same interval (i.e., $V^{S,C}_{s',k,s'} = 1$), Eq. (5.84) enforces the temperature change of cold stream s' to be the same as the size of the temperature grid; in other words, cold stream s' should start the heat exchanger at the interval boundary. Similarly, in the opposite case where a hot stream starts and a cold stream ends in the same interval, Eq. (5.85) enforces the temperature change of the hot stream to be the same as the size of the temperature grid. Effects of Eqs. (5.84) and

(5.85) are illustrated in **Figure 5.7B**. Even though some solutions are excluded from these constraints, the impact is not significant when a moderate grid size is used. Also, to have a higher driving force to reduce the heat exchanger area, the optimal solution tends to have a higher temperature difference than the minimum.

Area calculation and objective function

As discrete temperatures on the grids are known, we can calculate the log-mean temperature difference between interval k and k' (i.e., $\Delta T^{lm}_{k,k'}$). Using the log-mean temperature difference, we calculate the heat exchanger area using a linear approximation,

$$A_{s,s'} = \sum_{k\in\mathbf{K}^{\mathrm{I}}} \sum_{k'\in\mathbf{K}^{\mathrm{I}}} \frac{Q^{EX}_{s,k,s'}(h_{s,k}+h_{s',k'})}{h_{s,k}h_{s',k'}\Delta T^{lm}_{k,k'}} \quad s,s' \in \mathbf{S} \tag{5.86}$$

where $h_{s,k}$ denotes the heat transfer coefficient of stream s in interval k. When a moderate interval size is used (e.g., 5 - 10K), the approximation is sufficiently close (deviation between 0.004 - 1.143%, See appendix D.2) to the calculation with the true log-mean temperature difference of a heat exchanger.

Then, the number of heat exchangers between a pair of streams ($N^{EX}_{s,s'}$) is calculated,

$$N^{EX}_{s,s'} = \sum_{k\in\mathbf{K}^{\mathrm{I}}} V^{S,H}_{s,k,s'} = \sum_{k\in\mathbf{K}^{\mathrm{I}}} V^{E,H}_{s,k,s'} = \sum_{k'\in\mathbf{K}^{\mathrm{I}}} V^{S,C}_{s',k',s} = \sum_{k'\in\mathbf{K}^{\mathrm{I}}} V^{E,C}_{s',k',s} \quad s,s' \in \mathbf{S} \tag{5.87}$$

Further, to avoid cyclic matching (i.e., multiple matching between a pair of streams) and to reduce the complexity of the resulting HEN, $N^{EX}_{s,s'}$ is bounded,

$$N^{EX}_{s,s'} \leq \eta \quad s,s' \in \mathbf{S} \tag{5.88}$$

where η can be set to 1 to avoid the cyclic matching. The objective is to minimize the total cost of the HEN, which is calculated using hot/cold utility cost, exchanger area

capital cost, and heat exchanger unit cost.

$$\begin{aligned} C = \quad & \mu^H \sum_{s\in\mathbf{S}^{\mathrm{HU}}} \sum_k \sum_{s'\neq s} \bar{Q}^H_{s,k,s'} + \mu^C \sum_{s'\in\mathbf{S}^{\mathrm{CU}}} \sum_{k'} \sum_{s\neq s'} \bar{Q}^C_{s',k',s} \\ & + \mu^A \sum_{s\in\mathbf{S}} \sum_{s'\in\mathbf{S}} A_{s,s'} + \mu^U \sum_{s\in\mathbf{S}} \sum_{s'\in\mathbf{S}} N^{EX}_{s,s'} \end{aligned} \tag{5.89}$$

Parameter μ^H/μ^C is annual operating cost for hot/cold utility ($\$/\mathrm{kW}-\mathrm{yr}$); μ^A is the annualized capital cost of area ($\$/\mathrm{m}^2-\mathrm{yr}$); and μ^U is the annualized fixed cost for the heat exchanger unit ($\$/\mathrm{yr}$).

5.2.4 Extensions

Non-isothermal mixing

The model can be extended to handle general non-isothermal mixing of split streams, which, in some cases, can be beneficial. However, we present non-isothermal mixing only in the same interval because this can be readily introduced without additional variables or constraints. By using Eqs. (5.90) and (5.91) instead of Eqs. (5.66) and (5.67), non-isothermal mixing configurations in **Figure 5.8A** can be allowed.

$$\tilde{F}^{tot,H}_{s,k} \leq \overline{\delta}_s (1 - W^H_{s,k,s'} + V^{E,H}_{s,k,s'}) \quad s, s' \in \mathbf{S}, k \in \mathbf{K} \tag{5.90}$$

$$\tilde{F}^{tot,C}_{s',k'} \leq \overline{\delta}_{s'} (1 - W^C_{s',k',s} + V^{E,C}_{s',k',s}) \quad s, s' \in \mathbf{S}, k' \in \mathbf{K} \tag{5.91}$$

Note that non-isothermal mixing in the middle of the interval is allowed only if all the split streams end in the same interval. This is illustrated in **Figure 5.8A**. In interval k1, two of split streams are mixed at the boundary, which is feasible without the extension. However, the mixing in interval k2 is allowed only if the extension is introduced, because mixing occurs in the middle of the interval; Notably, all the split streams end in the same interval k2.

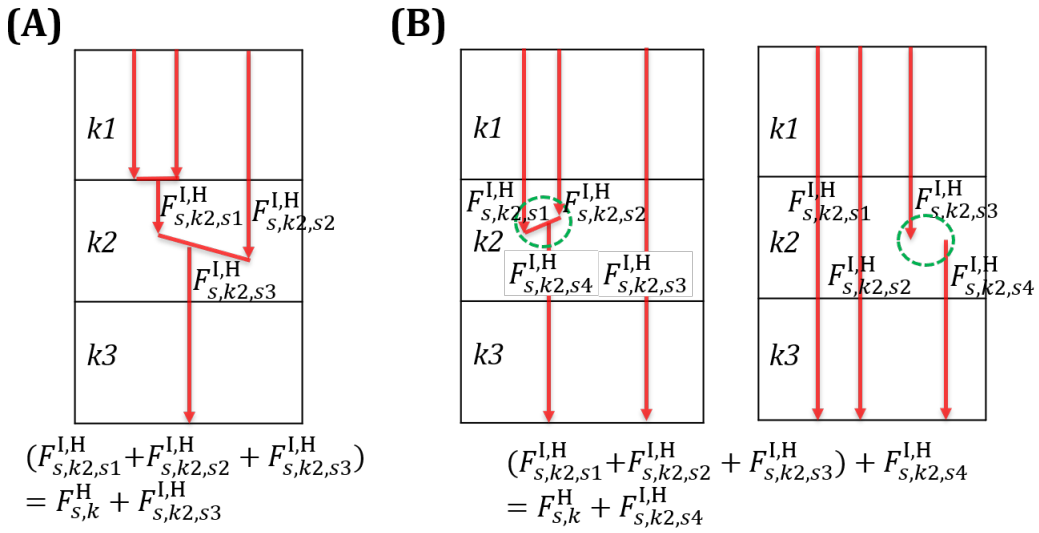

Figure 5.8: (A): Feasible configuration with relaxation for non-isothermal mixing; (B): Configurations that cannot be found with relaxation for non-isothermal mixing

However, configurations illustrated in **Figure 5.8B** cannot be found even with the extended model because they require non-zero dummy variables for the flow rate balance (i.e., $\tilde{F}^{tot,H}_{s,k}, \tilde{F}^{tot,C}_{s',k'}$) due to the repetitive flow rate calculation in the circled region, but the dummy variables are deactivated due to the split stream that does not end in the same interval. In the first configuration in **Figure 5.8B**, two streams are mixed in interval k2, but there is another split stream which is not mixed (end) in that interval. In this case, $\tilde{F}^{tot,H}_{s,k2}$ cannot have a non-zero value because the right-hand side of Eq. (5.90) is 0 ($W^{H}_{s,k2,s3} = 1, V^{E,H}_{s,k2,s3} = 0$). The same is true in the second configuration in **Figure 5.8B**; due to the streams that are not mixed in interval k2, $\tilde{F}^{tot,H}_{s,k2}$ is deactivated. We note that since non-isothermal mixing can only occur in the same interval, the size of the interval does affect the temperature range of such mixing.

Non-uniform temperature grid

In some cases, many intervals are needed, although it is not computationally effective, to map stream data onto the temperature grid accurately or to reduce the error of the linear approximation of the heat exchanger area. To address this challenge, we propose to use a non-uniform grid where the size of each interval can be adjusted, thereby considerably reducing the number of intervals while mapping accurate stream information.

5.3 Illustrative Examples

We used GAMS 25.0.1, and the computing platform was a Dell OptiPlex 7010 with 3.40 GHz Intel® CPU and 8 GB of RAM. The MILP models are solved by OSIGUROBI, and the MINLP models are solved by SCIP.

5.3.1 Simultaneous Process Synthesis and Utility Targeting

Here, we illustrate how the proposed utility targeting model can be seamlessly integrated with a process synthesis/intensification model, and the computational efficiency of the resulting integrated model. We compare the solution obtained by the proposed targeting model against the solution obtained by a nonlinear targeting model [59]. Due to nonlinear constraints in the process synthesis model (e.g., unit costs, mass balances), the combined model is a MINLP model for both cases. Interestingly, while the proposed targeting model has more variables than the nonlinear targeting model, it is easier to solve when it is combined with process synthesis model.

A process from Kong et al. [59] with some modifications found in Li et al. [66] is investigated (See **Figure 5.9**). There are 3 reactors and 3 separators. The objective

is to maximize profit. The feed includes 2 kmol/s of A and 1 kmol/s of B. In the first reaction, A and B react to form an intermediate C (A + B $\rightarrow$ C). Since the stoichiometry of A and B is 1 in the first reaction, B is the limiting reactant. There are two candidate catalysts, operating at different reactor temperatures, for this reaction, so one important decision is the selectin of the catalyst/reactor system. The first catalyst has to be operated at 340 K, while the second should be operated at 450 K. The second catalyst yields higher conversion than the first (90% vs. 60%), but its capital cost is also higher. Effluents from the reactors can be recycled directly to increase yield. After this reaction, C is separated from A and B in the sharp distillation tower (SEP1). In the following step, C is converted to product D (C $\rightarrow$ D) in reactor CSTR2. The reaction reaches equilibrium. The operating temperature of CSTR2 is fixed at 450 K, and the enthalpies of reaction in all the reactors are assumed to be negligible; these assumptions are lifted later in section 5.3.4 to include variable temperature isothermal stream in the HEN design. Finally, product D is separated from C in two consecutive distillation towers (SEP2, SEP3). Only 60 % of C is separated in SEP2 and sharp distillation is achieved in SEP3. Streams 2 and 7 can be either hot or cold streams depending on the operating temperature of the reactor. The classification of these streams is determined simultaneously by solving the optimization problem. The optimal solution is shown in **Figure 5.9**, where unselected units are dimmed. Streams 1 and 12 are mixed with recycling streams. While the temperature of the mixer outlet streams, 2 and 13, can be mapped exactly on one of the temperatures of the discrete temperature grid, this might lead to suboptimal solutions where some portion of the recycling stream is purged to satisfy the energy balance. To address this, we allowed some deviation between the temperature in the heat integration model (i.e., T_s^{HI}) and that in the heat integration

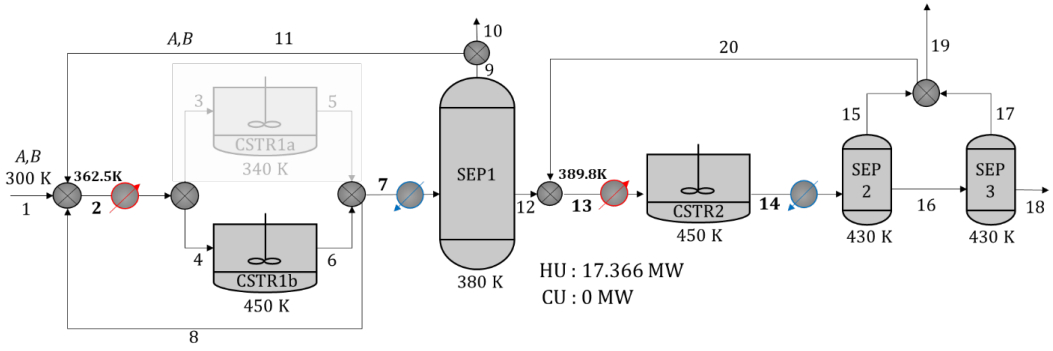

Figure 5.9: Problem configuration and its optimal solution for simultaneous process synthesis and utility targeting

model (i.e., T_s^{PS}). This is achieved using slack variable $\tilde{T}_s$,

$$T_s^{HI} = T_s^{PS} + \tilde{T}_s \quad s \in \mathbf{S} \tag{5.92}$$

which is bounded in $[-\Delta T^{grid}/2, \Delta T^{grid}/2]$. We use a uniform grid with $\Delta T^{grid} = 5$K, leading to 64 intervals. In the optimal solution, CSTR1b is selected, so stream 2 is cold and stream 7 is hot. The integrated model using the proposed model requires 25.07 s, while the one with the nonlinear model requires 14820 s. The optimal solution obtained using the proposed model has a profit of \$58.925 MM/year, employing 17.366 MW of hot utility (\$1.389 MM/year). The solution using the nonlinear model, has a profit equal to \$58.863 MM/year, with 18.135 MW of hot utility (\$1.451 MM/year). Note that the objective values are different because of the approximation of the temperature.

5.3.2 Cyclic Matching

When there is few streams to exchange heat, cyclic matching, where a pair of streams might be matched multiple times, can be beneficial, and the proposed model can handle

it. We adopt an example from Biegler et al. [11] with three streams with pre-determined classifications. A grid with $\Delta T^{grid} = 1$K is used to map exact stream information, leading to 220 intervals. Since there is only one hot stream, cyclic matching can be promising. The maximum number of cyclic matching (η) is set to 2. The example is

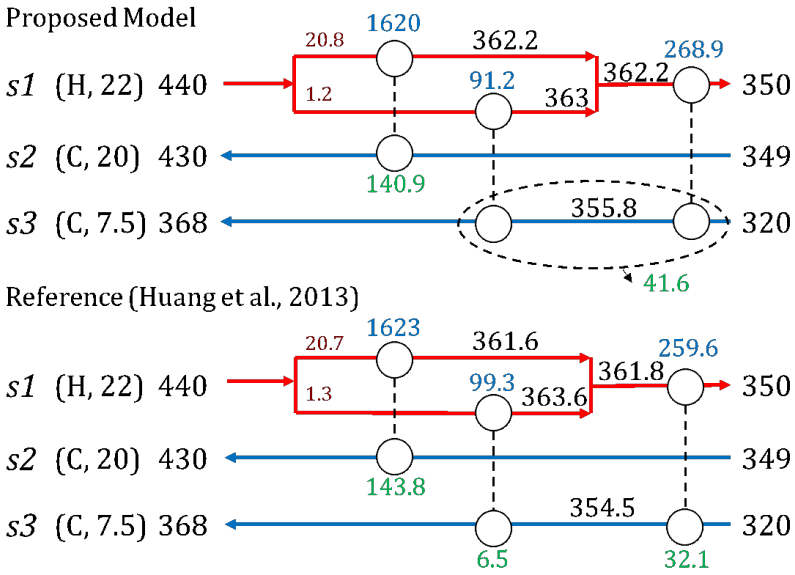

Figure 5.10: Optimal structures from the proposed HENS model and reference. Flow rates given in dark red, heat load (kW) and exchange area (m^2) given in blue and green.

solved in 107.23 s with an objective function value of \$78,399/yr (See **Figure 5.10**). The solution has a cyclic matching between streams s1 and s3. However, since the model only calculates the total area between a pair of streams (i.e., $A_{s,s'}$), the area for each heat exchanger cannot be directly obtained. Nevertheless, it is also possible to calculate the heat duty in each exchanger, thus area can be obtained using the information from the solution. We compare the solution with previously obtained one [49]. Since a nonlinear cost function with log-mean temperature is used in the previous paper, the comparison

between the two optimal objective function values is conducted after calculating the area cost using the original nonlinear function, referred to as adjusted cost. The adjusted cost ($76,459/yr) has a good agreement with the reference value [49] ($76,327/yr).

5.3.3 Stream Splitting

This example is from Yee et al. [108]. Stream splitting is likely to occur in this example because there is only one cold and multiple hot streams. We investigate the impact of non-isothermal mixing changing the interval size. **Figure 5.11** shows solution quality, of both models, as a function of the interval size; $\Delta T^{min} = 10$K is used in all cases. Non-isothermal mixing improves the solution quality considerably when a moderate size interval (e.g., 10 K) is used, but the improvement becomes smaller when we have a smaller interval. This is because using a smaller interval makes the range of the non-isothermal mixing smaller. This result shows that when non-isothermal mixing is expected, then it is better to use a moderate, rather than small, interval size. Non-isothermal mixing is likely to lead to better solutions when, for example, there is a hot stream with large flow rate and multiple cold streams, all with small flow rates, spanning the same intervals.

In general, we can observe improvement of the optimal objective function value with smaller intervals. This is from the two reasons: 1) better approximation achieved through the linear area calculation (we are overestimating the area with a large size interval) 2) more degree of freedom of mixing and splitting temperature with more intervals. This improvement, however, is not observed in the solution with 1 K interval with non-isothermal mixing. With 1 K interval, the optimal objective function value is

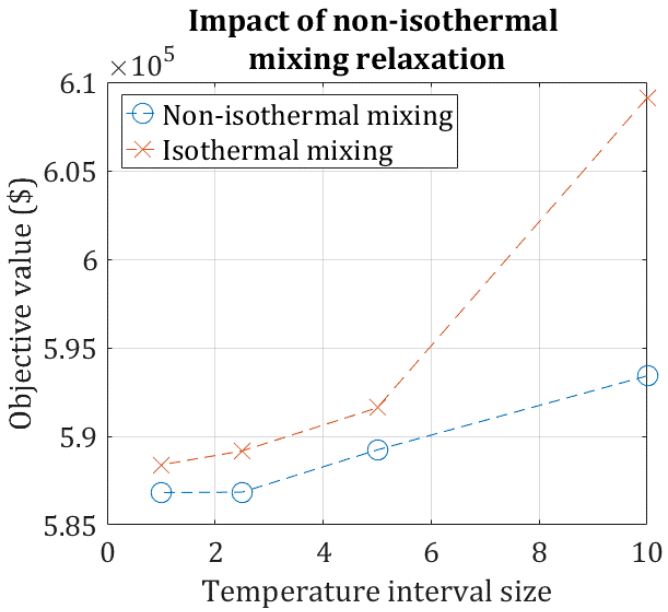

Figure 5.11: Impact of interval sizes of the grid for non-isothermal mixing

worse than that with 2.5 K interval because non-isothermal mixing within 1 K intervals does not lead to noticeable improvements even though the approximation is improved.

When we use $\Delta T^{min} = 1, \Delta T^{grid} = 1$ to map exact temperature information, the optimal objective function values with and without the adjustment are \$578,193/\$579,547, respectively, which are slightly inferior (1.4/1.6 %, respectively) to the reported value (\$570,362, [49]) due to the limited range for non-isothermal mixing. The optimal solution without the adjustment is represented in **Figure 5.12**. The solution has a serial stream splitting (i.e., splitting of the stream that is already split stream). Stream s6 splits at 290 K into s6a (13.33 kW/K) and s6b (4.67 kW/K) to exchange heat with s5 and s4. After exchanging heat with s5, s6a splits again into s6c (7.98 kW/K) and s6d (5.36 kW/K) at 344 K to exchange heat with s1 and s3. Finally, all the split streams are mixed non-isothermally, and the mixed stream becomes 456.6 K.

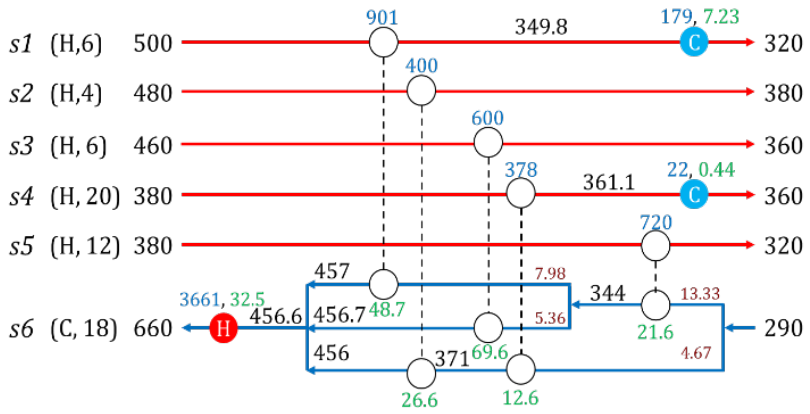

Figure 5.12: Optimal heat exchanger network of the example in Section 5.3.3

5.3.4 Simultaneous Process and HEN Synthesis

We study simultaneous process and HEN synthesis. The overall process configuration for this example is the same as the one in section 5.3.1, but a couple of important modifications are made. First, the heat of reaction of reaction 2 in CSTR2 (exothermic) is considerable (it was ignored previously), so an isothermal cooling duty for reactor r1 is introduced. Second, the operating temperature of CSTR2 varies within 350 $\sim$ 450 K, making streams 13 and 14 unclassified. Thus, the operating temperature of the reactor affects not only yield but also heat exchanger design. All the streams except the one representing the reactor duty are treated as unclassified streams. We use a nonlinear cost function for heat exchangers (i.e., $\mu^U + \mu^A A^{0.6}$) although we still use the linear approximation to calculate the area. The number of heat exchangers for CSTR2 is limited to one to consider practical constraints. Note that this type of constraints cannot be readily implemented in models that do not identify actual matching between streams (e.g., area targeting models). The optimization problem is solved to 0.32 % gap after 108,000 s, returning an objective function value of \$59.502 MM/yr. The optimal

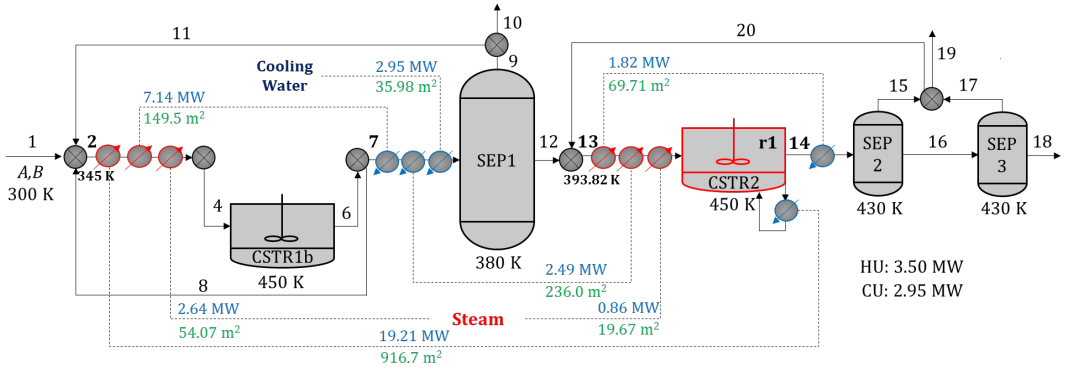

Figure 5.13: Optimal process configuration found with simultaneous process and HEN synthesis. Heat load (kW) and exchange area (m^2) given in blue and green

solution is represented in **Figure 5.13**. The annualized cost of the HEN (area + unit) is \$0.215 MM/yr while that of utility is \$0.339 MM/yr. There are seven heat exchangers with total exchanger area of 1481.64 m^2. The loads of hot and cold utilities are 3.50 and 2.95 MW, respectively. A 96.1 % total yield of product D from limiting reactant B is obtained with recycling of unreacted reactants (components A and B by streams 8 and 11, component C by stream 20) to the reactors.

In the optimal solution, CSTR1b is selected, so stream 2 becomes a cold stream; it exchanges heat with the reactor stream (r1) (exothermic reaction) and stream 7 that needs to be cooled down before the separation (SEP1). The optimal temperature of the CSTR2 is 450 K which is at the upper operating temperature bound; stream 13/14 is determined as cold/hot stream accordingly. Interestingly, the temperature is at the upper bound despite the reaction 2 being exothermic, because the gain in the yield by lowering the operating temperature of CSTR2 is outweighed by the gains in the HEN. One thing to note is that the total yield can be increased by recycling even though the single pass yield in the reactor is low due to the high temperature. This simple example

shows the advantage of considering simultaneous process synthesis with HENS. Other solution details can be found in the supporting information of the original work [82].

5.3.5 Non-uniform Grid

This example illustrates the advantage of using a non-uniform temperature grid. When the size of the problem is medium (e.g., 10 $\sim$ 15 streams), the proposed model with uniform temperature grid can be computationally expensive. By using a non-uniform grid, we can reduce the number of intervals while preserving stream information. This example has 15 streams with one hot and one cold utility. Streams 8 and 9 are unclassified with variable inlet/outlet temperature; the range of the inlet temperature of stream 8/9 is (110 $\sim$ 130)/(180 $\sim$ 280), while the range of the outlet temperature is (40 $\sim$ 250)/(190 $\sim$ 220). In addition, streams 4, 7, 8, and 14 have variable flow rates. Detailed parameters can be found in the supporting information of the original work [82]. The non-uniform grid has 27 intervals, leading to a model with 209,564 variables, of which 20,730 are discrete variables; and 138,519 constraints. The maximum size of the intervals is 40 K and the minimum 5 K. The model is solved to 3.01 % optimality gap in 40,000 s. The best solution is found after 19,749 s. The objective function value is \$1,163,923/yr, and the corresponding configuration is shown in **Figure 5.14**. Unclassified streams (i.e., s8 and s9) are determined to be hot streams. The adjusted cost, calculated using the log-mean temperature method based on the optimal configuration, is \$1,086,212/yr, which is 6.7 % lower than the cost calculated using the original cost function.

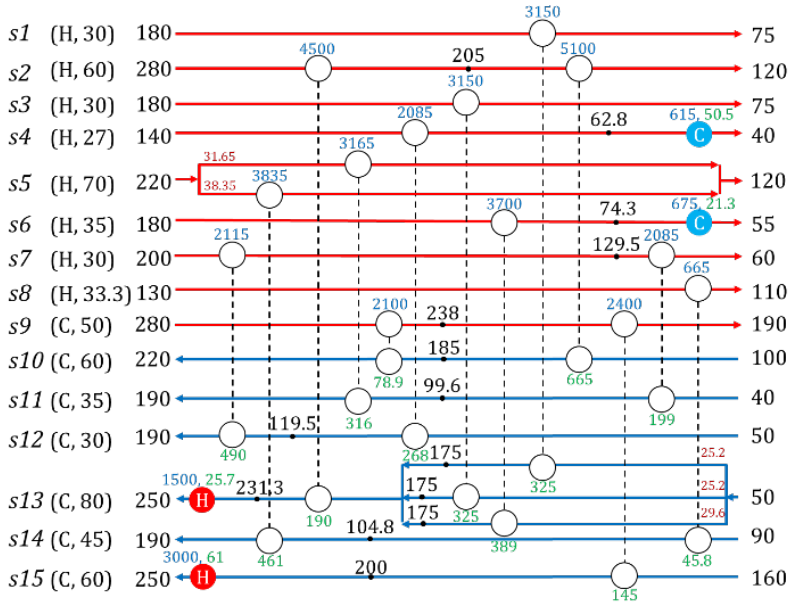

Figure 5.14: Optimal heat exchanger network with 15 streams. Streams 8 and 9 are determined to be hot streams. Flow rates given in dark red, heat load (kW) and exchange area (m^2) given in blue and green.

5.3.6 Phase Changes

In this example, phase change during the heat exchange is modeled by decomposing the stream into sub-streams corresponding to each phase (vapor, 2-phase, and liquid) as previous works [59, 54]. Bubble/dew points are assumed to be fixed (assuming constant stream pressure and composition). Since we can adjust the size of each interval, we can exactly map bubble/dew point of the stream on the discrete temperature grid. A subset of stream $\mathbf{S}^{\text{PHC}}$ is defined to represent the streams that might have phase changes. Streams in this subset are referred to as parent streams. Also, for each parent stream, we generate three sub-streams ($\mathbf{S}_s^{\text{SPHC}}$): vapor ($v_s$), 2-phases ($2p_s$), and liquid ($l_s$). All the sub-streams are considered as normal process streams. As shown in **Figure 5.15**, the set

of temperature intervals $\mathbf{K}^{\mathrm{I}}$ in hot/cold stream grid is divided into three subsets depending on the relative location with respect to the bubble/dew point of the parent stream on the grid. The subsets of the temperature interval ($\mathbf{K}_s^{\mathrm{V,H}}/\mathbf{K}_s^{\mathrm{V,C}}, \mathbf{K}_s^{\mathrm{2P,H}}/\mathbf{K}_s^{\mathrm{2P,C}}, \mathbf{K}_s^{\mathrm{L,H}}/\mathbf{K}_s^{\mathrm{L,C}}$) denote the temperature range of each phase of parent stream s in the hot/cold stream grids. We refer to these subsets of temperature interval as *phase regions*.

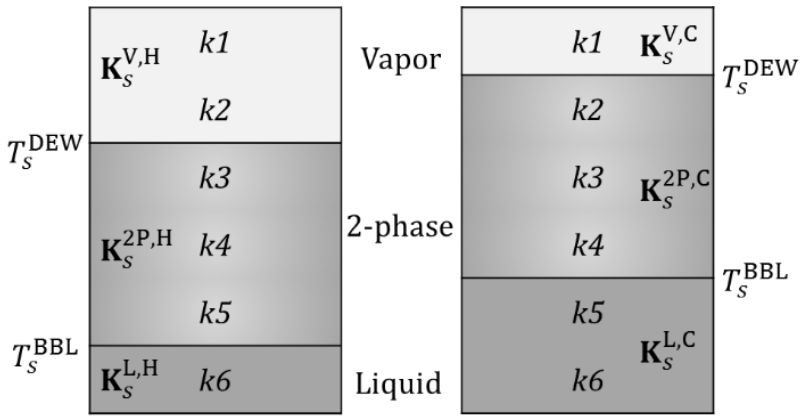

Figure 5.15: Phase regions in hot/cold stream temperature grid

The spanning of a sub-stream for a certain interval is determined by that of the parent stream; thus, we can equate the binary variables for the interval spanning of the parent stream to those of the sub-streams.

$$Z_{s,k}^{H} = Z_{v_s,k}^{H} \quad k \in \mathbf{K}_s^{\mathrm{V,H}}, s \in \mathbf{S}^{\mathrm{PHC}} \tag{5.93}$$

$$Z_{s,k}^{H} = Z_{2p_s,k}^{H} \quad k \in \mathbf{K}_s^{\mathrm{2P,H}}, s \in \mathbf{S}^{\mathrm{PHC}} \tag{5.94}$$

$$Z_{s,k}^{H} = Z_{l_s,k}^{H} \quad k \in \mathbf{K}_s^{\mathrm{L,H}}, s \in \mathbf{S}^{\mathrm{PHC}} \tag{5.95}$$

$$Z_{s,k}^{C} = Z_{v_s,k}^{C} \quad k \in \mathbf{K}_s^{\mathrm{V,C}}, s \in \mathbf{S}^{\mathrm{PHC}} \tag{5.96}$$

$$Z_{s,k}^{C} = Z_{2p_s,k}^{C} \quad k \in \mathbf{K}_s^{\mathrm{2P,C}}, s \in \mathbf{S}^{\mathrm{PHC}} \tag{5.97}$$

$$Z^C_{s,k} = Z^C_{l_s,k} \quad k \in \mathbf{K}^{\mathrm{L,C}}_s, s \in \mathbf{S}^{\mathrm{PHC}} \tag{5.98}$$

Note that the equalities of the spanning variable between the parent stream and the sub-streams are satisfied only in the corresponding phase region in Eqs. (5.93) - (5.98), ensuring correct decomposition of the parent stream into the sub-streams.

Binary variables are introduced to denote the existence of a certain phase during the heat exchange ($\hat{Z}^{V,H}_s, \hat{Z}^{V,C}_s, \hat{Z}^{2P,H}_s, \hat{Z}^{2P,C}_s, \hat{Z}^{L,H}_s, \hat{Z}^{L,C}_s$). If a certain phase (i.e., V, 2-P, L) appears during the heat exchange of parent stream s, the corresponding binary variable for the sub-stream is activated (Eqs. (5.99) – (5.104)). In contrast, if the parent stream does not span the phase region (i.e., $Z^H_{s,k}/Z^C_{s,k} = 0$), the corresponding binary variable is deactivated accordingly.

$$Z^H_{s,k} \leq \hat{Z}^{L,H}_s \leq \textstyle\sum_k Z^H_{s,k} \quad s \in \mathbf{S}^{\mathrm{PHC}}, k \in \mathbf{K}^{\mathrm{L,H}}_s \tag{5.99}$$

$$Z^C_{s,k} \leq \hat{Z}^{L,C}_s \leq \textstyle\sum_k Z^C_{s,k} \quad s \in \mathbf{S}^{\mathrm{PHC}}, k \in \mathbf{K}^{\mathrm{L,C}}_s \tag{5.100}$$

$$Z^H_{s,k} \leq \hat{Z}^{V,H}_s \leq \textstyle\sum_k Z^H_{s,k} \quad s \in \mathbf{S}^{\mathrm{PHC}}, k \in \mathbf{K}^{\mathrm{V,H}}_s \tag{5.101}$$

$$Z^C_{s,k} \leq \hat{Z}^{V,C}_s \leq \textstyle\sum_k Z^C_{s,k} \quad s \in \mathbf{S}^{\mathrm{PHC}}, k \in \mathbf{K}^{\mathrm{V,C}}_s \tag{5.102}$$

$$Z^H_{s,k} \leq \hat{Z}^{2P,H}_s \leq \textstyle\sum_k Z^H_{s,k} \quad s \in \mathbf{S}^{\mathrm{PHC}}, k \in \mathbf{K}^{\mathrm{2P,H}}_s \tag{5.103}$$

$$Z^C_{s,k} \leq \hat{Z}^{2P,C}_s \leq \textstyle\sum_k Z^C_{s,k} \quad s \in \mathbf{S}^{\mathrm{PHC}}, k \in \mathbf{K}^{\mathrm{2P,C}}_s \tag{5.104}$$

When phase change occurs, flow rate (i.e., heat duty) in each phase is different . We can change the flow rate of the parent stream according to each phase using sub-streams. If a sub-stream denoting a certain phase does not exist, then the flow rate of the sub-stream is deactivated via Eqs. (5.105) – (5.107).

$$F_{v_s} \leq \overline{\delta}_{v_s}(\hat{Z}^{V,H}_s + \hat{Z}^{V,C}_s) \quad s \in \mathbf{S}^{\mathrm{PHC}} \tag{5.105}$$

$$F_{2p_s} \leq \overline{\delta}_{2p_s}(\hat{Z}_s^{2P,H} + \hat{Z}_s^{2P,C}) \quad s \in \mathbf{S}^{\text{PHC}} \tag{5.106}$$

$$F_{l_s} \leq \overline{\delta}_{l_s}(\hat{Z}_s^{L,H} + \hat{Z}_s^{L,C}) \quad s \in \mathbf{S}^{\text{PHC}} \tag{5.107}$$

To illustrate this extension, a small example with 5 streams is considered. The bubble point of stream s5 is 320 °C and its dew point is 335 °C. The inlet temperature of s5 is between 207 and 405 °C and the outlet temperature between 330 and 340 °C, so it can undergo phase change. In addition, it is an unclassified stream. We assume that the ratio of specific heat capacities between liquid, 2-phase, and vapor is 2:4:1. The optimal configuration is shown in **Figure 5.16**, where s5 is used as a cold stream undergoing a phase change from liquid to 2-phases; vapor phase does not appear during the heat exchange.

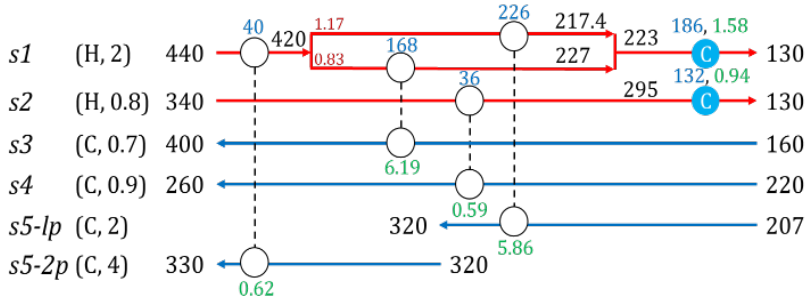

Figure 5.16: Optimal heat exchanger network with phase change

Chapter 6

Conclusions and Future Works

6.1 Distillation Network Synthesis

We proposed a versatile and computationally efficient shortcut distillation column model and a separation energy targeting model, which are well-suited for superstructure-based process synthesis. They can seamlessly handle systems in the presence of undetermined feeds, which can naturally appear in process synthesis problems. The proposed distillation column models can automatically identify adequate key components and calculate the corresponding energy requirement of a separation task. Also, they can be readily adopted as submodules in distillation network synthesis approaches. The proposed separation energy targeting model can calculate an energy target for the separation of a mixture without designing the network. Henceforth, this targeting model can be effectively used in a preliminary synthesis step to identify promising systems among multiple alternatives. As a demonstration, we applied the proposed model into the bio-refinery optimization for ethanol upgrading, which unveiled several promising ethanol upgrading strategies. Also, the solution obtained with the proposed energy targeting model can be used as a good starting point for more rigorous process synthesis/design. Potential future works in this area include developing generalized column models and targeting models that can handle non-ideal mixtures. One way is to extend existing shortcut

approaches for non-ideal mixtures to consider the undetermined feed. Approaches with data-driven surrogate models are also promising.

Next, we proposed a superstructure-based distillation network synthesis model with extended modeling features. It can account for multiple undetermined sources and unspecified outlets to facilitate the integration with reactor network synthesis models. Furthermore, bypass streams and thermal coupling can be considered to find more energy/cost efficient distillation networks. Bypass streams can be utilized to avoid unnecessary separations, and thermal coupling can be adopted to avoid re-mixing. Due to its extended modeling capability, the proposed approach enabled seamless integration of reactor and separation network synthesis and led to solutions that cannot be found using existing models employed in a sequential approach. For future works, addressing large scale problems would require the development of specialized solution methods. Also, introducing various heat integration options between columns can be an interesting future research topic.

In addition, we illustrated how simple graphically-inspired feasibility constraints can be used in conjunction with superstructure-based approaches for distillation network synthesis. This approach can allow the use of surrogate models for distillation columns, to improve computational efficiency of superstructure-based approaches, while enforcing approximate feasibility constraints of distillation tasks. An interesting future research direction is the derivation of and integration with similar feasibility constraints for (1) non-ideal mixtures and (2) liquid-liquid equilibrium.

6.2 Heat Integration

We proposed mathematical programming models for 1) utility targeting and 2) heat exchanger network synthesis (HENS). By using a discrete temperature grid approach, we were able to formulate linear models (with integer variables) even in the case where unclassified streams with variable temperatures and flow rates are present. This approach allows the formulation of computationally more tractable process synthesis models with integrated HENS. Further, the HENS model can be extended to address non-isothermal mixing of split streams, within a limited range, as well as phase changes during heat exchange. To further reduce the computational cost, a non-uniform temperature grid can be adopted. For future research, the comprehensive consideration of non-isothermal mixing can be explored. Also, to tackle large scale problems, developing solution methods that are specialized in solving HENS model would be needed.

Appendix A

Chapter 2 Appendix

A.1 Role of Inactive Roots[9]

We briefly illustrate the role of Eqs. (2.5) and (2.6) with inactive roots, while more thorough discussion can be found in the works by Halvorsen et al. [44] and Gooty et al. [101]. Let's consider a saturated liquid feed with four components ($\mathbf{I} = \{\mathrm{A}, \mathrm{B}, \mathrm{C}, \mathrm{D}\}$; $(\alpha_\mathrm{A}, \alpha_\mathrm{B}, \alpha_\mathrm{C}, \alpha_\mathrm{D}) = \{5, 2, 1.1, 1\}$; $F_i = 0.25$). From the feed equation, roots are calculated as $(\phi_\mathrm{A}, \phi_\mathrm{B}, \phi_\mathrm{C}) = (3.161, 1.466, 1.044)$. We need to achieve 90% recovery of component B in the distillate stream and 70% recovery of component C in the bottom stream.

If we select B/C as the light/heavy key (only ϕ_B is active) with recoveries of 0.9/0.7 in the distillate/bottom stream, $V1 = V2 = 0.97$ and $(D_\mathrm{A}, D_\mathrm{B}, D_\mathrm{C}, D_\mathrm{D}) = (0.25,\ 0.225,\ 0.075,\ 0)$ are calculated by Eqs. (2.2) and (2.3). Then, if we calculate Eqs. (2.5) and (2.6) with one of inactive roots ϕ_C,

$$\sum_{i\in\mathbf{I}} \frac{\alpha_i D_i}{\alpha_i - \phi_\mathrm{C}} = \frac{5\times 0.25}{5-\phi_\mathrm{C}} + \frac{2\times 0.225}{2-\phi_\mathrm{C}} + \frac{1.1\times 0.075}{1.1-\phi_\mathrm{C}} = 2.252 > V1 = 0.97 \tag{A.1}$$

$$\sum_{i\in\mathbf{I}} -\frac{\alpha_i B_i}{\alpha_i - \phi_\mathrm{C}} = -\frac{2\times 0.025}{2-\phi_\mathrm{C}} - \frac{1.1\times 0.175}{1.1-\phi_\mathrm{C}} - \frac{1\times 0.188}{1-\phi_\mathrm{C}} = 2.252 > V2 = 0.97 \tag{A.2}$$

Eqs. (2.5) and (2.6) are violated; this implies that the resulting component distributions are not obtainable with the minimum vapor flow rate operating condition.

[9]The contents of this section appear in Ryu and Maravelias, *Comp. & Chem. Engr.* **2020**

On the other hand, if we select B/D as the light/heavy key (ϕ_{B} and ϕ_{C} are active) with recoveries of 0.9/0.753, $V1 = V2 = 0.837$ and $(D_{\mathrm{A}}, D_{\mathrm{B}}, D_{\mathrm{C}}, D_{\mathrm{D}}) = (0.25,\ 0.225,\ 0.075,\ 0.062)$ are calculated by Eqs. (2.2) and (2.3). These components distributions can be obtained with the minimum vapor flow rate operating condition because the resulting minimum vapor flow rates and component distributions satisfy Eqs. (2.5) and (2.6) for all inactive roots (i.e., ϕ_{A}).

A.2 Reformulation of Eqs. (2.53) and (2.54)[10]

Eqs. (2.53) and (2.54) are reformulated as follows,

$$\overline{U}^{D}_{i,i'}(1 - \frac{\phi_{i'}}{\alpha_i}) = \overline{D}_{i,i'} \qquad i \in \mathbf{I},\ i' \in \mathbf{I}^{\mathrm{R}} \tag{A.3}$$

$$\overline{U}^{B}_{i,i'}(1 - \frac{\phi_{i'}}{\alpha_i}) = -\overline{B}_{i,i'} \qquad i \in \mathbf{I},\ i' \in \mathbf{I}^{\mathrm{R}} \tag{A.4}$$

$$-\frac{1}{\omega}\overline{D}_{i,i'} \leq \overline{U}^{D}_{i,i'} \leq \frac{1}{\omega}\overline{D}_{i,i'} \qquad i \in \mathbf{I},\ i' \in \mathbf{I}^{\mathrm{R}} \tag{A.5}$$

$$-\frac{1}{\omega}\overline{B}_{i,i'} \leq \overline{U}^{B}_{i,i'} \leq \frac{1}{\omega}\overline{B}_{i,i'} \qquad i \in \mathbf{I},\ i' \in \mathbf{I}^{\mathrm{R}} \tag{A.6}$$

A.3 Column Model with Only Active Roots[11]

When only high recoveries of heavy/light key components (e.g., $> 99\%$) are considered, calculating inactive roots to check Eqs. (2.5) and (2.6) might be redundant because they are implicitly satisfied for all inactive roots. In this case, Kong and Maravelias proposed a column model to handle an undetermined feed, where only active roots are calculated [61]. However, this model becomes computationally inefficient when the number of

[10] The contents of this section appear in Ryu and Maravelias, *Comp. & Chem. Engr.* **2020**

[11] The contents of this section appear in Ryu and Maravelias, *AIChE J.* 2020

components in the system increases. We briefly touch this model here and introduce improvements we proposed, which dramatically improve computational efficiency. Major difference of the previous model [61] from **M2** is that all Underwood roots are constrained to be between the relative volatilities of the keys to calculate only active roots,

$$\sum_{i\in\mathbf{I}}(\alpha_i+\sigma)Y_i^{HK} \le \phi_{i'} \le \sum_{i\in\mathbf{I}}(\alpha_i-\sigma)Y_i^{LK} \quad i'\in\mathbf{I}^{\mathrm{R}} \tag{A.7}$$

where parameter σ is a small number ($10^{-3}\sim10^{-2}$) to make the roots strictly between the relative volatilities of the keys.

Then, binary variable X_i is defined, where $X_i=1$ if and only if component $i+1$ is distributed (i.e., $Z_{i+1}=1$) and has a positive molar flow rate in the feed (i.e., $Y_{i+1}=1$),

$$X_i = Z_{i+1}Y_{i+1} \quad i\in\mathbf{I}^{\mathrm{RD}} \tag{A.8}$$

where the set $\mathbf{I}^{\mathrm{RD}}=\mathbf{I}^{\mathrm{R}}\backslash\{i=n-1\}$ denotes the intervals between the Underwood roots. Note that Eq. (A.8) can be reformulated as a set of linear constraints. Then, the difference between adjacent Underwood roots, Δ_i, is constrained as follows,

$$\phi_i-\phi_{i+1}=\Delta_i \quad i\in\mathbf{I}^{\mathrm{RD}} \tag{A.9}$$

$$\epsilon X_i \le \Delta_i \le (\overline{\alpha}-\underline{\alpha})X_i \quad i\in\mathbf{I}^{\mathrm{RD}} \tag{A.10}$$

where Δ_i is positive when $X_i=1$; otherwise, it is equal to 0, making adjacent roots identical. For instance, when components A and D are selected as the light and heavy keys, respectively, but component C has zero flow, then $X_{\mathrm{A}}=1$ ($Z_{\mathrm{B}}=Y_{\mathrm{B}}=1$) and $X_{\mathrm{B}}=0$ ($Z_{\mathrm{C}}=1, Y_{\mathrm{C}}=0$) are enforced by Eq. (A.8); thus, $\phi_{\mathrm{A}}-\phi_{\mathrm{B}}=\Delta_{\mathrm{A}}\ge\epsilon$ and $\phi_{\mathrm{B}}-\phi_{\mathrm{C}}=\Delta_{\mathrm{B}}=0$ are enforced by Eqs. (A.9) and (A.10) to ensure the existence of two distinct roots ($\phi_{\mathrm{A}}>\phi_{\mathrm{B}}=\phi_{\mathrm{C}}$). Note that $\overline{\alpha}$ can be set as the relative volatility of the lightest component and $\underline{\alpha}$ can be set as 1.

With only Eqs. (A.7) $\sim$ (A.10), the Underwood roots are bounded only by the relative volatilities of the heavy and light keys (i.e., Eq. (A.7)) and the relationships between the roots (i.e., Eqs. (A.9) and (A.10)).

Consider a feed with 5 components, $\mathbf{I} = \{\mathrm{A}, \mathrm{B}, \mathrm{C}, \mathrm{D}, \mathrm{E}\}$, with positive component molar flow rates, ($Y_i = 1,\ \forall i \in \mathbf{I}$). If component A/D is selected as the light/heavy key, B and C are distributed components ($Z_\mathrm{B} = Z_\mathrm{C} = 1$). Binary variables X_A and X_B are activated ($X_\mathrm{A} = X_\mathrm{B} = 1$) while $X_\mathrm{C} = 0$ (because $Z_\mathrm{D} = 0$), enforcing three distinct roots with Eqs. (A.7) $\sim$ (A.10):

$$\alpha_\mathrm{A} > \phi_\mathrm{A} > \phi_\mathrm{B} > \phi_\mathrm{C} = \phi_\mathrm{D} > \alpha_\mathrm{D} > \alpha_\mathrm{E} = 1 \tag{A.11}$$

However, based on the Underwood equations, we know that the roots should satisfy

$$\alpha_\mathrm{A} > \phi_\mathrm{A} > \alpha_\mathrm{B} > \phi_\mathrm{B} > \alpha_\mathrm{C} > \phi_\mathrm{C} = \phi_\mathrm{D} > \alpha_\mathrm{D} > \alpha_\mathrm{E} = 1 \tag{A.12}$$

Accordingly, additional valid constraints are introduced, enforcing that if $X_i = 1$, the relative volatility of component $i+1$ (α_{i+1}) should be between ϕ_i and ϕ_{i+1}.

$$X_i = 1 \rightarrow \phi_i > \alpha_{i+1} > \phi_{i+1} \quad i \in \mathbf{I}^\mathrm{RD} \tag{A.13}$$

Eq. (A.13) can be re-written as follows,

$$\phi_i \geq (\alpha_{i+1} + \sigma)X_i + \underline{\alpha}(1 - X_i) \quad i \in \mathbf{I}^\mathrm{RD} \tag{A.14}$$

$$\phi_{i+1} \leq (\alpha_{i+1} - \sigma)X_i + \overline{\alpha}(1 - X_i) \quad i \in \mathbf{I}^\mathrm{RD} \tag{A.15}$$

Eqs. (A.14) and (A.15) constrain each root depending on the key selection and the existence of components in the feed, thereby enhancing the computational performance of the model. In the previous example, since $X_\mathrm{A} = 1$ and $X_\mathrm{B} = 1$, $\phi_\mathrm{A} > \alpha_\mathrm{B} > \phi_\mathrm{B}$ and $\phi_\mathrm{B} > \alpha_\mathrm{C} > \phi_\mathrm{C}$ are enforced by the valid root constraints, respectively.

Note that roots are correctly constrained even when some flow rates are zero. For example, if $F_C = 0$ ($Y_C = 0$) in the previous example, then $X_B = X_C = 0$ while $X_A = 1$; thus, only two distinct roots exist, and they should satisfy,

$$\alpha_A > \phi_A > \alpha_B > \phi_B = \phi_C = \phi_D > \alpha_D > \alpha_E = 1 \tag{A.16}$$

where $\phi_B = \phi_C$ is enforced because $X_B = 0$. In Eqs. (A.14) and (A.15), $X_A = 1$ enforces $\phi_A > \alpha_B > \phi_B$ while $X_B = 0$ and $X_C = 0$ lead to redundant constraints (i.e., $\phi_B \geq \underline{\alpha}$, $\phi_C \leq \overline{\alpha}$ and $\phi_C \geq \underline{\alpha}$, $\phi_D \leq \overline{\alpha}$). Note that root ϕ_C, which is identical with ϕ_B and ϕ_D, is constrained by Eq. (A.15) on ϕ_B (i.e., $\alpha_B > \phi_B$) and by Eq. (A.7) on ϕ_D (i.e., $\phi_D > \alpha_D$).

A.4 Extension of Column Model with Only Active Roots for Non-Sharp Splits[12]

We introduce an extension of the column model with only active roots to consider non-sharp splits using constraints inspired from the Fenske equation [27].

A.4.1 Practical Feasibility of Non-sharp Splits

In the Underwood equations, we assume that the column has an infinite number of trays and is operated at minimum vapor flow rates for the specified recoveries of the keys. We refer to the design (i.e., vapor flow rates and the number of trays (equilibrium stages)) obtained from the Underwood equations for the specific keys and their recoveries as the *theoretical design*. Note that there can be multiple theoretical designs with different key selections to achieve a separation task. As the recoveries of LLKs/HHKs increase with

[12]The contents of this section appear in Ryu and Maravelias, *AIChE J.* **2020**

more trays, we can assume that they are perfectly recovered in the theoretical design, which can significantly simplify the calculation of component distributions. We refer to this assumption as the *perfect recovery assumption*.

However, a distillation column is typically designed with vapor flow rates between 1.1 and 1.5 times the minimum flow rates and a (finite) number of trays between 3 and 5 times the minimum number of trays, calculated by the Fenske equation [27] based on the recoveries of the key components [56]. Accordingly, we refer to the design with 1.1 $\sim$ 1.5 times the minimum vapor flow rates and 3 $\sim$ 5 times the minimum number of trays based on the theoretical design as the *practical design*. Note that the theoretical and practical designs should achieve the same recoveries of the key components.

It is desirable that the component distributions in the theoretical design can be closely achieved in the corresponding practical design. If the component distributions in the theoretical design are vastly different from those in the corresponding practical design, then the desired separation task may not be achieved in practice. Henceforth, a theoretical design is termed *practically feasible* if the predicted component distributions can be closely achieved in the corresponding practical design. Conversely, a theoretical design is termed *practically infeasible* if its corresponding practical design results in significantly different component distributions. For non-sharp splits where the recoveries of the keys are not high (e.g., < 0.8), perfect recoveries of non-distributed components may not be achievable in the practical design. This is especially true when the relative volatilities of the keys and those of the non-distributed components are close [56]. In this case, other methods such as the Hengstebeck method [46] can be used to calculate component distributions of LLKs/HHKs instead of using the perfect recovery assumption.

However, the incorporation of such methods adds considerable complexity (and nonlinearities). Instead, we propose an approach to select adequate keys and their recoveries to safely use the perfect recovery assumption.

For example, if we need 60 % recovery of component B in the distillate stream and 99 % recovery of component C in the bottom stream for a ternary mixture feed with $\mathbf{I} = \{\mathrm{A}, \mathrm{B}, \mathrm{C}\}$, there are two options as shown in **Figure A.1**; the first option is to

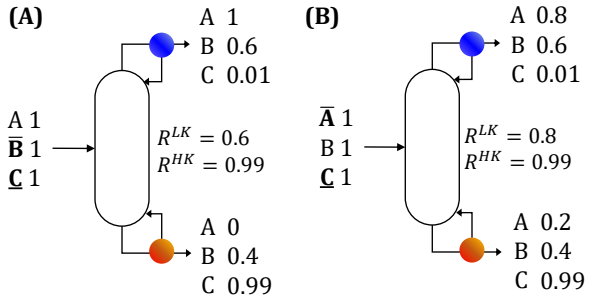

Figure A.1: Two options to recover 60 % of component B in the distillate stream and 99 % of component C in the bottom stream. The light/heavy key is shown as a bold letter with over/under bar. R^{LK}/R^{HK} denotes the recovery of the light/heavy key; (A): Component B/C is selected as the light/heavy key. Component A is perfectly recovered in the distillate stream in the theoretical design, so the corresponding practical design needs to achieve it; (B): A/C is selected as the light/heavy key. Component A can be distributed into the distillate and bottom streams in the theoretical and practical designs.

choose component B as the light key and C as the heavy key in the Underwood equations, resulting in the theoretical design with $R^{LK} = 0.6$ and $R^{HK} = 0.99$ (see **Figure A.1A**). Also, component A (LLK) is perfectly recovered in the distillate stream. For this theoretical design to be practically feasible, component A should be almost perfectly

recovered in the distillate stream in the corresponding practical design. However, if the relative volatility of component A (i.e., LLK) is very close to that of B (i.e., LK), the perfect recovery of A may not be achievable in the corresponding practical design.

This can be addressed by changing the key selection from B/C to A/C in the Underwood equations (see **Figure A.1B**), which allows A to appear in the bottom stream in the theoretical design and its corresponding practical design. Note that if there is no component A in the feed (i.e., $F_{\mathrm{A}} = 0$), it should not affect the practical feasibility of the theoretical design.

Even though the recovery of component B in the distillate stream ($D_{\mathrm{B}}/F_{\mathrm{B}}$) is the same in the two cases, the selection of the keys and their recoveries in the theoretical designs are different depending on practical feasibility, which is affected by 1) the proximity of the relative volatilities between the keys and non-distributed components and 2) the presence of components.

A.4.2 Practical Feasibility Constraints

To determine the practical feasibility of a theoretical design, we augment the Fenske equation. Under the total reflux condition where all vapor stream from the top tray and all liquid stream from the bottom tray are recycled back to the column, Fenske showed that the logarithms of the recovery factors, defined as D_i/B_i, of all components are on a straight line with respect to the logarithms of the relative volatilities,

$$\ln \frac{D_i}{B_i} = m \ln \alpha_i + b \quad i \in \mathbf{I} \tag{A.17}$$

where m/b denotes the slope/intercept of the line. If the recovery of the light key (R^{LK}) and that of the heavy key (R^{HK}) are specified, we can calculate the distributions of

other components as follows,

$$\ln \frac{D_i}{B_i} = N^{MIN} \ln \alpha_i - \frac{\ln \alpha_{\mathrm{LK}} \ln \left[R^{HK}/(1-R^{HK})\right] + \ln \alpha_{\mathrm{HK}} \ln \left[R^{LK}/(1-R^{LK})\right]}{\ln \left(\alpha_{\mathrm{LK}}/\alpha_{\mathrm{HK}}\right)} \quad i \in \mathbf{I} \tag{A.18}$$

where we refer to Eq. (A.18) as the Fenske equation. The slope of the line, N^{MIN}, is the minimum number of trays calculated in terms of the recoveries and relative volatilities of the keys.

$$N^{MIN} = \frac{\ln[R^{LK}/(1-R^{LK})] + \ln \left[R^{HK}/(1-R^{HK})\right]}{\ln \left(\alpha_{\mathrm{LK}}/\alpha_{\mathrm{HK}}\right)} \tag{A.19}$$

In **Figure A.2**, three different component distributions with the same recoveries of the keys are shown based on the work of Stupin and Lockhart [96]. The x-axis denotes the logarithm of the relative volatility, and the y-axis denotes the logarithm of the recovery factor. The blue curve represents component distributions in the theoretical design. $\hat{\phi}^{LK+}$ is the Underwood root between the relative volatility of the light key and that of the LLK adjacent to the light key (referred to as LLK1) while $\hat{\phi}^{HK-}$ is the root between the relative volatility of the heavy key and that of the HHK adjacent to the heavy key (referred to as HHK1). When the relative volatility of a component approaches $\hat{\phi}^{LK+}/\hat{\phi}^{HK-}$, the logarithm of its recovery factor becomes $\infty/-\infty$. Since the relative volatilities of LLKs/HHKs are greater/less than $\hat{\phi}^{LK+}/\hat{\phi}^{HK-}$, they are perfectly recovered in the distillate/bottom stream.

The red curve represents component distributions in a practical design based on the theoretical design. The black line represents component distributions calculated by the Fenske equation based on the recoveries of the keys. Notably, the recovery factor of a LLK from the Fenske equation can be used as a lower bound on its recovery factor in the practical design ($D^{FS}_{\mathrm{LLK}}/B^{FS}_{\mathrm{LLK}} \leq D_{\mathrm{LLK}}/B_{\mathrm{LLK}}$). Also, the recovery factor of a HHK

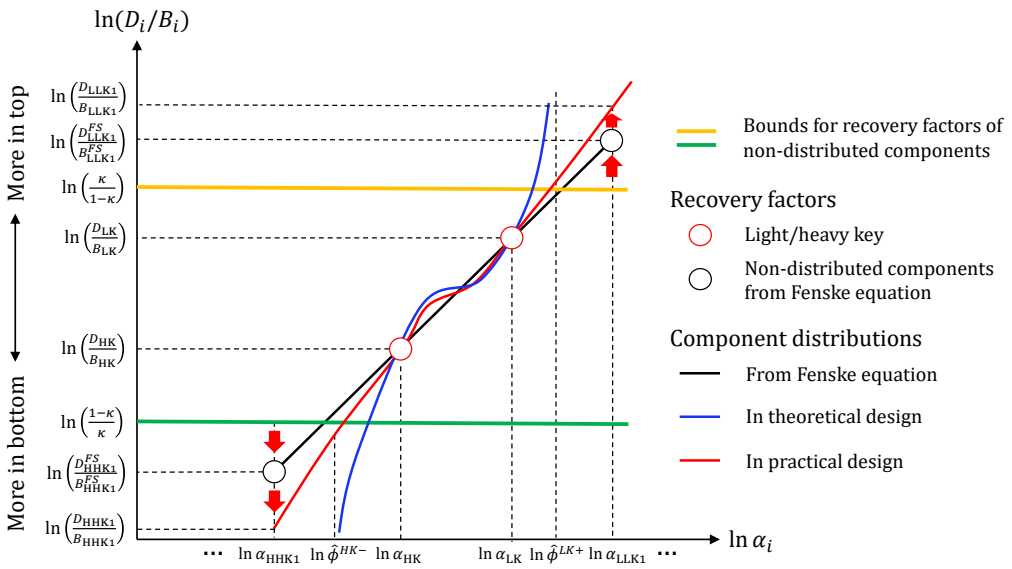

Figure A.2: (Blue/Red) Component distributions in theoretical/practical design; (Black): Component distributions from the Fenske equation. Recovery factors calculated by the Fenske equation are denoted with superscript FS; (Orange/Green): Bound for recovery factors of LLKs/HHKs.

from the Fenske equation can be used as an upper bound on its recovery factor in the practical design ($D^{FS}_{\mathrm{HHK}}/B^{FS}_{\mathrm{HHK}} \geq D_{\mathrm{HHK}}/B_{\mathrm{HHK}}$). Similar arguments have been used to develop heuristic rules for non-sharp splits. [5, 17, 68]

Then, if we introduce a bound for the recovery factors of LLKs/HHKs calculated by the Fenske equation, we can indirectly introduce a lower bound, κ, on their recoveries in the practical design. For example, in **Figure A.2**, we introduce the bound (i.e., $\kappa/(1-\kappa)$, orange line) for the recovery factors of LLKs from the Fenske equation. Since $D^{FS}_{\mathrm{LLK1}}/B^{FS}_{\mathrm{LLK1}} \leq D_{\mathrm{LLK1}}/B_{\mathrm{LLK1}}$, if $\kappa/(1-\kappa) \leq D^{FS}_{\mathrm{LLK1}}/B^{FS}_{\mathrm{LLK1}}$ holds as shown in **Figure**

A.2, the following holds,

$$\frac{\kappa}{1-\kappa} \leq \frac{D^{FS}_{\mathrm{LLK1}}}{B^{FS}_{\mathrm{LLK1}}} \leq \frac{D_{\mathrm{LLK1}}}{B_{\mathrm{LLK1}}} = \frac{(D_{\mathrm{LLK1}}/F_{\mathrm{LLK1}})}{1-(D_{\mathrm{LLK1}}/F_{\mathrm{LLK1}})} \tag{A.20}$$

which implies, in the practical design, that $D_{\mathrm{LLK1}}/F_{\mathrm{LLK1}} > \kappa$. Similarly, we introduce the bound (i.e., $(1-\kappa)/\kappa$, green line) for the recovery factors of HHKs from the Fenske equation. If $(1-\kappa)/\kappa \geq D^{FS}_{\mathrm{HHK1}}/B^{FS}_{\mathrm{HHK1}}$ holds as shown in **Figure A.2**, the following holds,

$$\frac{1-\kappa}{\kappa} \geq \frac{D^{FS}_{\mathrm{HHK1}}}{B^{FS}_{\mathrm{HHK1}}} \geq \frac{D_{\mathrm{HHK1}}}{B_{\mathrm{HHK1}}} = \frac{1-(B_{\mathrm{HHK1}}/F_{\mathrm{HHK1}})}{B_{\mathrm{HHK1}}/F_{\mathrm{HHK1}}} \tag{A.21}$$

which implies $B_{\mathrm{HHK1}}/F_{\mathrm{HHK1}} > \kappa$. Note that if these conditions are satisfied for LLK1 and HHK1, they are automatically satisfied for the components that are lighter than LLK1 or heavier than HHK1. If Eqs. (A.20) and (A.21) hold with the parameter κ sufficiently close to 1, the theoretical design is more likely to be practically feasible because LLKs/HHKs can be almost perfectly recovered in the practical design.

Based on these criteria, two inequalities are introduced, which lead to designs that are more likely to be implementable in practice,

$$\ln\frac{\kappa}{1-\kappa} \leq (\theta^{LLK}_{i,i',i-m}+1)\bar{R}^{LK} + \theta^{LLK}_{i,i',i-m}\bar{R}^{HK} + \mu(3-Y^{LK}_{i}-Y^{HK}_{i'}-Y_{i-m})$$
$$1<i<n,\ i<i'\in\mathbf{I},\ 1\leq i-m\leq i-1 \tag{A.22}$$

$$\ln\frac{1-\kappa}{\kappa} \geq \theta^{HHK}_{i,i',i'+m}\bar{R}^{LK} + (\theta^{HHK}_{i,i',i'+m}-1)\bar{R}^{HK} - \mu(3-Y^{LK}_{i}-Y^{HK}_{i'}-Y_{i'+m})$$
$$1<i'<n,\ i<i'\in\mathbf{I},\ i'+1\leq i'+m\leq n \tag{A.23}$$

$$\bar{R}^{LK} = \ln\left[R^{LK}/(1-R^{LK})\right] \tag{A.24}$$

$$\bar{R}^{HK} = \ln\left[R^{HK}/(1-R^{HK})\right] \tag{A.25}$$

where the parameter μ is used to relax the inequalities, and parameters $\theta^{LLK}_{i,i',i-m}$ and $\theta^{HHK}_{i,i',i'+m}$ are defined as follows,

$$\theta^{LLK}_{i,i',i-m} = \frac{\ln\left(\alpha_{i-m}/\alpha_i\right)}{\ln\left(\alpha_i/\alpha_{i'}\right)} \quad 1 < i < n,\ i < i' \in \mathbf{I},\ 1 \leq i-m \leq i-1 \tag{A.26}$$

$$\theta^{HHK}_{i,i',i'+m} = \frac{\ln\left(\alpha_{i'+m}/\alpha_{i'}\right)}{\ln\left(\alpha_i/\alpha_{i'}\right)} \quad 1 < i' < n,\ i < i' \in \mathbf{I},\ i'+1 \leq i'+m \leq n \tag{A.27}$$

where detailed derivations can be found in the supporting information of the original work [84]. In Eq. (A.22), components i and i' denote candidates for the light and heavy keys, respectively; while $i-m$ denotes a LLK when i is selected as the light key ($1 \leq i-m \leq i-1$). When $Y^{LK}_i = Y^{HK}_{i'} = Y_{i-m} = 1$, Eq. (A.22) enforces the recovery of component $i-m$ (LLK) in the practical design to be higher than κ; otherwise, it becomes a redundant constraint. In Eq. (A.23), components i and i' denote the light and heavy key candidates, while $i'+m$ denotes a HHK ($i'+1 \leq i'+m \leq n$). When $Y^{LK}_i = Y^{HK}_{i'} = Y_{i'+m} = 1$, Eq. (A.23) enforces the recovery of component $i'+m$ (HHK) in the practical design to be higher than κ.

Note that the parameter κ can be adjusted; if κ is closer to 1, the perfect recoveries of LLKs/HHKs are more likely to be achieved in the practical design while the recoveries of the keys are also more tightly constrained, leading to a smaller feasible space for non-sharp splits. With the proposed approach, we can take the proximity of relative volatilities into account instead of simply enforcing a fixed lower bound on the recoveries of the keys (e.g., $R^{HK}, R^{LK} > \bar{\gamma}^R$).

The recoveries of the light and heavy keys (R^{LK}, R^{HK}) are constrained as follows,

$$D_i = F_i R^{LK} + \hat{D}^{LK+}_i - \hat{D}^{LK-}_i \quad i \in \mathbf{I} \tag{A.28}$$

$$B_i = F_i R^{HK} + \hat{B}^{HK+}_i - \hat{B}^{HK-}_i \quad i \in \mathbf{I} \tag{A.29}$$

where dummy variables $\hat{D}_i^{LK+}$, $\hat{D}_i^{LK-}$, $\hat{B}_i^{HK+}$, $\hat{B}_i^{HK-}$ are introduced. Dummy variables $\hat{D}_i^{LK+}$ and $\hat{D}_i^{LK-}$ are deactivated if component i is selected as the light key,

$$\hat{D}_i^{LK+} \leq \delta_i^D (1 - Y_i^{LK}) \quad i \in \mathbf{I} \tag{A.30}$$

$$\hat{D}_i^{LK-} \leq \delta_i^D (1 - Y_i^{LK}) \quad i \in \mathbf{I} \tag{A.31}$$

while $\hat{B}_i^{HK+}$ and $\hat{B}_i^{HK-}$ are deactivated when component i is selected as the heavy key.

$$\hat{B}_i^{HK+} \leq \delta_i^B (1 - Y_i^{HK}) \quad i \in \mathbf{I} \tag{A.32}$$

$$\hat{B}_i^{HK-} \leq \delta_i^B (1 - Y_i^{HK}) \quad i \in \mathbf{I} \tag{A.33}$$

When deactivated, $D_i = F_i R^{LK}$ and $B_i = F_i R^{HK}$ are enforced in Eqs. (A.28) and (A.29), respectively; if component i is not selected as the light key, $\hat{D}_i^{LK+}$ and $\hat{D}_i^{LK-}$ can be positive, relaxing the equality between D_i and $F_i R^{LK}$. Similarly, if component i is not selected as the heavy key, $\hat{B}_i^{HK+}$ and $\hat{B}_i^{HK-}$ can be positive, so the equality between B_i and $F_i R^{HK}$ is relaxed.

Appendix B

Chapter 3 Appendix[13]

B.1 Distillation Column Model

In the column model [84], the set of intervals between postulated components is defined for each mixture node as $\mathbf{I}^{\mathrm{R}}_{jk} = \{i \in \mathbf{I} | i^L_{jk} \leq i \leq i^H_{jk} - 1\}$, where interval i denotes the interval between components i and $i+1$. Then, the Underwood root (ϕ_{ijk}) is defined for each interval ($\phi_{ijk} \geq \phi_{i+1,jk}$). For example, if node (1,1) has $\mathbf{I}^{\mathrm{C}}_{11} = \{\mathrm{A}, \mathrm{B}, \mathrm{C}, \mathrm{D}\}$, there are three intervals, $\mathbf{I}^{\mathrm{R}}_{11} = \{\mathrm{A}, \mathrm{B}, \mathrm{C}\}$, with three Underwood roots ($\phi_{\mathrm{A}11} \geq \phi_{\mathrm{B}11} \geq \phi_{\mathrm{C}11}$). The Underwood roots satisfy the following,

$$\sum_{i \in \mathbf{I}} \frac{\alpha_i F^C_{ijk}}{\alpha_i - \phi_{i'jk}} = V1_{jk} - V2_{jk} \qquad i' \in \mathbf{I}^{\mathrm{R}}_{jk}, (j,k) \in \mathbf{N}^{\mathrm{DM}} \tag{B.1}$$

The roots are constrained between the relative volatilities of the light and heavy keys,

$$\sum_{i \in \mathbf{I}} \alpha_i Y^{HK}_{ijk} \leq \phi_{i'jk} \leq \sum_{i \in \mathbf{I}} \alpha_i Y^{LK}_{ijk} \qquad i' \in \mathbf{I}^{\mathrm{R}}_{jk}, (j,k) \in \mathbf{N}^{\mathrm{DM}} \tag{B.2}$$

to calculate only *active* roots which are required to calculate the minimum vapor flow rates. Binary variable Z_{ijk} denotes whether component i is a distributed component. Also, the correct number of distinct active roots is enforced by $X^R_{ijk} \in \{0,1\}$ as follows,

$$\epsilon X^R_{ijk} \leq \phi_{ijk} - \phi_{i+1,jk} \leq (\overline{\alpha} - \underline{\alpha}) X^R_{ijk} \qquad i \in \mathbf{I}^{\mathrm{RD}}_{jk} \tag{B.3}$$

$$X^R_{ijk} = Y_{i+1,jk} Z_{i+1,jk} \qquad i \in \mathbf{I}^{\mathrm{RD}}_{jk}, (j,k) \in \mathbf{N}^{\mathrm{DM}} \tag{B.4}$$

[13]The contents of this chapter appear in Ryu and Maravelias, *Chem. Eng. Sci.* **2021**

where set $\mathbf{I}^{\mathrm{RD}}_{jk} = \{i \in \mathbf{I} | i^L_{jk} \leq i \leq i^H_{jk} - 2\}$ denotes intervals between the Underwood roots; ϵ denotes a lower bound on the absolute difference between adjacent roots; $\overline{\alpha}/\underline{\alpha}$ is the lowest/highest relative volatility (i.e., $\overline{\alpha} = \alpha_{\mathrm{A}}$, $\underline{\alpha} = 1$). If component $i+1$ is present and distributed, $X^R_{ijk} = 1$ is enforced by Eq (B.4), and $\phi_{ijk} - \phi_{i+1,jk} \geq \epsilon$ is enforced by Eq (B.3); if $X^R_{ijk} = 0$, $\phi_{ijk} - \phi_{i+1,jk} = 0$ is enforced by Eq. (B.3). Also, valid constraints for the roots are introduced as follows,

$$\phi_{ijk} \geq (\alpha_{i+1} + \sigma) X^R_{ijk} + \underline{\alpha}(1 - X^R_{ijk}) \qquad i \in \mathbf{I}^{\mathrm{RD}}_{jk}, (j,k) \in \mathbf{N}^{\mathrm{DM}} \tag{B.5}$$

$$\phi_{i+1,jk} \leq (\alpha_{i+1} - \sigma) X^R_{ijk} + \overline{\alpha}(1 - X^R_{ijk}) \qquad i \in \mathbf{I}^{\mathrm{RD}}_{jk}, (j,k) \in \mathbf{N}^{\mathrm{DM}} \tag{B.6}$$

where σ is a small number ($10^{-3} \sim 10^{-4}$) and $\underline{\alpha}/\overline{\alpha}$ denotes a lower/upper bound on relative volatilities (e.g., $\underline{\alpha} = 1/\overline{\alpha} = \alpha_{\mathrm{A}}$ can be set). For example, consider node (1,1) with $\mathbf{I}^{\mathrm{C}}_{11} = \{\mathrm{A}, \mathrm{B}, \mathrm{C}, \mathrm{D}\}$ and $Y_{\mathrm{C}11} = 0$. Then, if component A/D is selected as the light/heavy key (i.e., $Y^{LK}_{\mathrm{A}11} = 1$ and $Y^{HK}_{\mathrm{D}11} = 1$), components B and C are distributed (i.e., $Z_{\mathrm{B}11} = 1$ and $Z_{\mathrm{C}11} = 1$). By Eq (B.4), $X^R_{\mathrm{A}11} = 1$ and $X^R_{\mathrm{B}11} = 0$ are enforced, so $\phi_{\mathrm{A}11} - \phi_{\mathrm{B}11} \geq \epsilon$ and $\phi_{\mathrm{B}11} - \phi_{\mathrm{C}11} = 0$ are enforced by Eq (B.3). Then, Eqs. (B.5) and (B.6) enforce $\phi_{\mathrm{A}11} > \alpha_{\mathrm{B}}$ and $\phi_{\mathrm{B}11} < \alpha_{\mathrm{B}}$, constraining the roots as $\alpha_{\mathrm{A}} > \phi_{\mathrm{A}11} > \alpha_{\mathrm{B}} > \phi_{\mathrm{B}11} = \phi_{\mathrm{C}11} > 1$.

The vapor flow rates are constrained as follows,

$$\sum_{i \in \mathbf{I}} \frac{\alpha_i D_{ijk}}{\alpha_i - \phi_{i'jk}} \leq V1_{jk} \qquad i' \in \mathbf{I}^{\mathrm{R}}_{jk}, (j,k) \in \mathbf{N}^{\mathrm{DM}} \tag{B.7}$$

$$\sum_{i \in \mathbf{I}} \frac{-\alpha_i B_{ijk}}{\alpha_i - \phi_{i'jk}} \leq V2_{jk} \qquad i' \in \mathbf{I}^{\mathrm{R}}_{jk}, (j,k) \in \mathbf{N}^{\mathrm{DM}} \tag{B.8}$$

where inequalities are used because some columns can be operated above its minimum vapor flow rates due to thermal coupling [12]. Although not necessary, minimum recoveries of key components ($\gamma^{LK}_{jk}/\gamma^{HK}_{jk}$ for the light/heavy key) can be imposed for each

column.

$$D_{ijk} \geq \gamma_{jk}^{LK} F_{ijk}^{C} - \zeta_{ijk}^{D}(1 - Y_{ijk}^{LK}) \qquad i \in \mathbf{I}, (j,k) \in \mathbf{N}^{\mathrm{DM}} \tag{B.9}$$

$$B_{ijk} \geq \gamma_{jk}^{HK} F_{ijk}^{C} - \zeta_{ijk}^{B}(1 - Y_{ijk}^{HK}) \qquad i \in \mathbf{I}, (j,k) \in \mathbf{N}^{\mathrm{DM}} \tag{B.10}$$

B.2 Light and Heavy Key Candidates

There are two types of separation tasks depending on whether there are distributed components or not. First, let's consider a separation task with distributed components. For example, in **Figure B.1**, top arc from node (1,1) ($\mathbf{I}_{11}^{\mathrm{C}} = \{\mathrm{A}, \mathrm{B}, \mathrm{C}, \mathrm{D}, \mathrm{E}\}$) to node (1,3) ($\mathbf{I}_{13}^{\mathrm{C}} = \{\mathrm{A}, \mathrm{B}, \mathrm{C}\}$) and the bottom arc from node (1,1) to node (3,3) ($\mathbf{I}_{33}^{\mathrm{C}} = \{\mathrm{C}, \mathrm{D}, \mathrm{E}\}$) are active. Thus, in column (1,1), component B/D can be the light/heavy key while C is distributed. However, if B is not present in the source (i.e., $Y_{\mathrm{B}} = 0$), then it cannot be chosen as the light key due to Eq. (3.35). In this case, the next heaviest component, which is A, should be chosen as the light key. On the other hand, if $Y_{\mathrm{D}} = 0$, D cannot be chosen as the heavy key due to Eq. (3.36), so the next lightest component, which is E, should be selected as the heavy key. Thus, depending on components present in the source, the light/heavy key for one separation task can change. For the separation task defined by an active top arc $(j,k,j',k') \in \mathbf{A}_{jk}^{\mathrm{TS}}$ and an active bottom arc $(j,k,j'',k'') \in \mathbf{A}_{jk}^{\mathrm{BS}}$, the set of light/heavy key *candidates* ($\mathbf{I}_{j'k'j''k''}^{\mathrm{LK}}$/$\mathbf{I}_{j'k'j''k''}^{\mathrm{HK}}$) can be defined as follows,

$$\mathbf{I}_{j'k'j''k''}^{\mathrm{LK}} = \{i \in \mathbf{I} | i_{j'k'}^{L} \leq i \leq i_{j''k''}^{L} - 1\} \quad (j',k',j'',k'') \in \{(j',k',j'',k'') | i_{j''k''}^{L} \leq i_{j'k'}^{H}\} \tag{B.11}$$

$$\mathbf{I}_{j'k'j''k''}^{\mathrm{HK}} = \{i \in \mathbf{I} | i_{j'k'}^{H} + 1 \leq i \leq i_{j''k''}^{H}\} \quad (j',k',j'',k'') \in \{(j',k',j'',k'') | i_{j''k''}^{L} \leq i_{j'k'}^{H}\} \tag{B.12}$$

where $i^L_{j''k''} \leq i^H_{j'k'}$ denotes there are distributed components. However, if there is no distributed component (i.e., $i^L_{j''k''} > i^H_{j'k'}$), the light/heavy key selection is simpler. For example, in **Figure B.1**, top arc from node (1,1) to node (1,4) ($\mathbf{I}^{\mathrm{C}}_{14} = \{\mathrm{A}, \mathrm{B}\}$) and bottom arc from node (1,1) to node (3,3) ($\mathbf{I}^{\mathrm{C}}_{33} = \{\mathrm{C}, \mathrm{D}, \mathrm{E}\}$) are active, so component B/C can be selected as the light/heavy key because the activation of nodes (1,4) and (3,3) implies $Y_{\mathrm{B}} = 1$ and $Y_{\mathrm{C}} = 1$, respectively, by Eq. (3.17). Thus, when there is no distributed component, the light/heavy key can be uniquely identified as follows,

$$\mathbf{I}^{LK}_{j'k'j''k''} = \{i \in \mathbf{I} | i = i^H_{j'k'}\} \qquad (j', k', j'', k'') \in \{(j', k', j'', k'') | i^L_{j''k''} > i^H_{j'k'}\} \tag{B.13}$$

$$\mathbf{I}^{HK}_{j'k'j''k''} = \{i \in \mathbf{I} | i = i^L_{j''k''}\} \qquad (j', k', j'', k'') \in \{(j', k', j'', k'') | i^L_{j''k''} > i^H_{j'k'}\} \tag{B.14}$$

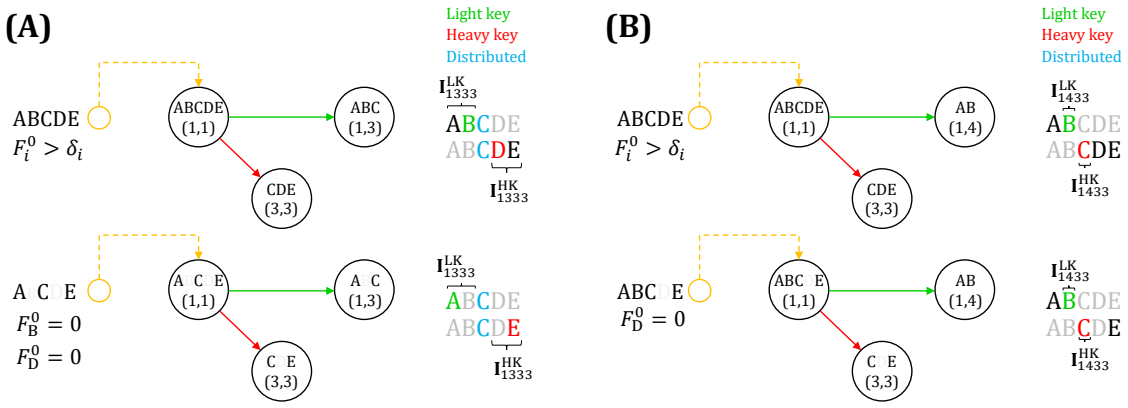

Figure B.1: Light and heavy key candidates when active top and bottom arcs are given. Light/heavy keys are represented in green/red while distributed components are represented in blue; (A): When there are distributed components between the distillate and bottom streams. The light/heavy key is determined depending on whether component B/D is present in the source. (B): When there is no distributed component. Component B is present in the source, which is implied by the activation of node (1,4). Similarly, component C is present, which is implied by the activation of node (3,3). Thus, the light/heavy key is determined as B/C regardless of the presence of other components.

Appendix C

Chapter 4 Appendix[14]

C.1 Distillation Network Model

We define ordered set $\mathbf{I} = \{\mathrm{A}, \mathrm{B}, ...\}$ to denote components in the system in decreasing order of volatility. Sets $\mathbf{S}^{\mathrm{IN}}$ and $\mathbf{S}^{\mathrm{OUT}}$ are defined to denote inlets and outlets, respectively. An inlet stream can be sent to columns and/or outlets,

$$\sum_{l \in \mathbf{L}} E^{IC}_{s,l} + \sum_{s' \in \mathbf{S}^{\mathrm{OUT}}} E^{IO}_{s,s'} = 1 \qquad\qquad s \in \mathbf{S}^{\mathrm{IN}} \tag{C.1}$$

where $E^{IC}_{s,l}$ and $E^{IO}_{s,s'}$ denote the split fractions of inlet stream s to column l and outlet s', respectively. When the inlet stream is sent to column l, then the corresponding binary variable $Y^{IC}_{s,l}$ is set to 1. Similarly, when the inlet stream is sent to an outlet s', then the corresponding binary variable $Y^{IO}_{s,s'}$ is set to 1.

$$\underline{\delta}^{IC}_{s,l} Y^{IC}_{s,l} \leq E^{IC}_{s,l} \leq Y^{IC}_{s,l} \qquad\qquad s \in \mathbf{S}^{\mathrm{IN}}, l \in \mathbf{L} \tag{C.2}$$

$$\underline{\delta}^{IO}_{s,s'} Y^{IO}_{s,s'} \leq E^{IO}_{s,s'} \leq Y^{IO}_{s,s'} \qquad\qquad s \in \mathbf{S}^{\mathrm{IN}}, s' \in \mathbf{S}^{\mathrm{OUT}} \tag{C.3}$$

Parameter $\underline{\delta}^{IC}_{j,l} / \underline{\delta}^{IO}_{s,s'}$ denotes the lower bound on the split fraction when the connection is selected. Binary variable Y_l is introduced to denote whether column l is selected or not. When the column is not selected (i.e., $Y_l = 0$), the corresponding feed stream is

[14]The contents of this chapter appear in Ryu and Maravelias, *AIChE J.* **2022**

deactivated,

$$\underline{\delta}_{l,i} Y_l \leq F_{l,i} \leq \overline{\delta}_{l,i} Y_l \qquad i \in \mathbf{I}, l \in \mathbf{L} \tag{C.4}$$

where parameters $\underline{\delta}_{l,i}$ and $\overline{\delta}_{l,i}$ denote the lower and upper bounds, respectively, on the component molar flow rate of the feed stream. The distillate/bottom stream can be sent to other columns or outlets,

$$\sum_{l' \in \mathbf{L}} E^{DC}_{l,l'} + \sum_{s' \in \mathbf{S}^{\mathrm{OUT}}} E^{DO}_{l,s'} = 1 \qquad l \in \mathbf{L} \tag{C.5}$$

$$\sum_{l' \in \mathbf{L}} E^{BC}_{l,l'} + \sum_{s' \in \mathbf{S}^{\mathrm{OUT}}} E^{BO}_{l,s'} = 1 \qquad l \in \mathbf{L} \tag{C.6}$$

where $E^{DC}_{l,l'}$ and $E^{BC}_{l,l'}$ denote the split fractions of the distillate and bottom streams, respectively, to column l'; $E^{DO}_{l,s'}$ and $E^{BO}_{l,s'}$ denote the split fractions of the distillate and bottom stream, respectively, to outlet k. These split fractions are also constrained by the corresponding binary variables ($Y^{BC}_{l,l'}$,$Y^{DC}_{l,l'}$,$Y^{BO}_{l,s'}$, and $Y^{DO}_{l,s'}$).

$$\delta^{BC}_{l,l'} Y^{BC}_{l,l'} \leq E^{BC}_{l,l'} \leq Y^{BC}_{l,l'} \qquad l, l' \in \mathbf{L} \tag{C.7}$$

$$\delta^{DC}_{l,l'} Y^{DC}_{l,l'} \leq E^{DC}_{l,l'} \leq Y^{DC}_{l,l'} \qquad l, l' \in \mathbf{L} \tag{C.8}$$

$$\delta^{BO}_{l,s'} Y^{BO}_{l,s'} \leq E^{BO}_{l,s'} \leq Y^{BO}_{l,s'} \qquad l \in \mathbf{L}, s' \in \mathbf{S}^{\mathrm{OUT}} \tag{C.9}$$

$$\delta^{DO}_{l,s'} Y^{DO}_{l,s'} \leq E^{DO}_{l,s'} \leq Y^{DO}_{l,s'} \qquad l \in \mathbf{L}, s' \in \mathbf{S}^{\mathrm{OUT}} \tag{C.10}$$

Material balances for column feed streams and network outlet streams are as follows,

$$\sum_{s \in \mathbf{S}^{\mathrm{IN}}} F^{IC}_{s,l,i} + \sum_{l' \in \mathbf{L}} (D^{DC}_{l',l,i} + B^{BC}_{l',l,i}) = F_{l,i} \qquad l \in \mathbf{L}, i \in \mathbf{I} \tag{C.11}$$

$$\sum_{s \in \mathbf{S}^{\mathrm{IN}}} F^{IO}_{s,s',i} + \sum_{l \in \mathbf{L}} (D^{DO}_{l,s',i} + B^{BO}_{l,s',i}) = F^{OUT}_{s',i} \qquad s' \in \mathbf{S}^{\mathrm{OUT}}, i \in \mathbf{I} \tag{C.12}$$

$$F^{IC}_{s,l,i} = E^{IC}_{s,l} F^{IN}_{s,i} \qquad s \in \mathbf{S}^{\mathrm{IN}}, l \in \mathbf{L}, i \in \mathbf{I} \tag{C.13}$$

$$F^{IO}_{s,s',i} = E^{IO}_{s,s'} F^{IN}_{s,i} \qquad s \in \mathbf{S}^{\mathrm{IN}}, s' \in \mathbf{S}^{\mathrm{OUT}}, i \in \mathbf{I} \tag{C.14}$$

$$D^{DC}_{l,l',i} = E^{DC}_{l,l'} D_{l,i} \qquad l, l' \in \mathbf{L}, i \in \mathbf{I} \tag{C.15}$$

$$B^{BC}_{l,l',i} = E^{BC}_{l,l'} B_{l,i} \qquad l, l' \in \mathbf{L}, i \in \mathbf{I} \tag{C.16}$$

$$D^{DO}_{l,s',i} = E^{DO}_{l,s'} D_{l,i} \qquad l \in \mathbf{L}, s' \in \mathbf{S}^{\mathrm{OUT}}, i \in \mathbf{I} \tag{C.17}$$

$$B^{BO}_{l,s',i} = E^{BO}_{l,s'} B_{l,i} \qquad l \in \mathbf{L}, s' \in \mathbf{S}^{\mathrm{OUT}}, i \in \mathbf{I} \tag{C.18}$$

where $F^{IC}_{s,l,i}/F^{IO}_{s,s',i}$ denotes the molar flow rate of the inlet stream to the column/outlet; $D^{DC}_{l',l,i}/B^{BC}_{l',l,i}$ denotes the molar flow rate of the distillate/bottom stream to other columns; $D^{DO}_{l,s',i}/B^{BO}_{l,s',i}$ denotes the molar flow rate of the distillate/bottom stream to outlets; and $F^{IN}_{s,i}/F^{OUT}_{s',i}$ denotes the component molar flow rate of the inlet/outlet stream. Specifications for purities ($\rho^{P}_{s',i}$) and recoveries ($\rho^{R}_{s',i}$) can be imposed on outlet streams,

$$F^{OUT}_{s',i} \geq \rho^{P}_{s',i} \sum_{i' \in \mathbf{I}} F^{OUT}_{s',i'} \ \textit{or}\ F^{OUT}_{s',i} \leq \rho^{P}_{s',i} \sum_{i' \in \mathbf{I}} F^{OUT}_{s',i'} \qquad s' \in \mathbf{S}^{\mathrm{OUT}}, i \in \mathbf{I}^{\mathrm{S}}_{s'} \tag{C.19}$$

$$F^{OUT}_{s',i} \geq \rho^{R}_{s',i} \sum_{s \in \mathbf{S}^{\mathrm{IN}}} F^{IN}_{s,i'} \ \textit{or}\ F^{OUT}_{s',i} \leq \rho^{R}_{s',i} \sum_{s \in \mathbf{S}^{\mathrm{IN}}} F^{IN}_{s,i} \qquad s' \in \mathbf{S}^{\mathrm{OUT}}, i \in \mathbf{I}^{\mathrm{S}}_{s'} \tag{C.20}$$

where $\mathbf{I}^{\mathrm{S}}_{s'}$ denotes the set of components with specifications for the outlet stream associated with outlet s'. We also introduce constraints to limit the complexity of the optimal solution. First, we do not allow recycle within the distillation network.

$$Y^{DC}_{l,l'} + Y^{BC}_{l,l'} = 0 \qquad l > l', l, l' \in \mathbf{L} \tag{C.21}$$

$$Y^{DC}_{l,l'} + Y^{BC}_{l,l'} = 0 \qquad l > l', l, l' \in \mathbf{L} \tag{C.22}$$

Also, we only allow the connection between columns either through the distillate stream or through the bottom stream.

$$Y^{DC}_{l,l'} + Y^{BC}_{l,l'} \leq 1 \qquad l, l' \in \mathbf{L} \tag{C.23}$$

C.2 Reactor Network Model

We define set $\mathbf{R}$ to denote reactors. The reactor inlet ($F_{r,i}^{R,IN}$) consists of the initial feed ($\psi_{r,i}^{R,IT}$) and the recycle stream ($F_{s',i}^{OUT}$) from the distillation network,

$$F_{r,i}^{R,IN} = \psi_{r,i}^{R,IT} + \sum_{s' \in \mathbf{S}_r^{\mathrm{OUT}}} F_{s',i}^{OUT} \qquad r \in \mathbf{R}, i \in \mathbf{I} \tag{C.24}$$

where the set $\mathbf{S}_r^{\mathrm{OUT}}$ consists of outlet streams assigned for the recycle stream to reactor r. Each reactor has a fixed conversion (η_r) based on the limiting reactant (i_r^L),

$$F_{r,i}^{R,IN} + \nu_{r,i}\eta_r F_{r,i=i_r^L}^{R,IN} = F_{r,i}^{R,OUT} \qquad r \in \mathbf{R}, i \in \mathbf{I} \tag{C.25}$$

where $F_{r,i}^{R,OUT}$ denotes the component molar flow rate of the reactor outlet; and $\nu_{r,i}$ denotes the stoichiometry. The cost of a reactor is proportional to its total inlet molar flow rate,

$$C_r^R = \mu_r^R \sum_{i \in \mathbf{I}} F_{r,i}^{R,IN} \qquad r \in \mathbf{R} \tag{C.26}$$

where μ_r^R denotes the annualized cost parameter for the reactor.

Appendix D

Chapter 5 Appendix[15]

D.1 Projection of Stream Data onto Temperature Grid

Similar to the hot stream inlet temperature projection, the rest of the temperature ranges are projected onto the grid. Hot stream outlet temperature range is projected by identical algorithm as that for the inlet temperature range. Information of cold stream is projected onto the cold stream temperature grid instead with the same algorithm.

D.1.1 Hot Stream Outlet Preprocessing

$$\phi_{s,k}^{\mathrm{H,OUT,UP}} = \begin{cases} 1 & \text{if } k = \arg\min_{k'} \|\hat{T}_{k'}^{\mathrm{H}} - T_s^{\mathrm{OUT,UP}}\| \\ & \text{s.t.} \hat{T}_{k'}^{\mathrm{H}} \geq T_s^{\mathrm{OUT,UP}} \qquad s \in \mathbf{S}, k \in \mathbf{K} \\ 0 & \text{otherwise} \end{cases} \tag{D.1}$$

$$\phi_{s,k}^{\mathrm{H,OUT,LO}} = \begin{cases} 1 & \text{if } k = \arg\min_{k'} \|\hat{T}_{k'}^{\mathrm{H}} - T_s^{\mathrm{OUT,LO}}\| \\ & \text{s.t.} \hat{T}_{k'}^{\mathrm{H}} \leq T_s^{\mathrm{OUT,LO}} \qquad s \in \mathbf{S}, k \in \mathbf{K} \\ 0 & \text{otherwise} \end{cases} \tag{D.2}$$

[15]The contents of this chapter appear in Ryu and Maravelias, *Ind. Eng. Chem. Res.* **2019**

$$\psi_{s,k}^{\mathrm{H,OUT}} = \phi_{s,k}^{\mathrm{H,OUT,UP}} + \psi_{s,k-1}^{\mathrm{H,OUT}} - \phi_{s,k-1}^{\mathrm{H,OUT,LO}} \qquad s \in \mathbf{S}, k \in \mathbf{K} \tag{D.3}$$

D.1.2 Cold Stream Inlet Preprocessing

$$\phi_{s,k}^{\mathrm{C,IN,UP}} = \begin{cases} 1 & \text{if } k = \arg\min_{k'} \|\hat{T}_{k'}^{\mathrm{C}} - T_s^{\mathrm{IN,UP}}\| \\ & \text{s.t.} \hat{T}_{k'}^{\mathrm{C}} \leq T_s^{\mathrm{IN,UP}} \\ 0 & \text{otherwise} \end{cases} \qquad s \in \mathbf{S}, k \in \mathbf{K} \tag{D.4}$$

$$\phi_{s,k}^{\mathrm{C,IN,LO}} = \begin{cases} 1 & \text{if } k = \arg\min_{k'} \|\hat{T}_{k'}^{\mathrm{C}} - T_s^{\mathrm{IN,LO}}\| \\ & \text{s.t.} \hat{T}_{k'}^{\mathrm{C}} \geq T_s^{\mathrm{IN,LO}} \\ 0 & \text{otherwise} \end{cases} \qquad s \in \mathbf{S}, k \in \mathbf{K} \tag{D.5}$$

$$\psi_{s,k}^{\mathrm{C,IN}} = \phi_{s,k}^{\mathrm{C,IN,UP}} + \psi_{s,k-1}^{\mathrm{C,IN}} - \phi_{s,k-1}^{\mathrm{C,IN,LO}} \qquad s \in \mathbf{S}, k \in \mathbf{K} \tag{D.6}$$

D.1.3 Cold Stream Outlet Preprocessing

$$\phi_{s,k}^{\mathrm{C,OUT,UP}} = \begin{cases} 1 & \text{if } k = \arg\min_{k'} \|\hat{T}_{k'}^{\mathrm{C}} - T_s^{\mathrm{OUT,UP}}\| \\ & \text{s.t.} \hat{T}_{k'}^{\mathrm{C}} \leq T_s^{\mathrm{OUT,UP}} \\ 0 & \text{otherwise} \end{cases} \qquad s \in \mathbf{S}, k \in \mathbf{K} \tag{D.7}$$

$$\phi_{s,k}^{\mathrm{C,OUT,LO}} = \begin{cases} 1 & \text{if } k = \arg\min_{k'} \|\hat{T}_{k'}^{\mathrm{C}} - T_s^{\mathrm{OUT,LO}}\| \\ & \text{s.t.} \hat{T}_{k'}^{\mathrm{C}} \geq T_s^{\mathrm{OUT,LO}} \\ 0 & \text{otherwise} \end{cases} \qquad s \in \mathbf{S}, k \in \mathbf{K} \tag{D.8}$$

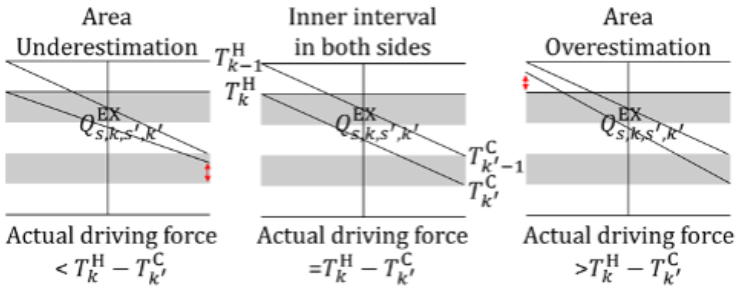

Figure D.1: Potential error in linearized area calculation in boundary intervals

$$\psi^{\mathrm{C,OUT}}_{s,k} = \phi^{\mathrm{C,OUT,UP}}_{s,k} + \psi^{\mathrm{C,OUT}}_{s,k-1} - \phi^{\mathrm{C,OUT,LO}}_{s,k-1} \qquad s \in \mathbf{S}, k \in \mathbf{K} \qquad \text{(D.9)}$$

D.2 Error in Linear Approximation of Heat Exchanger Area

The linear approximation of the area can over/underestimate the heat exchanger area at the start/end (boundary intervals) of the heat exchanger. Since we only have discrete temperatures on the grid, we cannot consider exact start/end temperature of the heat exchanger for the area calculation if that heat exchanger starts/ends in the middle of the temperature interval. In this case, driving force for that interval can be either over/underestimated so that numerical error can occur as **Figure D.1**. For fully spanned intervals, the linear approximation overestimates the area compared to method using log-mean temperature. With 20 K intervals, up to 4.4 % overestimation is observed compared to the log-mean temperature method. However, with 5 $\sim$ 10 degree intervals, error is small enough (0.004 % $\sim$ 1.143 %).

Table D.1: Approximation error of area calculation

	Moderate		High		Low	
Hot	420 K $\rightarrow$ 400K		620 K $\rightarrow$ 600 K		420 K $\rightarrow$ 400 K	
Cold	290 K $\rightarrow$ 330 K		290 K $\rightarrow$ 330 K		350 K $\rightarrow$ 390 K	
Size of interval (K)	Area (m^2)	Error (%)	Area (m^2)	Error (%)	Area (m^2)	Error (%)
20	0.40404	0.67250	0.13348	0.07415	1.06667	4.40614
10	0.40202	0.16914	0.13341	0.01855	1.03333	1.14345
5	0.40151	0.04235	0.13339	0.00464	1.02460	0.28894
1	0.40135	0.00170	0.13338	0.00019	1.02180	0.01160

Bibliography

[1] C. S. Adjiman, I. P. Androulakis, and C. A. Floudas, *Global optimization of mixed-integer nonlinear problems*, AIChE Journal, 46 (2000), pp. 1769–1797.

[2] A. Aggarwal and C. A. Floudas, *Synthesis of general distillation sequences-nonsharp separations*, Computers and Chemical Engineering, 14 (1990), pp. 631–653.

[3] M. J. Andrecovich and A. W. Westerberg, *An MILP formulation for heat-integrated distillation sequence synthesis*, AIChE journal, 31 (1985), pp. 1461–1474.

[4] P. Angelini, T. Armstrong, R. Counce, W. Griffith, T. LKlasson, G. Muralidharan, C. Narula, V. Sikka, G. Closset, and G. Keller, *Materials for separation technologies: Energy and emission reduction opportunities*, DOE, EERE Office, Washington, DC, (2005), p. 103.

[5] G. Bamopoulos, R. Nath, and R. L. Motard, *Heuristic synthesis of non-sharp separation sequences*, AIChE Journal, 34 (1988), pp. 763–780.

[6] A. Barbaro and M. J. Bagajewicz, *New Rigorous One-Step MILP Formulation for Heat Exchanger Network Synthesis*, Comput. Chem. Eng., 29 (2005), p. 1945.

[7] S. D. Barnicki and J. J. Siirola, *Process synthesis prospective*, Computers and Chemical Engineering, (2004).

[8] J. Bausa, R. v. Watzdorf, and W. Marquardt, *Shortcut methods for non-ideal multicomponent distillation: I. Simple columns*, AIChE Journal, 44 (1998), pp. 2181–2198.

[9] M. L. Bergamini, I. Grossmann, N. Scenna, and P. Aguirre, *An improved piecewise outer-approximation algorithm for the global optimization of minlp models involving concave and bilinear terms*, Computers & chemical engineering, 32 (2008), pp. 477–493.

[10] M. L. Bergamini, N. J. Scenna, and P. A. Aguirre, *Global optimal structures of heat exchanger networks by piecewise relaxation*, Industrial and Engineering Chemistry Research, 46 (2007), pp. 1752–1763.

[11] L. T. Biegler, I. E. Grossmann, and A. W. Westerberg, *Systematic methods for chemical process design*, Prentice Hall, Old Tappan, NJ (United States), 1997.

[12] J. A. Caballero and I. E. Grossmann, *Generalized Disjunctive Programming Model for the Optimal Synthesis of Thermally Linked Distillation Columns*, Industrial & Engineering Chemistry Research, 40 (2001), pp. 2260–2274.

[13] ——, *Design of distillation sequences: from conventional to fully thermally coupled distillation systems*, Computers & Chemical Engineering, 28 (2004), pp. 2307–2329.

[14] ——, *Synthesis of complex thermally coupled distillation systems including divided wall columns*, AIChE Journal, 59 (2013), pp. 1139–1159.

[15] J. Cerda, A. W. Westerberg, D. Mason, and B. Linnhoff, *Minimum utility usage in heat exchanger network synthesis A transportation problem*, Chemical Engineering Science, 38 (1983), pp. 373–387.

[16] Q. Chen and I. Grossmann, *Recent Developments and Challenges in Optimization-Based Process Synthesis*, Annual Review of Chemical and Biomolecular Engineering, 8 (2017), pp. 249–283.

[17] S. H. Cheng and Y. A. Liu, *Studies in Chemical Process Design and Synthesis. 8. A Simple Heuristic Method for the Synthesis of Initial Sequences for Sloppy Multicomponent Separations*, Industrial and Engineering Chemistry Research, 27 (1988), pp. 2304–2322.

[18] A. R. Ciric and C. A. Floudas, *Heat Exchanger Network Synthesis without Decomposition*, Comput. Chem. Eng., 15 (1991), p. 385.

[19] R. D. Colberg and M. Morari, *Area and capital cost targets for heat exchanger network synthesis with constrained matches and unequal heat transfer coefficients*, Computers and Chemical Engineering, 14 (1990), pp. 1–22.

[20] M. M. Daichendt and I. E. Grossmann, *Preliminary screening procedure for the minlp synthesis of process systems-ii. heat exchanger networks*, Computers and Chemical Engineering, 18 (1994), pp. 679–709. Cited By :37 Export Date: 22 March 2018.

[21] E. Davis and M. Ierapetritou, *A kriging-based approach to minlp containing black-box models and noise*, Industrial and Engineering Chemistry Research, (2008).

[22] M. F. Doherty and M. F. Malone, *Conceptual design of distillation systems*, McGraw-Hill,, 2001.

[23] A. W. Dowling and L. T. Biegler, *A framework for efficient large scale equation-oriented flowsheet optimization*, Computers and Chemical Engineering, (2015).

[24] M. A. Duran and I. E. Grossmann, *A mixed-integer nonlinear programming algorithm for process systems synthesis*, AIChE Journal, 32 (1986), pp. 592–606.

[25] I. Fahmi and S. Cremaschi, *Process synthesis of biodiesel production plant using artificial neural networks as the surrogate models*, Computers and Chemical Engineering, (2012).

[26] M. M. Faruque Hasan, G. Jayaraman, I. A. Karimi, and H. E. Alfadala, *Synthesis of heat exchanger networks with nonisothermal phase changes*, AIChE Journal, 56 (2010), pp. 930–945.

[27] M. Fenske, *Fractionation of straight-run Pennsylvania gasoline*, Industrial & Engineering Chemistry, 24 (1932), pp. 482–485.

[28] Z. T. Fidkowski, M. F. Doherty, and M. F. Malone, *Feasibility of separations for distillation of nonideal ternary mixtures*, AIChE journal, 39 (1993), pp. 1303–1321.

[29] Z. T. Fidkowski, M. F. Malone, and M. F. Doherty, *Nonideal multicomponent distillation: Use of bifurcation theory for design*, AIChE Journal, 37 (1991), pp. 1761–1779.

[30] G.-J. A. Fien and Y. Liu, *Heuristic Synthesis and Shortcut Design of Separation Processes Using Residue Curve Maps: A Review*, Ind Eng Chem Res, 33 (1994), pp. 2505–2522.

[31] C. A. Floudas, *Separation synthesis of multicomponent feed streams into multicomponent product streams*, AIChE Journal, 33 (1987), pp. 540–550.

[32] C. A. Floudas, *Synthesis of heat integrated nonsharp distillation sequences*, Computers & chemical engineering, 16 (1992), pp. 89–108.

[33] C. A. Floudas and S. H. Anastasiadis, *Synthesis of distillation sequences with several multicomponent feed and product streams*, Chemical Engineering Science, 43 (1988), pp. 2407–2419.

[34] C. A. Floudas and A. R. Ciric, *Strategies for Overcoming Uncertainties in Heat Exchanger Network Synthesis*, Comput. Chem. Eng., 13 (1989), p. 1133.

[35] C. A. Floudas, A. R. Ciric, and I. E. Grossmann, *Automatic synthesis of optimum heat exchanger network configurations*, AIChE Journal, 32 (1986), pp. 276–290. Cited By :338 Export Date: 22 March 2018.

[36] C. A. Floudas and G. E. Paules IV, *A mixed-integer nonlinear programming formulation for the synthesis of heat-integrated distillation sequences*, Computers & chemical engineering, 12 (1988), pp. 531–546.

[37] F. Friedler, K. Tarjan, Y. W. Huang, and L. T. Fan, *Graph-theoretic approach to process synthesis - axioms and theorems*, Chemical Engineering Science, 47 (1992), pp. 1973–1988.

[38] A. Giridhar and R. Agrawal, *Synthesis of distillation configurations: I. Characteristics of a good search space*, Computers and Chemical Engineering, 34 (2010), pp. 73–83.

[39] A. Gomez-Munoz and J. D. Seader, *Synthesis of distillation trains by thermodynamic analysis*, Computers and Chemical Engineering, 9 (1985), pp. 311–341.

[40] T. Gundersen, S. Duvold, and A. Hashemi-Ahmady, *"An extended vertical MILP model for heat exchanger network synthesis*, Computers and Chemical Engineering, 20 (1996), pp. S97–S102.

[41] T. Gundersen and I. E. Grossmann, *Improved optimization strategies for automated heat exchanger network synthesis through physical insights*, Computers and Chemical Engineering, 14 (1990), pp. 925–944.

[42] T. Gundersen, P. Traedal, and A. Hashemi-Ahmady, *Improved sequential strategy for the synthesis of near-optimal heat exchanger networks*, Computers and Chemical Engineering, 21 (1997), pp. S59–S64.

[43] I. J. Halvorsen and S. Skogestad, *Minimum energy consumption in multicomponent distillation. 2. Three-product Petlyuk arrangements*, Industrial and Engineering Chemistry Research, 42 (2003), pp. 605–615.

[44] I. J. Halvorsen and S. Skogestad, *Minimum energy consumption in multicomponent distillation. 3. More than three products and generalized Petlyuk arrangements*, Industrial & Engineering Chemistry Research, 42 (2003), pp. 616–629.

[45] C. A. Henao and C. T. Maravelias, *Surrogate-based superstructure optimization framework*, AIChE Journal, (2011).

[46] R. J. Hengstebeck, *Distillation: principles and design procedures*, Reinhold Pub. Corp., 1961.

[47] X. Hong, Z. Liao, B. Jiang, J. Wang, and Y. Yang, *New Transshipment Type MINLP Model for Heat Exchanger Network Synthesis*, Chem. Eng. Sci., 173 (2017), p. 537.

[48] K. F. Huang, E. M. Al-mutairi, and I. A. Karimi, *Heat exchanger network synthesis using a stagewise superstructure with non-isothermal mixing*, Chemical engineering science, 73 (2012), pp. 30–43.

[49] K. F. Huang and I. A. Karimi, *Simultaneous Synthesis Approaches for Cost-Effective Heat Exchanger Networks*, Chem. Eng. Sci., 98 (2013), p. 231.

[50] J. M. Jezowski, H. K. Shethna, and F. J. L. Castillo, *Area Target for Heat Exchanger Networks Using Linear Programming*, Ind. Eng. Chem. Res., 42 (2003), p. 1723.

[51] Z. Jiang, T. J. Mathew, H. Zhang, J. Huff, U. Nallasivam, M. Tawarmalani, and R. Agrawal, *Global optimization of multicomponent distillation configurations: Global minimization of total cost for multicomponent mixture separations*, Computers & Chemical Engineering, 126 (2019), pp. 249–262.

[52] A. José, Caballero and g. E. Grossmann, *Synthesis of complex thermally*

coupled distillation systems including divided wall columns, AIChe, 59 (2012), pp. 1139–1159.

[53] V. Julka and M. F. Doherty, *Geometric behavior and minimum flows for nonideal multicomponent distillation*, Chemical Engineering Science, 45 (1990), pp. 1801–1822.

[54] R. S. Kamath, L. T. Biegler, and I. E. Grossmann, *Modeling multistream heat exchangers with and without phase changes for simultaneous optimization and heat integration*, AIChE Journal, 58 (2012), pp. 190–204.

[55] M. R. Kilinç and N. V. Sahinidis, *Exploiting integrality in the global optimization of mixed-integer nonlinear programming problems with baron*, Optimization Methods and Software, 33 (2018), pp. 540–562.

[56] C. J. King, *Separation processes*, Courier Corporation, 2nd ed., 2013.

[57] G. R. Kocis and I. E. Grossmann, *Relaxation strategy for the structural optimization of process flow sheets*, Industrial & engineering chemistry research, 26 (1987), pp. 1869–1880.

[58] J. Koehler, P. Aguirre, and E. Blass, *Minimum reflux calculations for nonideal mixtures using the reversible distillation model*, Chemical Engineering Science, 46 (1991), pp. 3007–3021.

[59] L. Kong, V. Avadiappan, K. Huang, and C. T. Maravelias, *Simultaneous Chemical Process Synthesis and Heat Integration with Unclassified Hot/Cold Process Streams*, Comput. Chem. Eng., 101 (2017), p. 210.

[60] L. Kong and C. T. Maravelias, *Expanding the scope of distillation network synthesis using superstructure-based methods*, Computers & Chemical Engineering, 133 (2020), p. 106650.

[61] ——, *Generalized short-cut distillation column modeling for superstructure-based process synthesis*, AIChE Journal, 66 (2020), p. e16809.

[62] Q. Kong and N. Shah, *An optimisation-based framework for the conceptual design of reaction-separation processes*, Chemical Engineering Research and Design, 113 (2016), pp. 206–222.

[63] K. Kraemer, A. Harwardt, M. Skiborowski, S. Mitra, and W. Marquardt, *Shortcut-based design of multicomponent heteroazeotropic distillation*, Chemical Engineering Research and Design, 89 (2011), pp. 1168–1189.

[64] M. R. Kilinç and N. V. Sahinidis, *Exploiting integrality in the global optimization of mixed-integer nonlinear programming problems with BARON*, Optimization Methods and Software, 33 (2018), pp. 540–562.

[65] J. Leboreiro and J. Acevedo, *Processes synthesis and design of distillation sequences using modular simulators: a genetic algorithm framework*, Computers & Chemical Engineering, 28 (2004), pp. 1223–1236.

[66] J. Li, S. E. Demirel, and M. M. F. Hasan, *Process Synthesis Using Block Superstructure with Automated Flowsheet Generation and Optimization*, AIChE J., 64 (2018), p. 3082.

[67] P. Linke and A. Kokossis, *Attainable reaction and separation processes from a superstructure-based method*, AIChE Journal, 49 (2003), pp. 1451–1470.

[68] Y. A. Liu, T. E. Quantrille, and S. H. Cheng, *Studies in chemical process design and synthesis. 9. A unifying method for the synthesis of multicomponent separation sequences with sloppy product streams*, Industrial and Engineering Chemistry Research, 29 (1990), pp. 2227–2241.

[69] A. Lucia, A. Amale, and R. Taylor, *Distillation pinch points and more*, Computers & Chemical Engineering, 32 (2008), pp. 1342–1364.

[70] A. Lucia and R. Taylor, *The geometry of separation boundaries: I. Basic theory and numerical support*, AIChE journal, 52 (2006), pp. 582–594.

[71] M. Martín and T. A. Adams, *Future directions in process and product synthesis and design*, Computer Aided Chemical Engineering, 44 (2018).

[72] U. Nallasivam, V. H. Shah, A. A. Shenvi, J. Huff, M. Tawarmalani, and R. Agrawal, *Global optimization of multicomponent distillation configurations: 2. Enumeration based global minimization algorithm*, AIChE Journal, 62 (2016), pp. 2071–2086.

[73] N. Nishida, G. Stephanopoulos, and A. W. Westerberg, *A review of process synthesis*, AIChE Journal, 27 (1981), pp. 321–351.

[74] S. A. Papoulias and I. E. Grossmann, *A structural optimization approach in process synthesis - {III: Total processing systems}*, Comput. Chem. Eng., 7 (1983), pp. 723–734.

[75] S. A. Papoulias and I. E. Grossmann, *A structural optimization approach in process synthesis-I. Utility systems*, Computers and Chemical Engineering, 7 (1983), pp. 695–706.

[76] ——, *A Structural Optimization Approach in Process Synthesis-II. Heat Recovery Networks*, Comput. Chem. Eng., 7 (1983), p. 707.

[77] F. B. Petlyuk, *Thermodynamically optimal method for separating multicomponent mixtures*, Int. Chem. Eng., 5 (1965), pp. 555–561.

[78] J. M. Ponce-Ortega, A. Jiménez-Gutiérrez, and I. E. Grossmann, *Optimal synthesis of heat exchanger networks involving isothermal process streams*, Computers and Chemical Engineering, 32 (2008), pp. 1918–1942.

[79] J. M. Ponce-Ortega, M. Serna-González, and A. Jiménez-Gutiérrez, *Synthesis of heat exchanger networks with optimal placement of multiple utilities*, Industrial and Engineering Chemistry Research, 49 (2010), pp. 2849–2856.

[80] N. Quirante, I. E. Grossmann, and J. A. Caballero, *Disjunctive model for the simultaneous optimization and heat integration with unclassified streams and area estimation*, Computers and Chemical Engineering, (2018).

[81] J. Ryu, L. Kong, A. E. P. de Lima, and C. T. Maravelias, *A generalized superstructure-based framework for process synthesis*, Computers & Chemical Engineering, 133 (2020), p. 106653.

[82] J. Ryu and C. T. Maravelias, *Simultaneous process and heat exchanger network synthesis using a discrete temperature grid*, Industrial and Engineering Chemistry Research, 58 (2019), pp. 6002–6016.

[83] J. Ryu and C. T. Maravelias, *Computationally efficient optimization models for preliminary distillation column design and separation energy targeting*, Computers & Chemical Engineering, 143 (2020), p. 107072.

[84] ——, *Efficient generalized shortcut distillation model with improved accuracy for superstructure-based process synthesis*, AIChE Journal, 66 (2020), p. e16994.

[85] ——, *A generalized distillation network synthesis model*, Chemical Engineering Science, 244 (2021), p. 116766.

[86] R. W. H. Sargent and K. Gaminibandara, *Introduction: approaches to chemical process synthesis*, in Optimization in action, Academic Press London, 1976.

[87] P. Schäfer, A. Caspari, A. M. Schweidtmann, Y. Vaupel, A. Mhamdi, and A. Mitsos, *The potential of hybrid mechanistic/data-driven approaches for reduced dynamic modeling: Application to distillation columns*, Chemie Ingenieur Technik, 92 (2020), pp. 1910–1920.

[88] J. D. Seader and A. W. Westerberg, *A combined heuristic and evolutionary strategy for synthesis of simple separation sequences*, AIChE Journal, 23 (1977), pp. 951–954.

[89] V. H. Shah and R. Agrawal, *A matrix method for multicomponent distillation sequences*, AIChE journal, 56 (2010), pp. 1759–1775.

[90] M. D. Shelley and M. M. El-Halwagi, *Component-less design of recovery and allocation systems: a functionality-based clustering approach*, Computers & Chemical Engineering, 24 (2000), pp. 2081–2091.

[91] D. S. Sholl and R. P. Lively, *Seven chemical separations to change the world*, Nature, 532 (2016), pp. 435–437.

[92] M. Skiborowski, S. Recker, and W. Marquardt, *Shortcut-based optimization of distillation-based processes by a novel reformulation of the feed angle method*, Chemical Engineering Research and Design, 132 (2018), pp. 135–148.

[93] E. M. B. Smith and C. C. Pantelides, *A symbolic reformulation/spatial branch-and-bound algorithm for the global optimisation of nonconvex minlps*, Computers and Chemical Engineering, (1999).

[94] R. Smith and M. Jobson, *Distillation*, in Encyclopedia of separation science, I. D. Wilson, ed., Academic Press, Oxford, 2000, pp. 84–103.

[95] G. Stephanopoulos and A. W. Westerberg, *Studies in process synthesis—II: Evolutionary synthesis of optimal process flowsheets*, Chemical Engineering Science, 31 (1976), pp. 195–204.

[96] W. J. Stupin and F. J. Lockhart, *The distribution of non-key components in multicomponent distillation*, in AIChE 61st Annual Meeting, Los Angeles, CA (Dec. 1968), 1968.

[97] R. E. Swaney, *Thermal integration of processes with heat engines and heat pumps*, AIChE Journal, 35 (1989), pp. 1003–1016.

[98] M. Tawarmalani and N. V. Sahinidis, *A polyhedral branch-and-cut approach to global optimization*, Mathematical programming, 103 (2005), pp. 225–249.

[99] D. W. Tedder and D. F. Rudd, *Parametric studies in industrial distillation: Part I. Design comparisons*, AIChE Journal, 24 (1978), pp. 303–315.

[100] ——, *Parametric studies in industrial distillation: Part II. Heuristic optimization*, AIChE Journal, 24 (1978), pp. 316–323.

[101] R. Tumbalam Gooty, R. Agrawal, and M. Tawarmalani, *An MINLP formulation for the optimization of multicomponent distillation configurations*, Computers and Chemical Engineering, 125 (2019), pp. 13–30.

[102] K. Ulonska, M. Skiborowski, A. Mitsos, and J. Viell, *Early-stage evaluation of biorefinery processing pathways using process network flux analysis*, AIChE Journal, 62 (2016), pp. 3096–3108.

[103] A. J. V. Underwood, *Fractional distillation of multi-component mixtures*, Chem. Eng. Prog., 44 (1948), pp. 603–614.

[104] ——, *Fractional distillation of multicomponent mixtures*, Industrial & Engineering Chemistry, 41 (1949), pp. 2844–2847.

[105] A. W. Westerberg, *A retrospective on design and process synthesis*, Computers and Chemical Engineering, (2004).

[106] W. Wu, C. A. Henao, and C. T. Maravelias, *A superstructure representation, generation, and modeling framework for chemical process synthesis*, AIChE Journal, 62 (2016), pp. 3199–3214.

[107] T. F. Yee and I. E. Grossmann, *Simultaneous optimization models for heat integration-ii. heat exchanger network synthesis*, Computers and Chemical Engineering, 14 (1990), pp. 1165–1184. Cited By :669 Export Date: 22 March 2018.

[108] ——, *Simultaneous Optimization Models for Heat Integration-II. Heat Exchanger Network Synthesis*, Comput. Chem. Eng., 14 (1990), p. 1165.

[109] H. Yeomans and I. E. Grossmann, *A systematic modeling framework of superstructure optimization in process synthesis*, Computers & Chemical Engineering, 23 (1999), pp. 709–731.

[110] ——, *Optimal design of complex distillation columns using rigorous tray-by-tray disjunctive programming models*, Industrial & engineering chemistry research, 39 (2000), pp. 4326–4335.

[111] L. Yiqing, Y. Xigang, and L. Yongjian, *An improved pso algorithm for solving non-convex nlp/minlp problems with equality constraints*, Computers and Chemical Engineering, (2007).

[112] J. M. Zamora and I. E. Grossmann, *A global minlp optimization algorithm for the synthesis of heat exchanger networks with no stream splits*, Computers and Chemical Engineering, 22 (1998), pp. 367–384. Cited By :129 Export Date: 22 March 2018.